FABRICATION OF A SURFACE ENHANCED NICKEL ULTRACAPACITOR USING A POTASSIUM HYDROXIDE ELECTROLYTE

By

ROBIN LYNN WOMACK

Submitted in partial fulfillment of the requirements
For the degree of Master of Science

Thesis Advisor: Dr. Chung-Chiun Liu

Department of Chemical Engineering
CASE WESTERN RESERVE UNIVERSITY

May, 2009

CASE WESTERN RESERVE UNIVERSITY

SCHOOL OF GRADUATE STUDIES

We hereby approve the thesis/dissertation of

Robin Womack

candidate for the MS degree *.

(signed) Chung-Chiun Liu

(chair of the committee)

Heidi Martin

Uziel Landau

(date) December 3, 2008

*We also certify that written approval has been obtained for any proprietary material contained therein.

Dedication

I dedicate this work to my parents, Sandy and Donna Womack, who have supported and encouraged my education.

Table of Contents

LIST OF TABLES

LIST OF FIGURES

ACKNOWLEDGEMENTS

I would like to thank: Laurie Dudik for her assistance with the thick film screen printing; Dr. Lei Fang and Brandon Bartling for their assistance with day to day laboratory procedures; Donald McGervey for his assistance in setting up and understanding of the ultracapacitor experiments; Li-Ju Chen for her help in performing the experiments, particularly the XRD analysis; and Dr. Gerhard Welsch and C.C. Liu for guidance.

Funding for this work is gratefully acknowledged from the NSF grant number 0609128 NIRT: NanoElectro Mechanical Systems (NEMS) using Light-Driven Molecular Shuttles as Active Nanostructures.

Fabrication of a Surface Enhanced Nickel
Ultracapacitor Using a
Potassium Hydroxide Electrolyte

Abstract by

Robin Lynn Womack

Surface enhanced nickel and potassium hydroxide have been proven to be a successful electrode and electrolyte of an ultracapacitor, respectively. The thermal reduction of nickel oxide to form nickel can generate surface enhancement up to one thousand times greater than a nickel substrate that has not been surface enhanced. Three types of the nickel oxide samples were prepared: (1) thermal oxidation in air, (2) thick film screen printed nickel oxide and (3) thick film screen printed nickel oxide with a pore former. The effects of the thermal reduction of the nickel oxide were investigated using scanning electron microscopy, energy dispersive x-ray spectroscopy and x-ray diffraction. The specific capacitance of individual nickel electrodes were measured using an oscilloscope in a potassium hydroxide electrolyte. Finally, six surface enhanced nickel electrodes were aligned in parallel in order to obtain an estimated capacitance of 75mF compared to an estimated specific capacitance of 0.14mF for a nickel ultracapacitor prior to surface enhancement. Each electrode in both types of ultracapacitors was 1.56cm^2 in area. If these ultracapacitors were scaled up, it would be possible to build devices that could be competitive with commercially available ultracapacitors.

I. INTRODUCTION

The motivation for this research is based on the constantly growing demand for energy. Novel means to store and supply energy such as metal based ultracapacitors become attractive as the traditional energy storage methods are not meeting increasing demands. For example, traditional batteries and capacitors can not deliver both the high power and the energy density that are necessary in a complex electronic system.[1] Ultracapacitors may be able to supply both large quantities of power as well as energy in a single device.

In comparison to the commercially available products, ultracapacitors are similar to batteries. Both devices are used to store charge, although in a different way. Batteries store charge through oxidation and reduction reactions taking place whereas the ultracapacitors store charge electrostatically. One major downfall of primary batteries is that the charge storing process is not reversible. The materials used to construct a battery are generally more corrosive. These limitations lead to a much shorter lifetime of a battery as compared to an ultracapacitor. Consequently, the lifetime of a battery is from 1/100 to 1/1000 times shorter than a capacitor.[2] In general, an ultracapacitor will not demonstrate significant deterioration within several hundreds or thousands of cycles, which is not the case with a battery. One benefit that a battery may have over an ultracapacitor is that a battery has a much higher energy density. This means that the quantity of the charge that the battery is capable of storing is greater than that of an ultracapacitor.[2] An ultracapacitor, however, can have a higher power density. This suggests that the time required to discharge is faster for an ultracapacitor than that for a battery.[2]

There are differences between ultracapacitors that are being fabricated in this research and commercially available devices. First, most commercial products are carbon-based devices as opposed to a surface enhanced metal used in this research. A carbon based device has the potential to store a large quantity of charge since carbon structures can be created to have an extremely high surface area by creating thick porous materials. Commercial products also use complex organic electrolytes that have high operating voltages. The operating voltage of an ultracapacitor is determined by the decomposition voltage of the electrolyte and impacts the quantity of energy that can be stored in the device.[2] An alternative to the organic electrolytes are compounds with high conductivities such as potassium hydroxide or sulfuric acid. The relatively lower conductivity is one major disadvantage of using an organic electrolyte as opposed to an aqueous electrolyte. Another major drawback of the commercial products is the long discharge time required. Commercial devices take several seconds to discharge.[2] This long discharge time can be attributed to the depth of the pores. The device becomes mass transport limited since the charge cannot leave the pores quickly. By creating a structure of shallower pores, the discharge time can be increased significantly.

Thus, this research focuses on the fabrication of a high energy storing ultracapacitor that may provide both high power and energy density by creating high surface area metallic electrodes.

I.1 Background

Capacitance is a measurement of the quantity of the charges stored. The charge can be stored using a capacitor. A typical capacitor is constructed using two conducting plates separated by a dielectric layer, as shown in Figure 1.1.

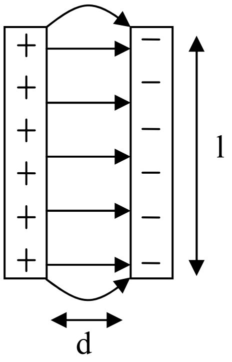

Figure 1.1: A typical parallel plate capacitor

The capacitance of this parallel plate capacitor can be calculated using the following equation[3]:

$$C = \kappa \varepsilon_o \frac{A}{d} \qquad [1.1]$$

where κ is the dielectric coefficient of the electrolyte, ε_o is the permittivity in a vacuum, A is the surface area of a plate and d is the distance between the two plates. The value of κ in a vacuum is 1 and all other values are greater than 1. Namely, ε_o is $8.85\text{x}10^{-12}$ F/m^3 and d should be much less than l, the length of the plate.[2] Typical values of the commercially available capacitors range in the order of picoFarads per square centimeters to microfarads per square centimeters. Once the capacitance is determined, the total quantity of energy stored can be determined using equation 1.2:

$$E = \frac{1}{2} C V_o^{\,2} \qquad [1.2]$$

where V_o is the applied voltage used to charge the capacitor. [2]

Ultracapacitors differ from capacitors in that ultracapacitors can have much higher energy densities. Capacitances on the order of Farads are possible with an ultracapacitor as opposed to only microFarads with regular capacitors. Hence, in order to optimize the performance of an ultracapacitor, it is beneficial to use the ultracapcitor in combination with other storage devices, such as a fuel cell or a battery.[1] Figure 1.2 illustrates the rationale of using an ultracapacitor. As shown in Figure 1.2, ultracapacitor can fill the gap between the traditional capacitors and the batteries in terms of the energy density and the power density.[2,4]

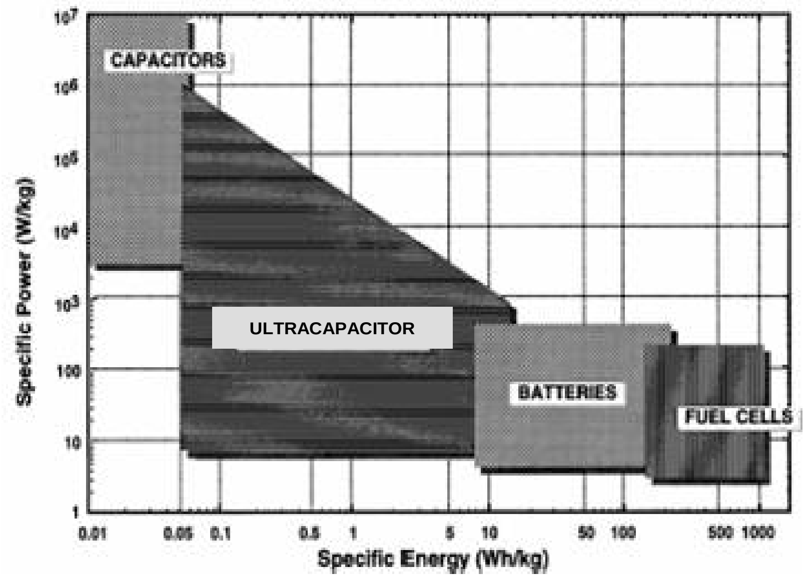

Figure 1.2: Ragone plot of energy storage devices[4]

Ultracapacitors can store charges in two ways: namely, Faradaic charge storage and non-Faradaic charge storage.[2] Faradaic charge storage is charges that are stored within the bulk of the electrode in a Faradaic capacitor. This is feasible due to a series of oxidation and reduction reactions that take place within the electrode material. This can be observed in selected metal oxides, specifically oxides of transition metals such as ruthenium, iridium and molybdenum.[2,5,6] These devices are typically known as supercapacitors. An ultracapacitor is an example of a non-Faradaic capacitor. This is a high energy charge storage device that is similar to a traditional capacitor in that the charges are simply accumulated on the surface of the electrode. The main difference is the high surface area of the electrodes. One approach to achieve a high surface area is by creating nanopores. This high surface area allows for more charge accumulation and results in a double layer capacitance which means the device operates as two capacitors in parallel.[2] Consequently, the total capacitance of a double layer capacitor in parallel can be calculated according to equation 1.3:

$$C_{tot} = C_1 + C_2 \qquad [1.3]$$

where C_{tot} is the total capacitance and C_1 and C_2 is the capacitance at either of the electrodes. This equation demonstrates that the total capacitance of the two capacitors in parallel will result in a higher total capacitance. If the electrodes are in series, equation 1.4 can then be used to calculate the total capacitance.

$$\frac{1}{C_{tot}} = \frac{1}{C_1} + \frac{1}{C_2} \qquad [1.4]$$

As shown, when the capacitors are in series, the total capacitance would be less than that of each single capacitor. Therefore, in order to obtain a higher capacitance, it is beneficial to align capacitors in parallel rather than in series.[2,3,4] On the other hand, if the capacitors are in series, the operating voltage will increase. According to equation 1.2, if the operating voltage increases, the total energy stored can also increase.[2,3]

Similarly to capacitors, resistors in parallel and in series can be calculated using equations 1.5 and 1.6 respectively:

$$\frac{1}{R_{tot}} = \frac{1}{R_1} + \frac{1}{R_2} \qquad [1.5]$$

$$R_{tot} = R_1 + R_2 \qquad [1.6]$$

where R_{tot} is the total resistance of the system and R_1 and R_2 are the resistances of two resistors in ohms.[3] Series resistance can negatively impact the operation of an ultracapacitor. Therefore it is desirable to not only maximize the capacitance but also minimize the resistance. If the capacitors are set up in parallel then the resistance of the system would add according to equation 1.6. Therefore by maximizing the capacitance, the series resistance would also be minimized.

If a capacitor is charged at using a resistor so that the resistance is constant, the result is an exponential function that follows equation 1.7:

$$V = V_o\left(1 - e^{-t/RC}\right) \qquad [1.7]$$

where V is the actual voltage of the capacitor, t is the time required to charge the capacitor and R is the resistance of the resistor used. Figure 1.3 shows the results of a typical voltage as a function of time of a capacitor charged at a constant resistance.[3]

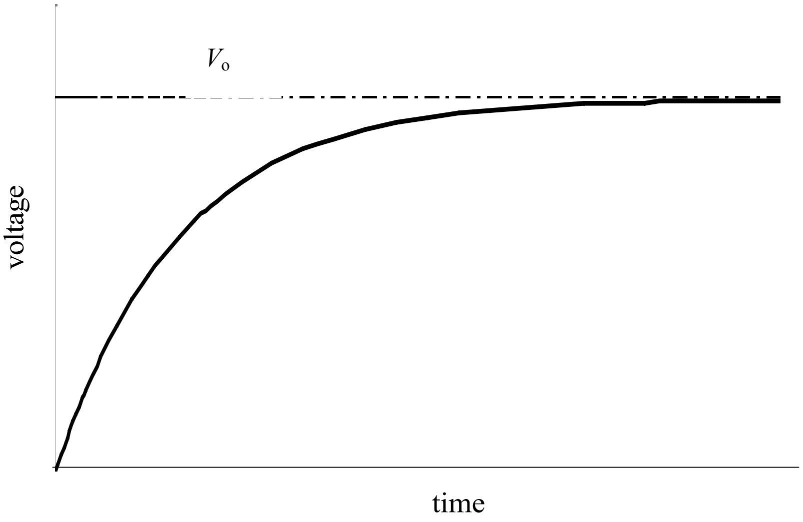

Figure 1.3: Voltage versus time of a capacitor charged at a constant resistance

If the capacitance of one electrode is known, the total capacitance of a system can then be determined. This can be accomplished by applying a square wave to the two capacitors in series. A square wave is a type of waveform that suddenly switches from voltage to another.[3] The time between the switching voltages can be varied in order to allow the capacitor to be fully charged and discharged. If the capacitor is fully charged, the maximum voltage of the device will equal the voltage applied by the square wave. Figure 4 illustrates the effect of a square wave on the capacitance.[3]

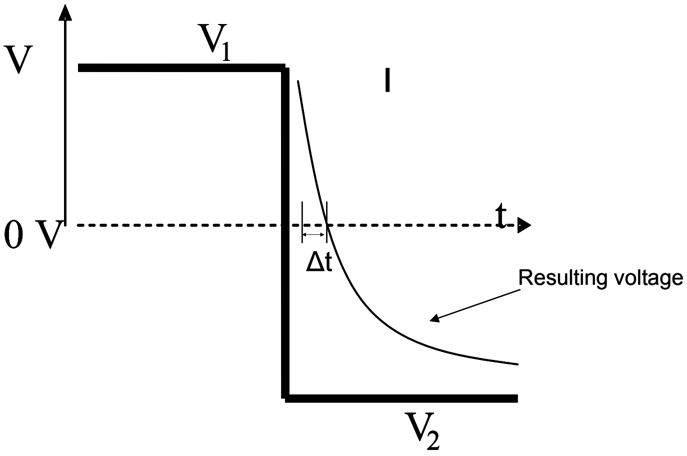

Figure 1.4: Square wave function and the effects on an ultracapacitor

The maximum and the minimum voltages of the square wave function are known as well as the change in time at V=0, the total capacitance can be determined. Equation 1.7 can be modified to form equation 1.8:

$$V = V_1 + (V_2 - V_1)\left(1 - e^{-t/RC_{tot}}\right) \qquad [1.8]$$

If V is assumed to be zero and $V_1 = -V_2$, then this equation becomes

$$C_{tot} = \frac{t}{R\ln(2)} \qquad [1.9]$$

Then, since C_{tot} and C_1 are known, equation 1.4 can be used to assess the value of C_2.[3]

In order to maximize the capacitance, the two electrodes should be placed as close as possible such that the distance the charges must travel through the electrolyte is minimized. Consequently, a thin membrane is used to separate the two electrodes. This membrane allows for the movement of the charges throughout the electrolyte but maintains the two electrodes from touching and shorting the device. An example of this can be seen in Figure 1.5.[2,7]

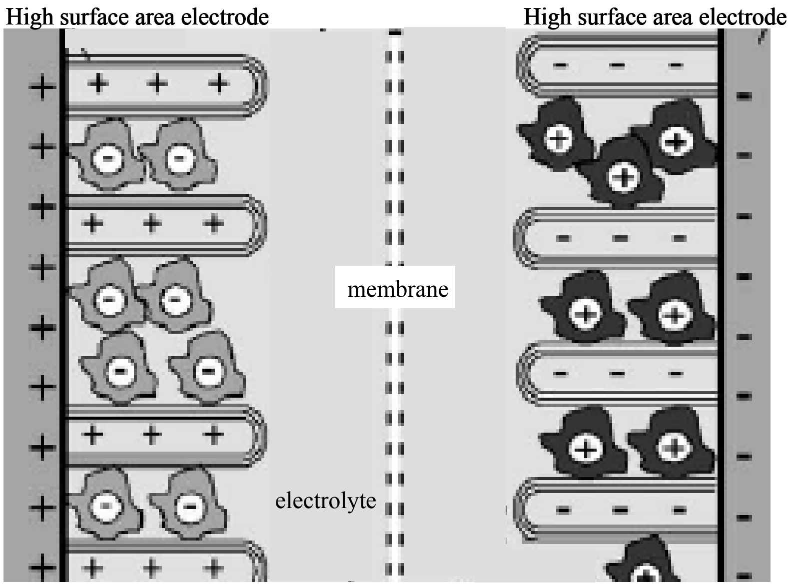

Figure 1.5: Schematic of an Ultracapacitor

Figure 1.5 is a schematic of an ultracapacitor. If a voltage is applied across the two electrodes, one electrode becomes negatively charged while the other becomes positively charged. The charged ions of the electrolyte accumulate at each of the electrodes forming a multiple double layer capacitor.

An approach to optimize the charge storage capabilities of this device involves a relatively conductive electrolyte and the high surface area electrodes. Common electrolytes used in this application are potassium hydroxide and sulfuric acid.[8] Both of these compounds have conductivities three orders of magnitude higher than that of water, which has a conductivity of 10^{-6}S/cm.[2,8] The electrolyte concentration electrolyte can affect its conductivity. If the conductivity of the electrolyte increases, the resistance of the system will decrease according to equation 1.10.

$$R = \frac{l}{A\kappa} \qquad [1.10]$$

Consequently, 1M-10M electrolyte solutions have conductivities that range from 0.1 to 1 S/cm.[9] Therefore, as concentration of the electrolyte increases, the conductivity would also increase, which would minimize the internal resistance of the system. Ideally, the conductivity of the electrolyte would continue to increase as the electrolyte concentration increased. This would be the case if there was no interaction between the ions in the electrolyte. Since this ideal case generally does not exist, the conductivity of the electrolyte will increase until a maximum conductivity is achieved. At this point, if the concentration is further increased, the conductivity will decrease.[9]

Other common electrolytes used are complex organic compounds.[10,11] The benefit of these organic compounds over potassium hydroxide and sulfuric acid is the higher operating voltage that can be applied. Organic electrolytes have operating voltages that range from 3V to 5V while aqueous electrolytes only have a maximum operating voltage of approximately 1V.[8] As shown in equation 1.2, the operating voltage influences the energy stored in the device. One disadvantage of the organic electrolytes is their relatively low conductivities. Most organic electrolytes do not have conductivities greater than 20mS/cm.[8] Another disadvantage is that the size of the ions of the electrolyte are larger than that of a simple, aqueous electrolyte. Consequently, this will limit the feasibility of allowing the large ions to pass through the pores of the electrode.[2,12]

Nickel is a conducting metal that is capable of storing charge.[14] A single plate of nickel in a 2M potassium hydroxide solution is capable of storing 25μF/cm^2. The standard free energy of formation of nickel oxide is negative up to about 2000°C. Thus, if nickel is heated in the presence of oxygen, nickel oxide will form. The only oxide of nickel that is stable at high temperatures is nickel II oxide, or in a one to one ratio of nickel to oxygen.[13, 14] Once a monolayer forms on the nickel surface, the kinetics of the reaction is no longer controlled by the heterogeneous reaction between the oxide and the metal.[14] Rather, mass transport becomes an issue since the oxygen must travel through the oxide surface in order to react with the metal underneath. If nickel is heated at 900°C in the presence of oxygen, the rate of formation of nickel oxide follows the parabolic law of oxidation. This law is governed by the equations 1.11 and 1.12, where equation 1.12 is the integrated form of equation 1.11.

$$\frac{dy}{dt} = \frac{A'}{y} \qquad [1.11]$$

$$y^2 = 2A't' + B \qquad [1.12]$$

In equations 1.11 and 1.12, y is the thickness of the oxide film, t' is the time of oxidation, A' is a constant dependent on the temperature and the nature of the film and B is an integration constant. Figure 1.6 illustrates the growth rate of the oxide film as a function of time.[14]

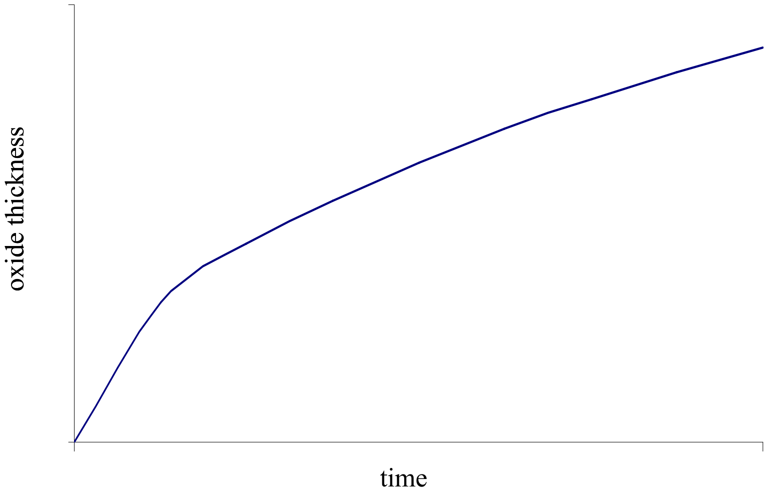

Figure 1.6: Parabolic Law of Oxidation

As this oxide film grows, the thickness of the overall sample also increases. If this sample is then reduced, instead of contracting back to its original form, the oxygen will be removed through the pores formed. This pore formation leaves behind an electrically conductive nickel sample with an extremely high surface area. This allows for a much larger surface area that is capable of storing charge.

A major issue that affects several aspects of this research is the mass transport, specifically the transport of oxygen into and out of the oxide layer, as well as the mass transport of the electrolyte into and out of the pores of the electrode. Mass transport of the oxygen into the nickel oxide layer impacts the rate of growth of the nickel oxide. This is because the oxygen must pass through the nickel oxide film in order to reach the nickel substrate in order to continue the oxidation of nickel. For this reason, the growth rate of nickel oxide on a nickel substrate is parabolic instead of linear. This relationship has been thoroughly studied in the past and is well understood.[14,15,16]

Mass transport of oxygen out of the oxide film also plays a role in the reduction of nickel oxide to form nickel. This has been studied as well.[13,17,18] However, the result is not as well defined since the reduction conditions, such as temperature and pressure, strongly impact the final result. Changes in these operating conditions will determine whether the different sub-oxides of nickel will exist or if pure nickel exists after reduction. In addition to the formation of nickel that exists after the reduction process, the reduction conditions can also impact the porous nature of the nickel. A large quantity of research has been carried out investigating the effects of hydrogen in nickel oxide reduction.[13,17] Methane and other natural gases are also options for the reduction of nickel oxide.[13] While this approach has been investigated, it has not been researched as extensively as hydrogen.[17] In order to obtain a high capacitance, a high surface area nickel is desired. Therefore the reduction conditions are important because they play an important role in the final structure of the nickel. The reduction conditions that result in a porous nickel structure are most desirable.

Finally, mass transport of the ions of the electrolyte will affect an ultracapacitor in terms of the diffusion of the ions to the surface of the electrode. As the pore size becomes smaller, the diffusion of the electrolyte into the pores of the electrode becomes more difficult. This can slow the charge and the discharge time of a capacitor significantly. An approach to avoid the issue of a slow charge and discharge time is to use an electrolyte with smaller ions. For instance, potassium hydroxide ions are much smaller than those of the complex organic electrolytes which are used in commercial products.[19] Shallower pores can also improve the charge and discharge time.[2,19,20] Finally, a higher operating voltage can also improve the mass transport of the ions since an increase in the voltage can decrease the series resistance of the electrolyte.[2,8,9]

I.2. Scope

The objective of this research is to design a high surface area ultracapacitor using nickel as the electrode and potassium hydroxide as the electrolyte. This nickel based ultracapacitor should exhibit a high power and energy density.

Three types of nickel electrodes were prepared and tested in this study. The first type was prepared by thermal oxidation and reduction of the nickel. First, a sheet of nickel was oxidized at 800^{o}C in the presence of air forming a layer of nickel oxide. This sample was then reduced in the presence of methane gas and heated forming the porous nickel. The thickness of the porous nickel depended on the oxidation time of the nickel. As the temperature and the length of time of oxidation increased, the thickness of the porous nickel layer increased. The thickness of the nickel oxide layer ranged from 5-20 microns. After oxidation, the nickel substrate would still remain underneath the nickel oxide layer. Figure 1.7 is the schematic of the oxidation and reduction process.

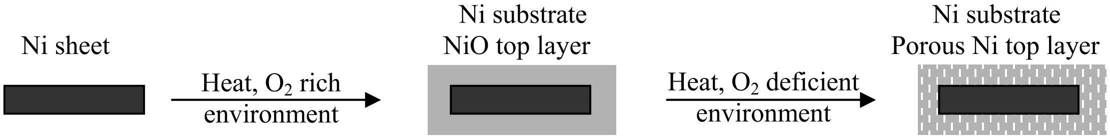

Figure 1.7: Schematic of oxidation and reduction procedure to obtain high surface area nickel

The other two nickel electrodes were prepared using commercially available nickel oxide pastes for thick-film screen-printing processing. The pastes were screen printed at the Electronics Design Center at Case Western Reserve University. Pastes #4410 and #4411 were purchased from ESL Electro-Science in King of Prussia, Pennsylvania and contained a nickel oxide powder and a binder mixed in a solvent. In addition to the nickel oxide powder, a binder and a solvent, paste #4411 also contained a pore forming agent. The substrate was the same nickel substrate from the thermal oxidation and reduction process used in the preparation of the previous sample. The thickness of the printed nickel films ranged from 10-25 microns. These electrodes were then heated and reduced in the presence of methane resulting in the formation of porous nickel. After the nickel electrodes were prepared, they were tested using a low frequency function generator and an oscilloscope to determine the capacitance of each type of the electrode. In addition to this, selected microscopic methods were used to analyze the morphology and the composition of the nickel and the nickel oxide layers. Finally, the electrodes were packaged as a capacitor in parallel in order to obtain a higher capacitance than a single capacitor.

The experimental work focused on obtaining the maximum capacitance of a high surface area ultracapacitor using a nickel electrode and a potassium hydroxide electrolyte. Although other metals and reducing methods could be viable options, this research was limited to the use of the nickel as the basic material for the potential ultracapacitor applications. It also should be recognized that the operational lifetime of such a device would not be assessed in this study.

Hence, this research would serve as the groundwork for the future study using a metal as ultracapacitor electrode. Since most research in ultracapacitors had been focused on carbon but not on metals, this study would serve as a valuable reference for the design of a device that could be competitive with commercially available devices in the future.

I.3. Significance

This research provided a new, novel method of storing a large quantity of electrical charges in a compact device using a relatively low cost material. It would also be possible to scale-up of the final device allowing manufacturing large electrical charge storage system. The commercial applications of both a small ultracapacitor as well as a large-scale device fabricated from similar materials will include telecommunication devices such as cell phones and pagers, stand-by power systems and electric/hybrid vehicles. Alternative methods of charge storage like ultracapacitors would be continually in high demand as the world's energy usage increases.[1]

I.4. References

1. Andrew Burke, *Ultracapacitors: why, how, and where is the technology*, Journal of Power Sources, **91** (2000) 37.

2. B.E. Conway. **Electrochemical Supercapacitors: Scientific Fundamental and Technological Applications**. Klumer Academic/Plenum Publishers, New York, 1999.

3. Richard C. Dorf. **Introduction to Electric Circuits**. 2nd Edition, John Wiley & Sons, Inc., New York, 1993.

4. A.G. Pandolfo, A.F. Hollenkamp, *Carbon properties and their role in supercapacitors*, Journal of Power Sources, **157** (2006) 11.

5. Il-Hwan Kim and Kwang-Bum Kim, *Ruthenium Oxide Thin Film Electrodes for Supercapacitors*, Electrochemical and Solid State Letters, **4** (2001) A62.

6. J.P. Zheng, P.J. Cygan, T.R. Jow, *Hydrous Ruthenium Oxide as an Electrode Material for Electrochemical Capacitors*, Journal of the Electrochemical Society, **142** (1995) 2699.

7. Ch. Emmenegger, Ph. Mauron, P. Sudan, P. Wenger, V. Hermann, R. Gallay, A. Züttel, *Investigation of electrochemical double-layer (ECDL) capacitors electrodes based on carbon nanotubes and activated carbon materials*, Journal of Power Sources, **124** (2003) 321.

8. Elzbieta Frackowiak, Françios Béguin, *Carbon materials for the electrochemical storage of energy in capacitors*, Carbon **39** (2001) 937.

9. Geoffrey Prentice. **Electrochemical Engineering Principles**. Prentice Hall, New Jersey, 1991.

10. T. Morimoto, K. Hiratsuka, Y. Sanada, K. Kurihara, *Electric double-layer capacitor using organic electrolyte*, Journal of Power Sources, **60** (1996) 239.

11. Makoto Ue, Kazuhiko Ida, Shoichiro Mori, *Electrochemical Properties of Organic Liquid Electrolytes Based on Quaternary Onium Salts for Electrical Double-Layer Capacitors*, Journal of the Electrochemical Society, **141** (1994) 2989.

12. P. Simon, A. Burke. *Nanostructured Carbons: Double-Layer Capacitance and More*. The Electrochemical Society **Interface**. Spring 2008. pp38-43.

13. Hong Yong Sohn, Milton E. Wadsworth. **Rate Processes af Extractive Metallurgy**. Plenum Press, New York, 1979.

14. Roger Hill Parker. **An Introduction to Chemical Metallurgy**. 1st Edition, Pergamon Press Ltd., Oxford, 1967.

15. Kazuo Fueki, J. Bruce Wagner, Jr., *Studies of the Oxidation of Nickel in the Temperature Range of 900^o to 1400^{o}C*, Journal of the Electrochemical Society, **112** (1965) 384.

16. Per Kofstad. **High Temperature Corrosion.** Elsevier Applied Science, New York, 1988.

17. Vladimir N. Ipatieff. **Catalytic Reactions at High Pressures and Temperatures**. The MacMillan Company, New York, 1936.

18. Giuseppe Parravano, *The Reduction of Nickel Oxide by Hydrogen*, Journal of the American Chemical Society, **74** (1952) 1194.

19. William D. Callister, Jr. **Materials Science and Engineering: An Introduction**. 7th Edition, John Wiley & Sons, Inc., New York, 2007.

20. Christie John Geankoplis. **Transport Processes and Separation Process Principles**. 4th Edition, Prentice Hall, New Jersey, 2003.

II. EXPERIMENTAL PROCEDURE

II.1. Preliminary Experiments

In this study, three preliminary experiments were performed. The first experiment was to obtain an oxidation curve similar to Figure 6 for oxidizing nickel to nickel oxide. This was accomplished by thermal oxidation of a nickel substrate in air at a given temperature. The nickel substrate was weighed periodically in order to determine the quantity of oxygen added to the nickel substrate. The thickness of the oxide layer was calculated using the following equation:

$$y = \frac{MW_{NiO}}{MW_o} \frac{\Delta m}{A_{avg} \rho_{NiO}} \qquad [2.1]$$

where Δm is the change in the mass after oxidation, MW_o and MW_{NiO} are the molecular weights of atomic oxygen and nickel oxide respectively, A_{avg} is the average area of the sample and ρ_{NiO} is the density of nickel oxide. The oxidation curve should be similar to equation 1.12 and served as a method of determining the total time needed to obtain a specific thickness of the oxide layer.

The second experiment was to determine the capacitance of a counter electrode that was used in the assessment. There were two identical counter electrodes used to determine the capacitance of the surface enhanced nickel samples. These counter electrodes were high surface area nickel screens obtained from INCOFoam. The density of these electrodes was $420g/m^2$, the pore size was 450μm and the thickness was 1.7mm. The dimensions of these electrodes were $9x3cm^2$. A schematic of the electrochemical cell set-up and the circuitry is shown in Figures 2.1 and 2.2 respectively.

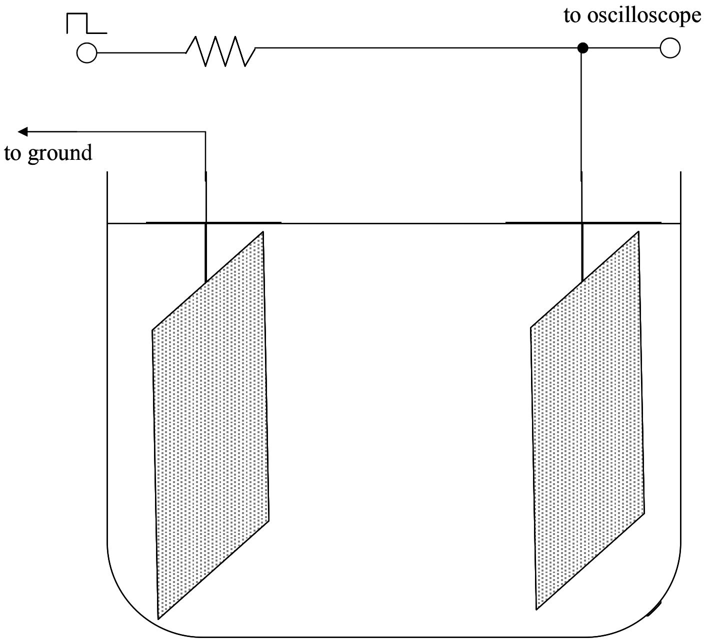

Figure 2.1: Schematic of cell set-up used to test capacitance of counter electrodes

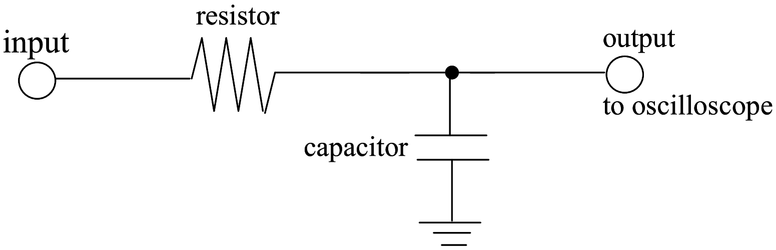

Figure 2.2: Circuitry set-up used to test capacitance of counter electrodes

In order to measure the capacitance of the samples, the function generator, the oscilloscope and the counter electrodes were each grounded. The function generator was connected to the input side of the resistor and the oscilloscope and the electrode was connected to the output side of the resistor. The counter electrodes were set up in series and equation 1.9 was used to determine the capacitance of the electrode. This experimental arrangement incorporated a resistor since this was necessary in order to calculate the total capacitance. A Gwinstek SFG-2110 Synthesized Function Generator was used to apply a square wave function to the cell. A Tektonix TDS 7054 Digital Phosphor Oscilloscope was used to measure the rise and fall time of the sample. The electrolyte was 2M potassium hydroxide. The applied frequency was 5.0Hz. The switching voltage of the square wave function was +20V and -20V.

The final preliminary test was to measure the capacitance of a sheet of nickel before the surface enhancement. This test was used as a comparison with the nickel samples that were surface enhanced later. This experiment was performed using a sheet of nickel that was 2.5x1x0.025cm^3. This sample was then set up in an electrochemical cell in series with the two counter electrodes. The electrolyte was 2M potassium hydroxide. Figure 2.3 shows a schematic of the electrochemical cell set-up used to perform this experiment.

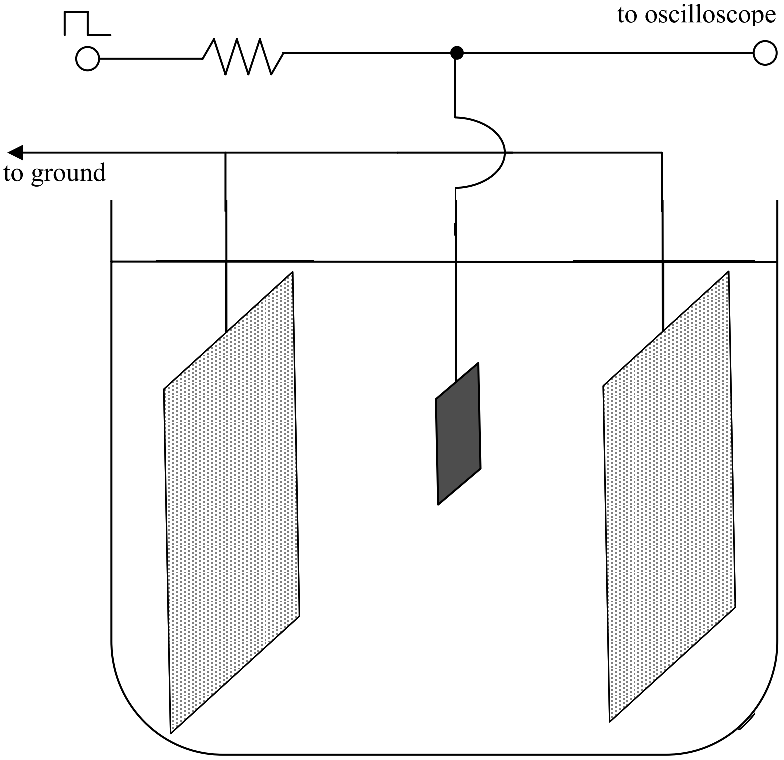

Figure 2.3: Schematic of electrochemical cell set-up used to test capacitance of nickel

II.2. Sample Preparation

The surface enhanced nickel samples were prepared in three different ways. The first one was a thermal oxidation-reduction procedure that involved oxidizing a nickel sample for several days forming a nickel oxide layer. In addition, two other types of samples were also prepared using screen printing paste to print a nickel oxide layer onto a nickel substrate. Different types of samples were used in order to optimize the final capacitance obtainable after reduction.

The first sample was prepared according to the following method. First, a strip of nickel was mechanically cut, weighed and placed in a furnace in the presence of air at $800^{o}C$ for four days. The original thickness of the sample was 0.025cm. The samples were then removed from the furnace and weighed again in order to determine the thickness of the oxide layer formed. The thickness of the nickel oxide after oxidation could be calculated using equation 2.1.

The screen printed nickel oxide samples were prepared using two different thick film pastes: type #4410 and #4411. These pastes were purchased from ESL Electro-Science. Paste #4410 was a proprietary standard paste that contained a nickel oxide powder, a binder and a solvent. Paste #4411 contained the nickel oxide powder, a binder, a solvent and a proprietary pore forming agent. A 325 mesh screen was used to pattern the designed samples on the nickel substrate. After the thick film pastes were applied to the nickel substrate, the samples were fired to remove the binder, solvent and pore forming agent to leave behind just the nickel oxide paste. The thicknesses of these pastes were measured using a laser profilometer. Table 2.1 summarizes the different methods of sample preparation used for this analysis.

Table 2.1: Summary of different porous nickel samples tested

Sample	Preparation Method
A	Nickel was oxidized to form nickel oxide then reduced to form porous nickel.
B	A nickel oxide paste was screen printed on a nickel substrate then reduced to form porous nickel.
C	A nickel oxide paste was screen printed on a nickel substrate then reduced to form porous nickel. This paste contained a pore forming agent.

In order to determine the morphology of the sample types A, B and C, a Philips XL30 Environmental Scanning Electron Microscope (ESEM) was used to examine the cross sections of the samples. The cross sections were prepared by mechanically cutting a small slit into the sample. A plier was then used to separate the rest of the sample. Energy Dispersive X-ray Spectroscopy (EDX) was used for qualitative analysis of the composition of the electrodes before the reduction process. Finally, a SCINTAG X-1 XRD x-ray diffraction tool was used to analyze the composition of the surface of the entire sample as well as the structure of the nickel oxide layer.

The conditions of the reduction of nickel oxide were varied in order to determine the optimal conditions that would yield the highest specific capacitance. All samples were reduced using the same experimental arrangement as shown in Figure 2.4.

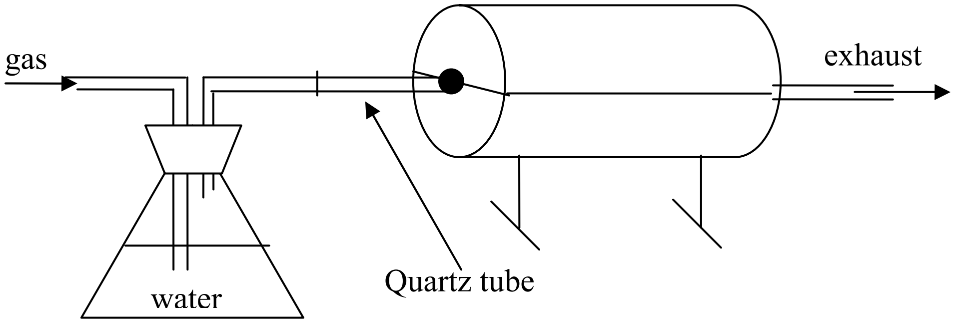

Figure 2.4: Schematic of the thermal reduction set-up

Samples were placed in a quartz tube, which was placed in a cylindrical furnace. Methane was used as the reducing gas. This gas first passed through a flask of water in order to control the flow rate. Subsequently, the gas entered the quartz tube and flowed over the sample. The gas reacted with the sample in order to reduce the nickel oxide layer to the surface enhanced nickel. The furnace was allowed to return to room temperature before sample reduction was started or before samples were removed from the furnace.

Several samples were reduced to determine the quality of surface enhancement after reduction. Sample types A, B and C were reduced at 700^{o}C in the presence of methane gas for 3 hours. The cross sections were prepared by mechanically cutting a small slit into the sample. A plier was then used to separate the rest of the sample. ESEM and EDX were used for qualitative analysis of the morphology and composition of the electrodes after the reduction process.

The specific parameters that were varied in this study of reducing the oxide were the temperature and the time in order to assess their effects on the porosity of the nickel. The purpose of these experiments was to determine the optimal reduction conditions of the nickel oxide that would result in the highest specific capacitance. The first experimental study was the effect of temperature on the porosity of the surface enhanced nickel sample. In order to determine this effect, the time of reduction was held constant. The temperature was varied from 700^{o}C-1000^{o}C in the interval of 100^{o}C. The reduction time was held constant at 24 hours and the reducing gas was methane. Sample types A, B and C were tested at these temperatures. After reduction, the cross sections of selected samples were analyzed using the ESEM. EDX was used for qualitative analysis of the composition of the electrode. Finally, additional SEM and Energy Dispersive Spectroscopy (EDS) assessment was carried out using an FEI Nova Nanolab 200 in order to obtain images on the order of tens of nanometers as well as more quantitative results about the composition of the samples. The surface morphology was also investigated using XRD.

The effect of a shorter reduction time was also investigated. The reducing gas was methane and the temperature of thermal reduction was varied from 600°C to 900°C and the time of reduction was 3 hours. The results of these experiments were compared to the results of thermally reducing the samples for 24 hours.

An experimental investigation involved the assessment of the time of reduction of Sample types A, B and C to investigate the effects on the porosity of each sample. Several time lengths were tested. These times were 1hr, 3hrs, 6hrs, 12hrs and 24hrs. Sample types A, B and C were tested at these time intervals. The temperature was held constant at 800°C and the reducing gas used was methane. After reduction, the cross sections of selected samples were analyzed using the ESEM. EDX was used for qualitative analysis of the composition of the electrode. Finally, additional SEM and Energy Dispersive Spectroscopy (EDS) assessment was carried out using an FEI Nova Nanolab 200 in order to obtain images on the order of tens of nanometers as well as more quantitative results about the composition of the samples. The surface morphology was also investigated using XRD.

The effect of a lower reduction temperature was also investigated. The reducing gas was methane and the time of thermal reduction was either 1hr, 3hrs, 6hrs, 12hrs or

24hrs and the reducing temperature was 700°C. The results of these experiments were compared to the results of thermally reducing the samples at 800°C.

II.3. Capacitance Measurements

These samples were tested to determine the capacitance using an experimental arrangement shown in Figure 2.5.

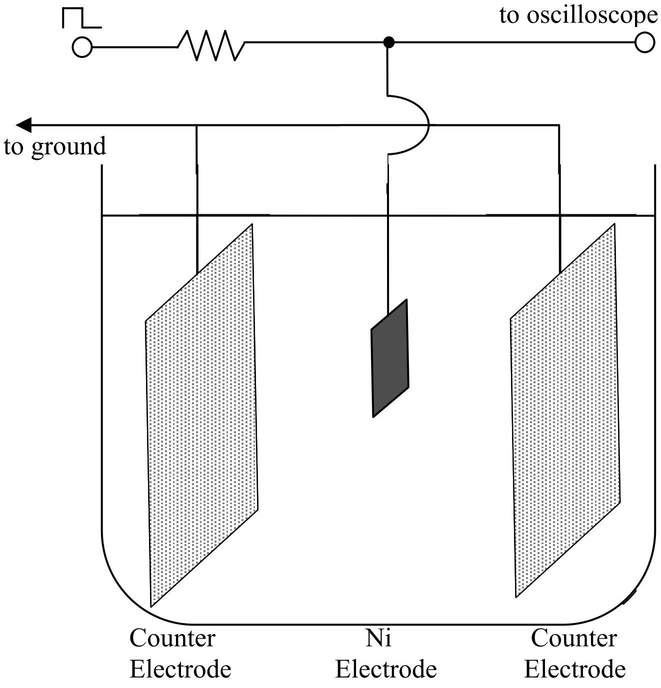

Figure 2.5: Experimental arrangement used to test samples

The counter electrode was set up in series with the surface enhanced nickel sample. The electrodes were attached to a low frequency function generator and the oscilloscope according to Figure 2.2. The resistance was held constant at 380Ω. The applied frequency was 0.1Hz. The switching voltage of the function generator was +20V and -20V. The value of V_o was determined by adding the voltage applied by the function generator to the maximum or minimum voltages measured by the oscilloscope. All of the samples were tested using a 2M potassium hydroxide electrolyte. The capacitance of each sample was calculated using equation 1.4.

Samples that were reduced for 3hrs in methane gas while varying the time of thermal reduction from 1hr to 24hrs were tested using different concentrations of potassium hydroxide in order to determine the effects of the concentration of the electrolyte of the ultracapacitor electrode. The specific capacitance was measured using the experimental arrangement shown in Figure 2.5. The counter electrode was set up in series with the surface enhanced nickel sample. The electrodes were attached to a low frequency function generator and the oscilloscope according to Figure 2.2. The resistance was held constant at 380Ω. The applied frequency was 0.1Hz. The switching voltage of the function generator was +20V and -20V. The value of V_o was determined by adding the voltage applied by the function generator to the maximum or minimum voltages measured by the oscilloscope. The different electrolyte concentrations were 0.1M, 1M, 2M and 3M potassium hydroxide. The capacitance of each sample was calculated using equation 1.4.

Ultracapacitors were built using six nickel electrodes. Two devices were built. The nickel electrodes of the first ultracapacitor were nickel plates before surface enhancement. The second ultracapacitor was built using six Sample type B electrodes. The samples were cut to 1.56cm^2 and then thermally reduced in methane at 700^{o}C for either 3 or 6 hours. Each sample had a 0.25mm diameter nickel wire spot welded to it and then the wires were spot welded together in groups of three. Each group would serve as either the positive or negative electrodes. The samples were then interwoven together with each electrode separated by a membrane. The membrane was a non-woven cellulose based separator that was 100μm thick. The membrane was purchased from Nippon Kodoshi Corporation in Agawa-Gun, Kochi-Ken, Japan and is product #PB100. Figure 2.6 shows the set-up of the electrodes.

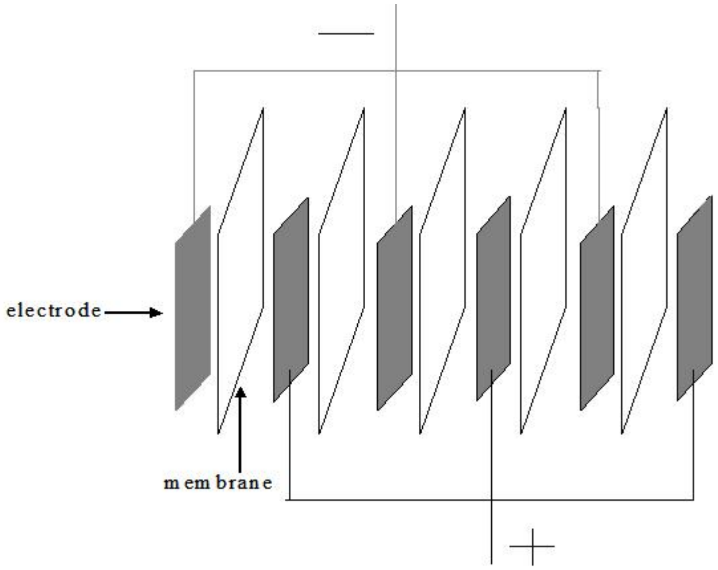

Figure 2.6: Schematic of the configuration of the electrodes used when building an ultracapacitor

In Figure 2.6, the six grey regions are the electrodes and the white regions are the separator membranes. The membranes were used to allow the electrodes to be as close together while not touching each other. If the electrodes were to touch each other, the device would be short circuited and no charge would be stored. This device was then placed inside of a 30mL plastic bottle and filled with the 2M potassium hydroxide electrolyte. The wires were places outside of the bottle and the bottle was sealed. Each side of the ultracapacitor was attached to the oscilloscope in order to determine the capacitance and the series resistance. Figure 2.7 shows the circuit set-up used to make these measurements.

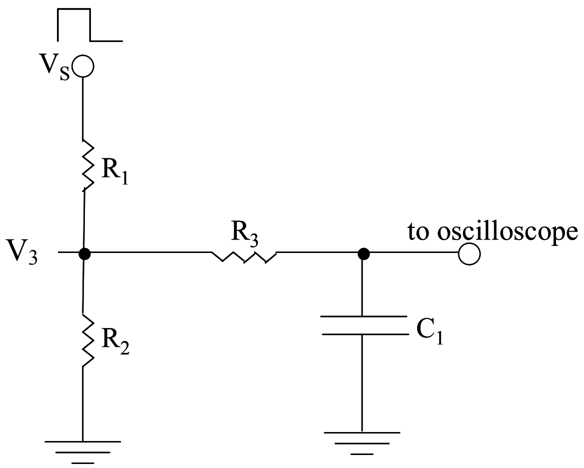

Figure 2.7: Circuit set-up used to measure the ultracapacitors

In Figure 2.7, V_s is the voltage of the square wave applied by the function generator, R_1 and R_2 are two resistors set up in parallel, V_3 is the voltage that results as a result of R_1 and R_2 and can be calculated using equation 2.2.

$$V_3 = V_S \frac{R_1}{R_1 + R_2} \qquad [2.2]$$

Consequently, R_3 is a resistor in series with the resultant resistance of R_1 and R_2 and C_1 is the ultracapacitor being tested. Table 2.2 summarizes the values of the components in Figure 2.7.

Table 2.2: Summary of values used to determine the capacitance of the ultracapacitors

V_s	1V
R_1	5Ω
R_2	330Ω
R_3	5Ω

The capacitance and the series resistance were measured using the experimental set-up shown in Figure 2.7. The capacitance of the system could be determined using equation 1.7, similarly to the calculations performed to determine the specific capacitance of one nickel electrode. The series resistance could be calculated using the following equation:

$$R_S = R_C \frac{\Delta V}{V_3} \tag{2.3}$$

where R_S is the series resistance, ΔV is the change in voltage of the square wave impacted by the resistance of the system, V_1 is the voltage in Figure 2.7 and R_C is the resistance applied to the ultracapacitor, calculated using equation 2.4.

$$R_C = \left(\frac{1}{R_1} + \frac{1}{R_2} \right)^{-1} + R_3 \tag{2.4}$$

In order to determine ΔV, a square wave is applied to the ultracapacitor and the instantaneous voltage is measured. This voltage is shown in Figure 2.8.

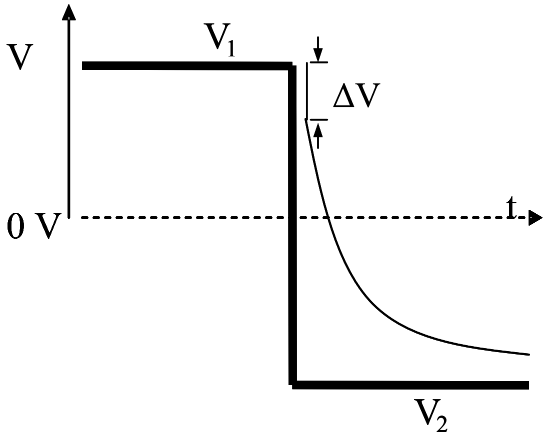

Figure 2.8: Schematic of square wave used to determine the value of ΔV

The capacitance of Sample type B was compared to the capacitance of a capacitor prepared using nickel electrode plates before the surface enhancement in order to determine if there is a significant increase in the capacitance after surface enhancement.

III. RESULTS AND DISCUSSION

III.1 Preliminary Experiments

Nickel was thermally oxidized in the presence of air at 800°C for 11 days forming nickel oxide. Figure 3.1 shows the thickness of nickel oxide formed as a function of oxidation time.

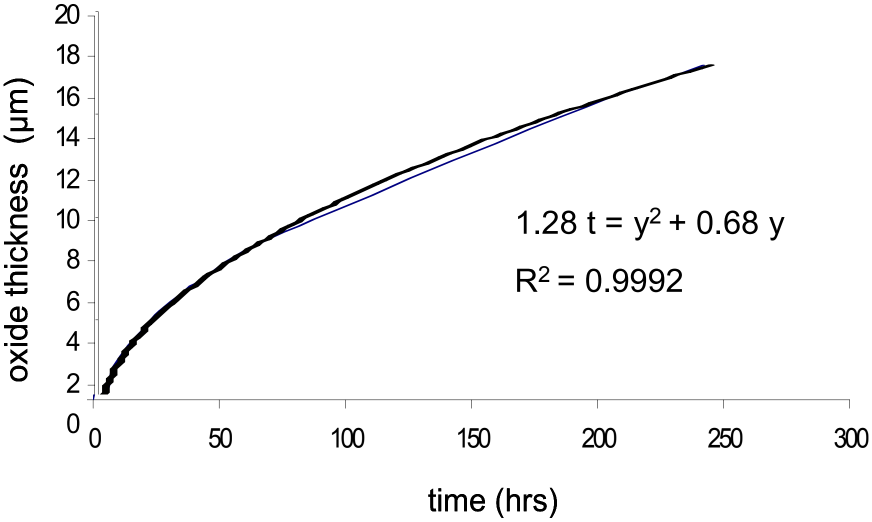

Figure 3.1: The thickness of nickel oxide as a function of time of oxidation

This figure shows that as the thickness of nickel oxide layer increases the length of the time needed to oxidize the nickel increased. Once a monolayer of the nickel oxide is formed on the nickel substrate, the diffusion of oxygen to the nickel surface becomes an issue in further oxidation. The initial mass of the nickel substrate was approximately 1.63g. The nickel sample was weighed several times in order to determine the thickness of oxide formed. The oxide thickness was calculated using equation 2.1 The trend line for Figure 3.1 is shown in equation 3.1:

$$y^2 = 0.68y - 1.28t' \qquad [3.1]$$

Equation 3.1 is similar to equation 1.12. In equation 1.12, B is an integration constant and corresponds to the thickness of the oxide when time equals zero. In this analysis, there was no nickel oxide layer initially, so B equals zero. The value of A' was -0.64. This value is one half of -1.28, the value before t'. There is an additional factor in equation 3.1, namely $0.68y$. The R^2 value for this equation was 0.9992. These two results show that the experimental data does not follow equation 1.12 exactly. This could be attributed to the sample cooling to room temperature periodically in order for weight measurements to be taken. This results in a discontinuity in the oxide layer. Therefore, in order to obtain a more accurate curve, it is necessary to weigh the sample without removing it from its heat source.

The capacitance of the counter electrode was determined by measuring the total capacitance of the two counter electrodes in series. The electrolyte used was a 2M potassium hydroxide solution. Since the capacitance of the references electrodes were assumed to be equal, equation 1.4 was used where C_1 equals C_2. The total capacitance of the counter electrodes in series equaled 3.64mF. The capacitance of each counter electrode was 7.28mF and the specific capacitance was 0.27mF/cm^2.

As seen in Figure 2.5, the counter electrodes are assembled in series with the nickel electrodes. Therefore, it is necessary that the counter electrode have a high capacitance. According to equation 1.4, if one electrode is much greater than the other electrode, the capacitive contribution of that electrode will approach zero, and consequently become insignificant in the value of total capacitance. Consequently, a value of 14.56mF should be large enough to serve as a counter electrode. The specific capacitance of the counter electrode is insignificant since the goal of this research is not to optimize the capacitance of the counter electrode. Therefore, it would be possible to make the counter electrode as large as necessary in order to measure the capacitance of the sample and the specific capacitance of each sample.

The capacitance of a nickel plate that was not surface enhanced was calculated by assembling the nickel electrode in series with the counter electrodes. Equation 1.4 was used to determine the capacitance of the nickel. In this approach, C_1 would be the value of the sum of the capacitance of the counter electrodes adding in parallel, with a total value of 14.56mF. Since the capacitance of the counter electrodes was much greater than that of nickel plate before surface enhancement, the inverse of C_1 approached zero and the equation 1.4 becomes

$$C_{tot} = C_2 \tag{3.2}$$

where C_2 is the capacitance of a nickel electrode before it is surface enhanced. The value of C_2 was estimated to be 70μF and the specific capacitance was 28μF/cm^2 since the total surface area of the sample was estimated to be 2.5cm^2. The value of 28μF/cm^2 would be comparable to the value of a commercially available capacitor. This observation indicated that a nickel capacitor was capable of storing charge and therefore it would be a viable option for using surface enhancement to produce a device for the storage of a large quantity of charge.

Sample type A was prepared by thermally oxidizing a plain nickel plate substrate for four days at 800°C. Table 3.1 summarizes the measurements that were performed in order to determine the thickness of the nickel oxide layer formed.

Table 3.1: Summary of values measured while thermally oxidizing nickel to nickel oxide

Initial mass of nickel	8.9470g
Final mass of nickel oxide	9.0545g
Change in mass of nickel oxide	0.1075g
Average area of nickel	37.5cm^2
Thickness of oxide layer formed	10.033µm

Equation 2.1 was used to calculate the thickness of the oxide layer formed. The oxidation curve shown in Figure 3.1 was used to determine the length of the time needed for the oxidation process. At a time of 100 hours, the oxide thickness shown in Figure 3.1 is approximately 10µm. This value is actually less than the actual thickness of the oxide layer formed on the nickel substrate. As stated, Figure 3.1 was obtained by weighing the nickel oxide periodically throughout the thermal oxidation process. Consequently, the sample was cooled to ambient temperature for each measurement. Therefore, when the nickel substrate was returned to the furnace, the sample had to be reheated to 800^{o}C. Thus, the actual thickness of the oxide layer would be less than the thickness would be if the substrate was heated continuously.

Sample types B and C were screen printed and the thickness was measured using a laser profilometer. Table 3.2 summarizes the thicknesses of sample types B and C.

Table 3.2: Nickel oxide paste thicknesses of sample type B and C

Sample	B		C	
	Top	Bottom	Top	bottom
thickness, µm	27.46	14.63	24.23	17.38
	16.80	12.39	18.22	27.49
	13.01	18.66	36.65	30.41
Average	19.09	15.23	26.37	25.09
avg, both sides	17.16µm		25.73µm	

Three separate measurements were carried out for both the top and bottom sides of the samples. The values reported in Table 3.2 were averaged values of both sides of the sample. Sample types B and C had an average thickness of 17.16μm and 25.73μm respectively. The thicknesses of the pasted samples are on the same order of magnitude as Sample type A and would serve as a method of comparison of the best method for the preparation of the surface enhanced nickel electrodes.

Figures 3.2-3.4 show the cross section of the SEM images of Sample types A, B and C before thermal reduction using methane. SEM analysis was performed in order to compare the morphology of samples before and after oxidation.

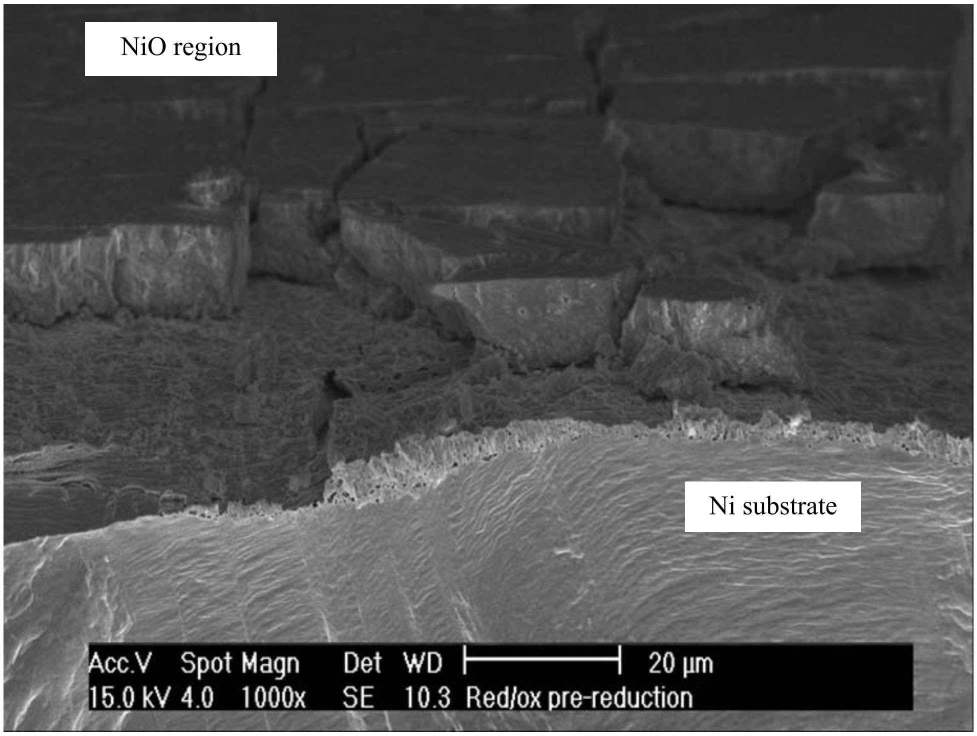

Figure 3.2: SEM cross section of Sample type A before thermal reduction

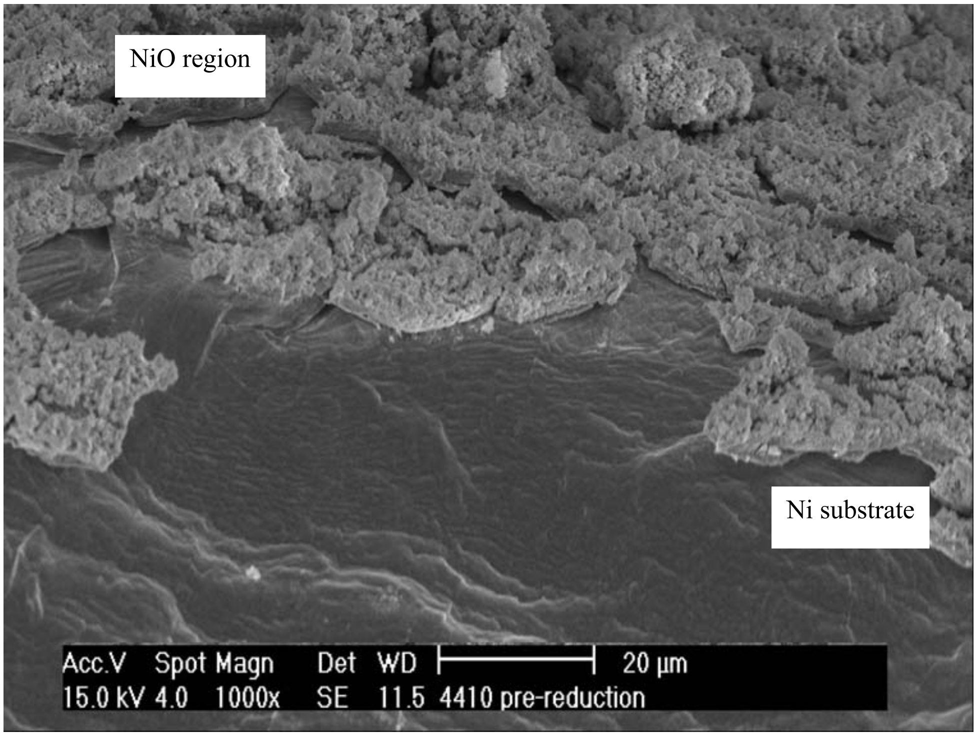

Figure 3.3: SEM cross section of Sample type B before thermal reduction

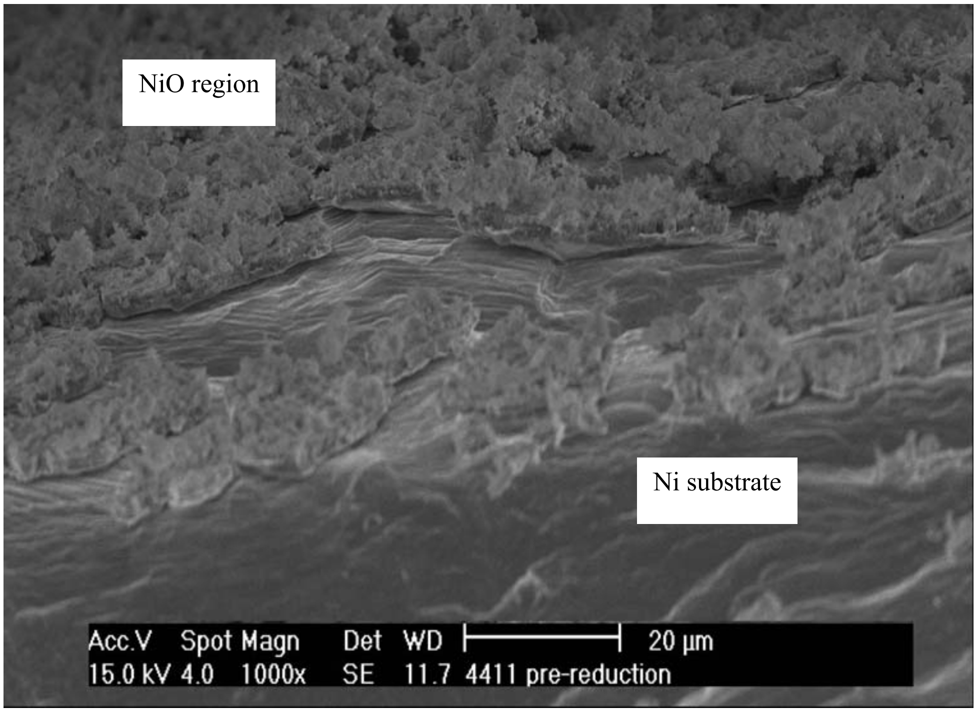

Figure 3.4: SEM cross section of Sample type C before thermal reduction

The three figures show that the interface occurred between the nickel and the nickel oxide. In each figure, the top region is the nickel oxide region and the bottom region is the nickel substrate. The preparation of the cross section for the SEM resulted in damage to the nickel oxide layer, however the different morphologies of the different regions of each sample is visible in Figures 3.2-3.4. It is important to recognize the differences between the nickel oxide layer in Figure 3.2 compared to those in Figures 3.3 and 3.4. The surfaces in Figures 3.3 and 3.4 are rougher than that in Figure 3.2. This would be the result of the method of preparation. When the nickel is thermally oxidized, the oxidation of the nickel would be uniform. Consequently, the surface morphology would be uniform. This would not be the case in the thick film screen printing, especially on the microscopic scale. The differences in the thickness of the samples can also be observed in Table 3.2.

In addition to SEM, the compositions of each region of the testing samples were confirmed qualitatively using EDX to analyze both the top nickel substrate and bottom nickel oxide regions of each sample. The EDX results are shown in Figures 3.5-3.10.

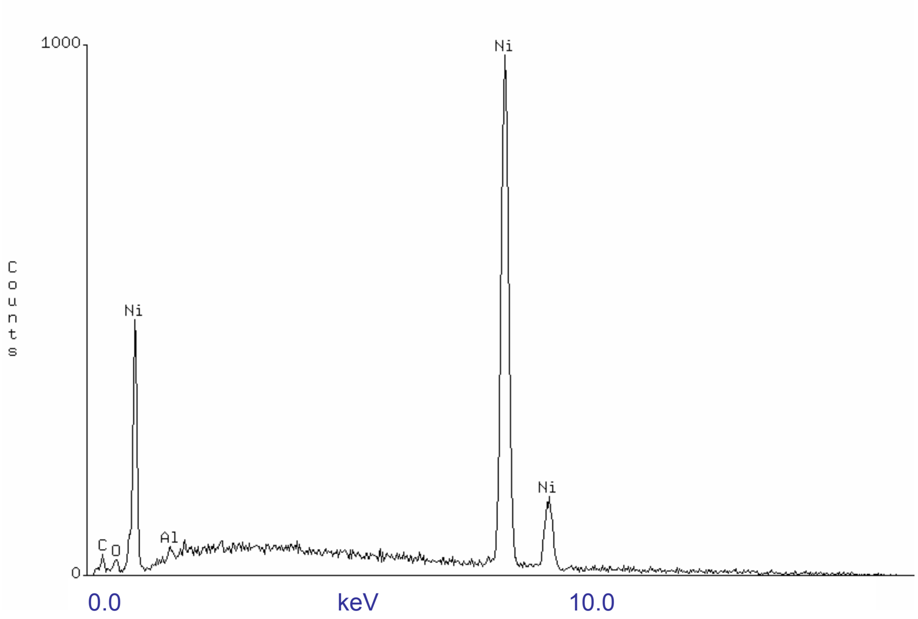

Figure 3.5: EDX of the nickel substrate region of
Sample type A before reduction

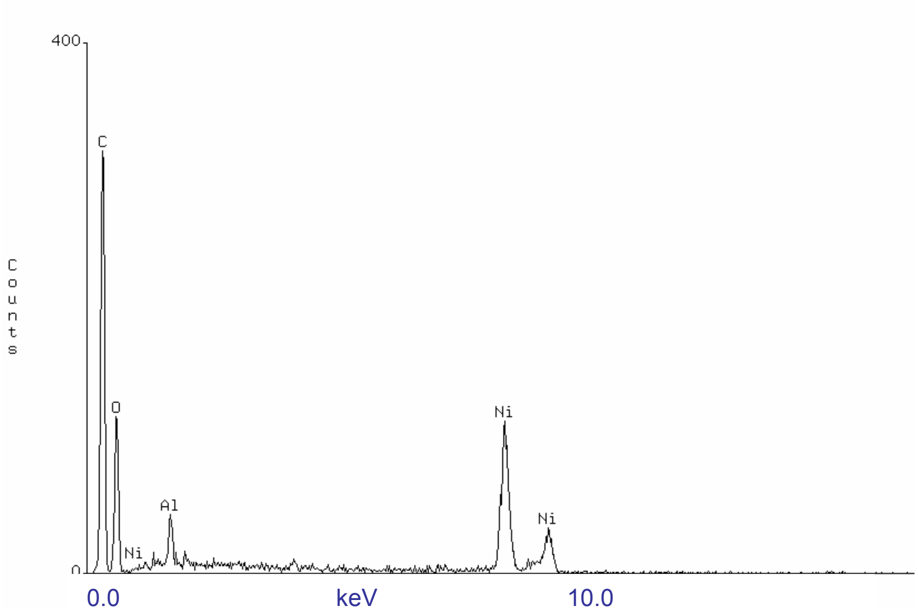

Figure 3.6: EDX of the nickel oxide region of
Sample type A before reduction

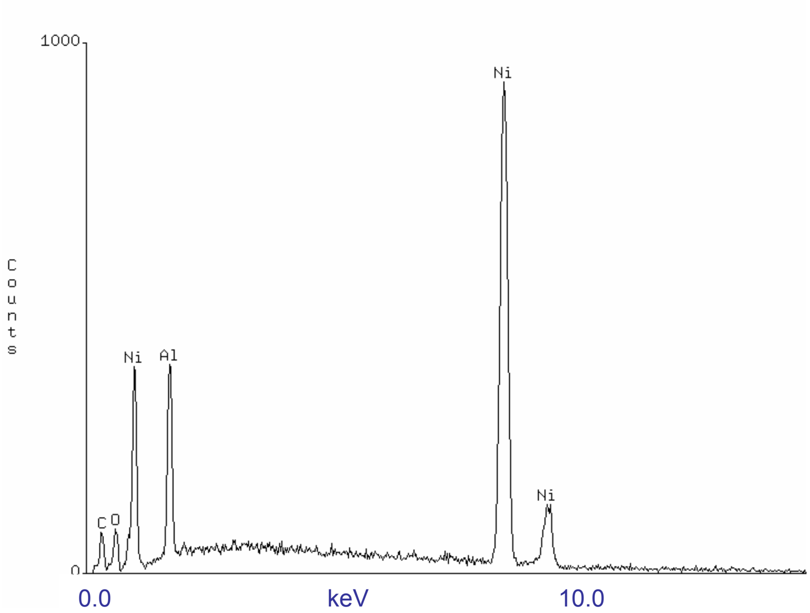

Figure 3.7: EDX of the nickel substrate region of Sample type B before reduction

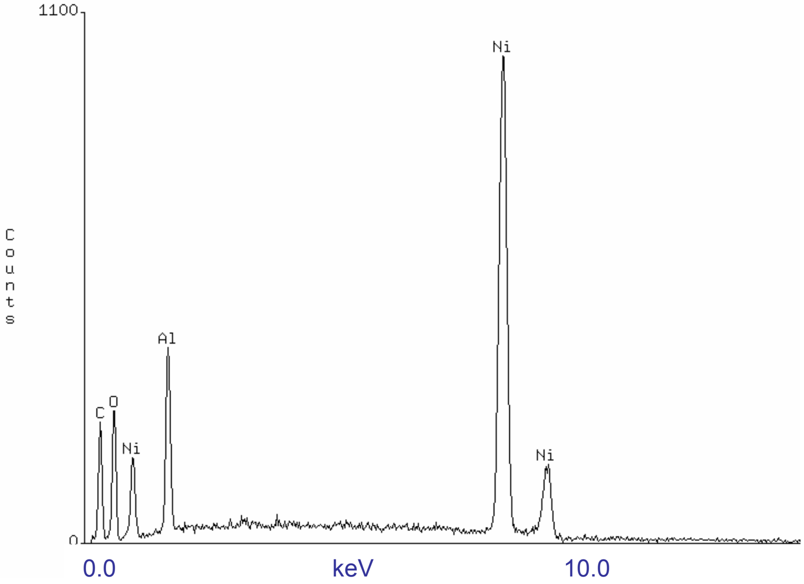

Figure 3.8: EDX of the nickel oxide region of Sample type B before reduction

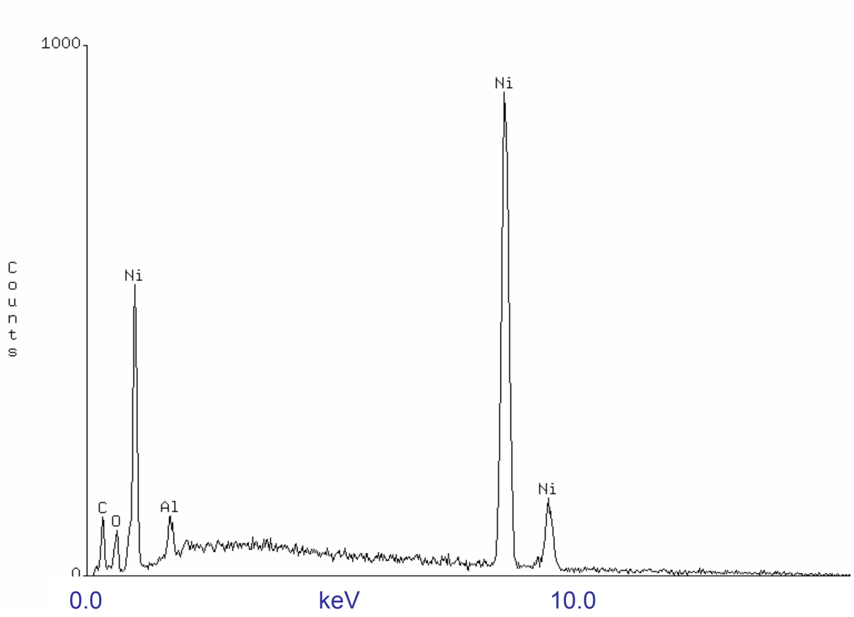

Figure 3.9: EDX of the nickel substrate region of
Sample type C before reduction

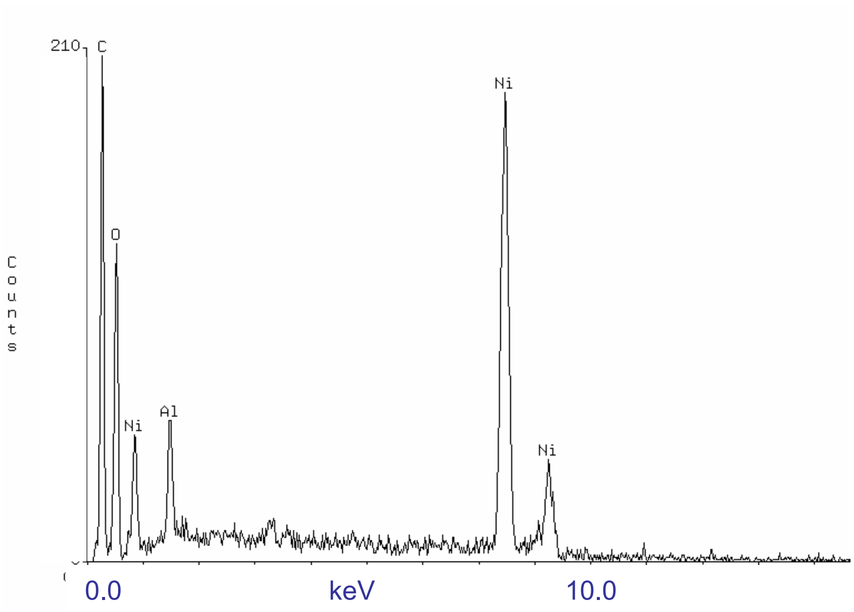

Figure 3.10: EDX of the nickel oxide region of
Sample type C before reduction

The EDX analysis was performed by analyzing several segments in both the nickel oxide region and the nickel substrate region. Figures 3.5, 3.7 and 3.9 are the EDX analysis of the nickel substrate of the testing samples, Sample types A, B and C, respectively. In general, the presence of the oxygen peak was smaller in these figures since only the surface was oxidized. The presence of oxygen would be unavoidable, however, due to the oxidation that occurs when nickel was in the presence of air, even at room temperature. The presence of carbon peaks was also unavoidable in both the nickel substrate and the nickel oxide regions once the sample was exposed to air. In addition to carbon, oxygen and nickel, there were also aluminum peaks presented. This could be attributed to the impurities present in the nickel substrate. Since aluminum was conductive, its presence would not impact the behavior of the electrode and it was not of concern.

Figures 3.6, 3.8 and 3.10 show the EDX analysis of Sample types A, B and C, respectively, before reduction in the nickel oxide region of each sample, as anticipated. In addition to the presence of carbon, nickel and aluminum, there was also a better defined oxygen peak. Due to the presence of a much larger oxygen peak, it could be determined that the presence of oxygen was much greater in the nickel oxide region as opposed to the nickel substrate region.

Figures 3.11-3.13 show the XRD analysis performed on Sample types A,B and C before thermal reduction using methane gas.

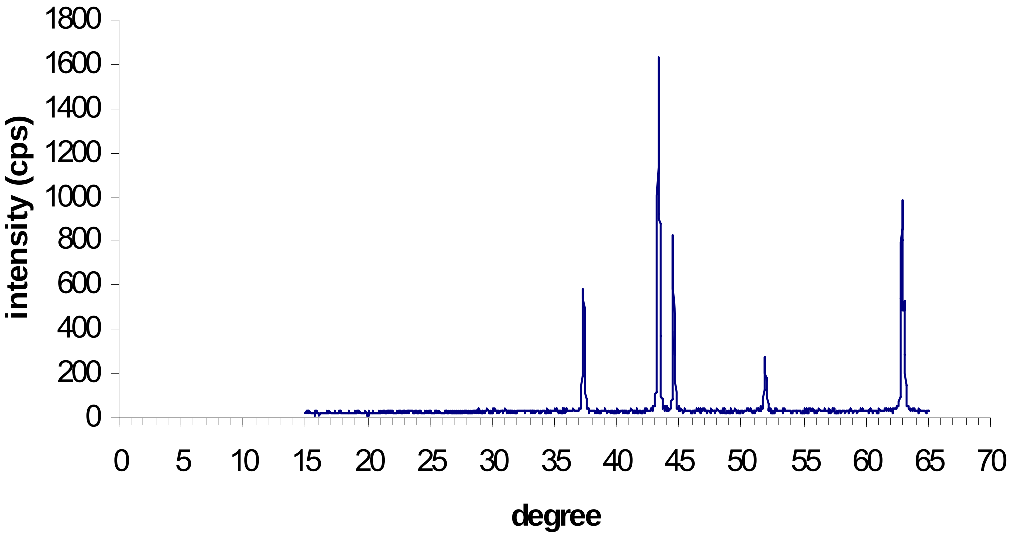

Figure 3.11 XRD results of Sample type A before reduction

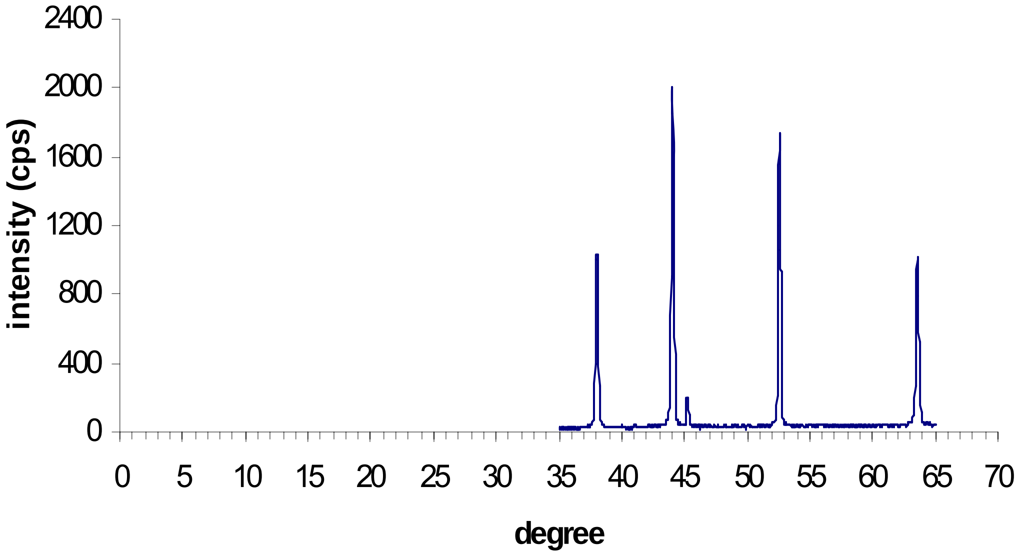

Figure 3.12: XRD results of Sample type B before reduction

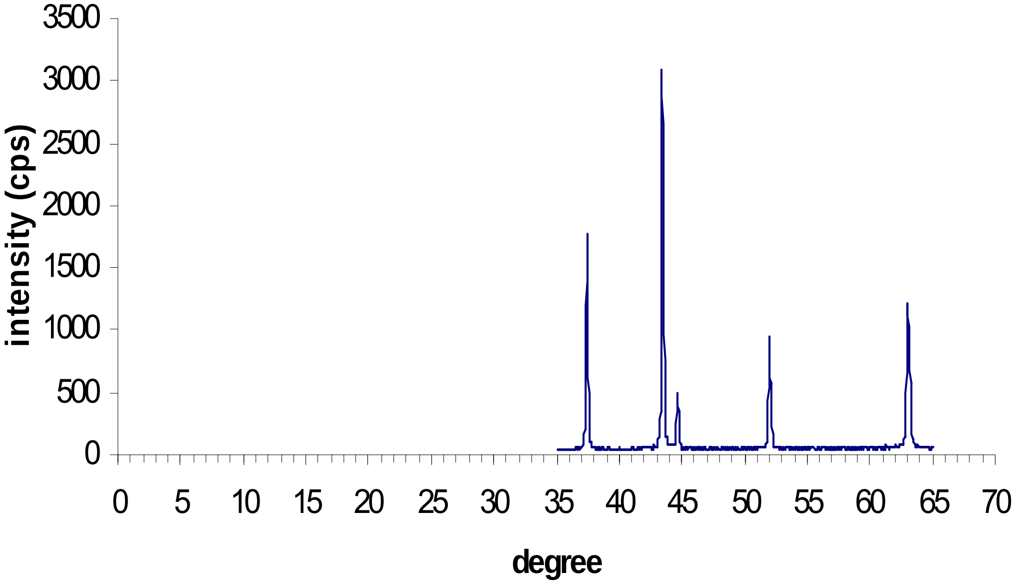

Figure 3.13: XRD results of Sample type C before reduction

The thickness of the nickel oxide layer of the three sample types were 10µm or greater and the XRD results showed only the composition of the nickel oxide layer of the samples. Figures 3.11-3.13 all show peaks at 44.5 and 51.9 degrees. These two peaks are indicative of the presence of nickel. More importantly, there are also three peaks at 37.3, 43.3 and 62.0 degrees. These peaks are indicative of nickel II oxide, or a one to one ratio of nickel to oxygen. The nickel oxide peaks have a higher intensity than the nickel peaks since the presence of nickel oxide is more dominant. While the EDX results show that selected regions of the electrodes are composed of nickel oxide, the XRD results show that the overall surface of the sample is composed of nickel oxide.[21]

The testing samples were further analyzed using SEM, EDX and XRD after thermal reduction of the nickel oxide forming the porous nickel. These results were compared to the results obtained before the nickel oxide reduction in order to determine if the reduction of the nickel oxide was feasible and the enhancement of the surface modification in the nickel was successful. Figures 3.14-3.16 show the SEM images of Samples A, B and C reduced for 3 hours at 700^{o}C, respectively.

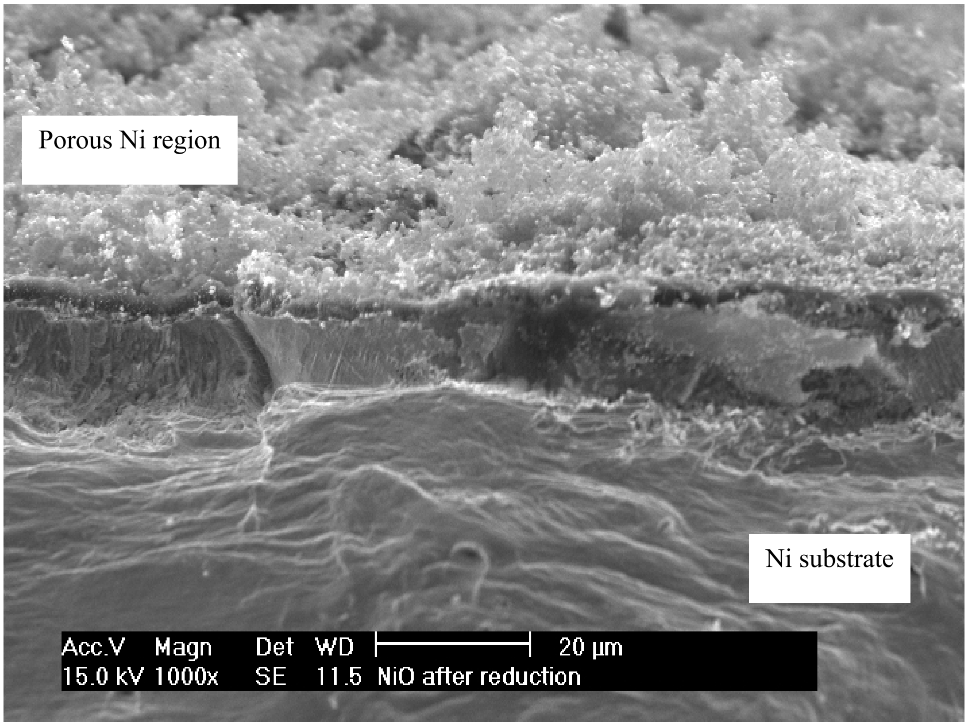

Figure 3.14: SEM cross section of Sample type A after thermal reduction at 700^{o}C for 3 hours in methane

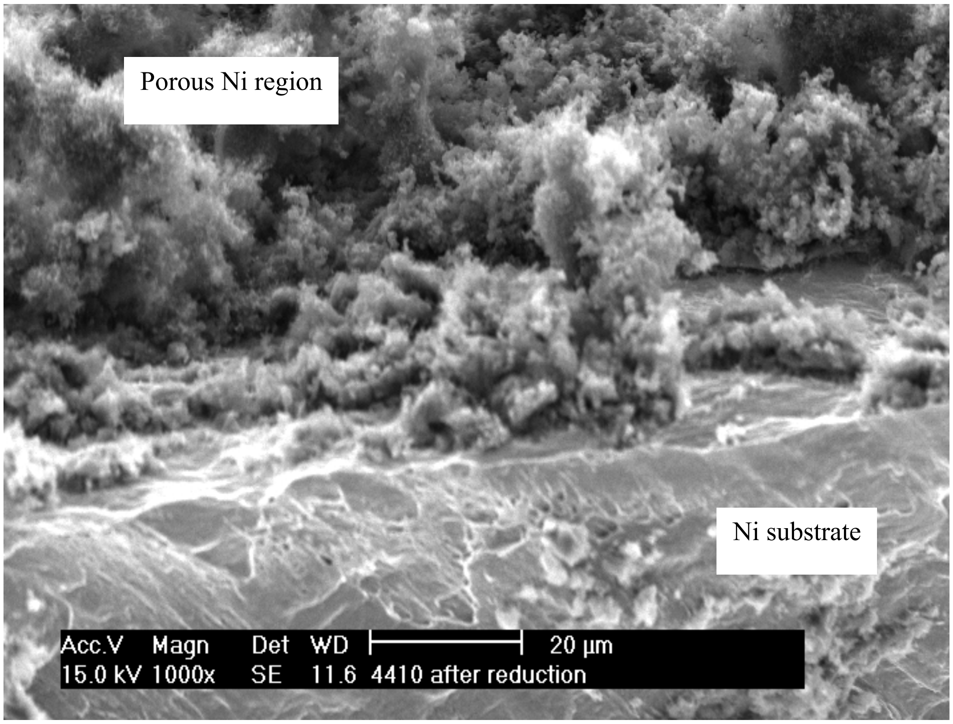

Figure 3.15: SEM cross section of Sample type B after thermal reduction at 700^{o}C for 3 hours in methane

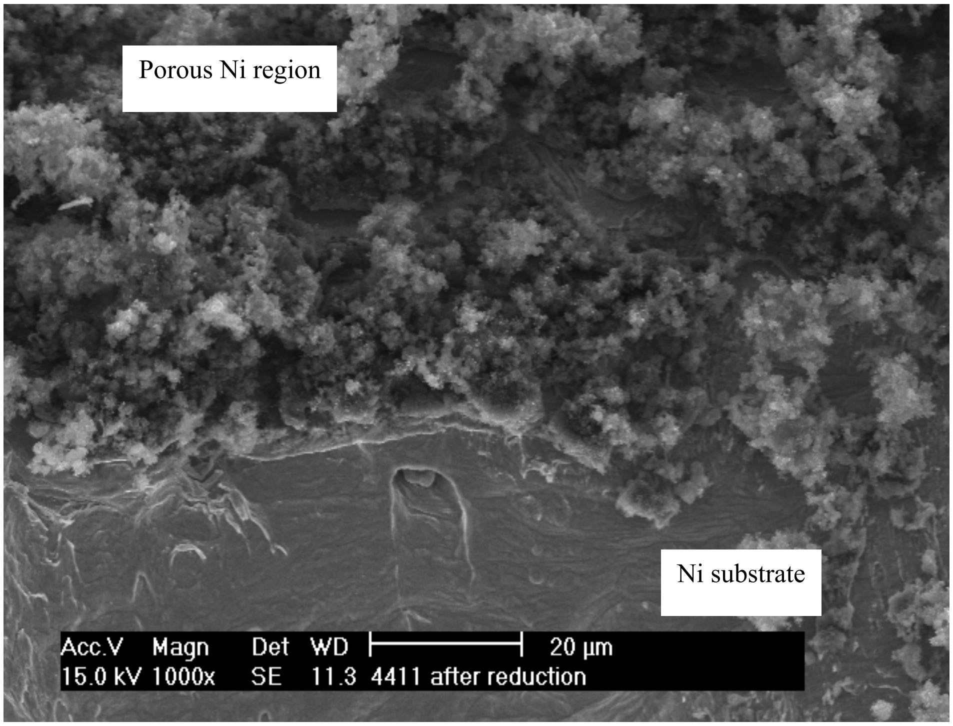

Figure 3.16: SEM cross section of Sample type C after thermal reduction at 700^{o}C for 3 hours in methane

Figures 3.14-3.16 show the nickel electrodes after the samples were reduced at 700°C in methane for three hours. The top regions of the samples were the porous nickel region and the bottom regions were the nickel substrate of Samples A, B and C, respectively. These figures indicated a significant amount of surface enhancement compared to the results shown in Figures 3.2-3.4. This surface enhancement can be attributed to the reduction of the oxide layer creating a rough, highly porous surface of the nickel layer. This increase in the surface area of this nickel layer would be highly desirable for an ultracapacitor.

Figures 3.17-3.22 show the EDX analysis of Samples A, B and C after reduction for 3hrs in methane at 700°C, respectively.

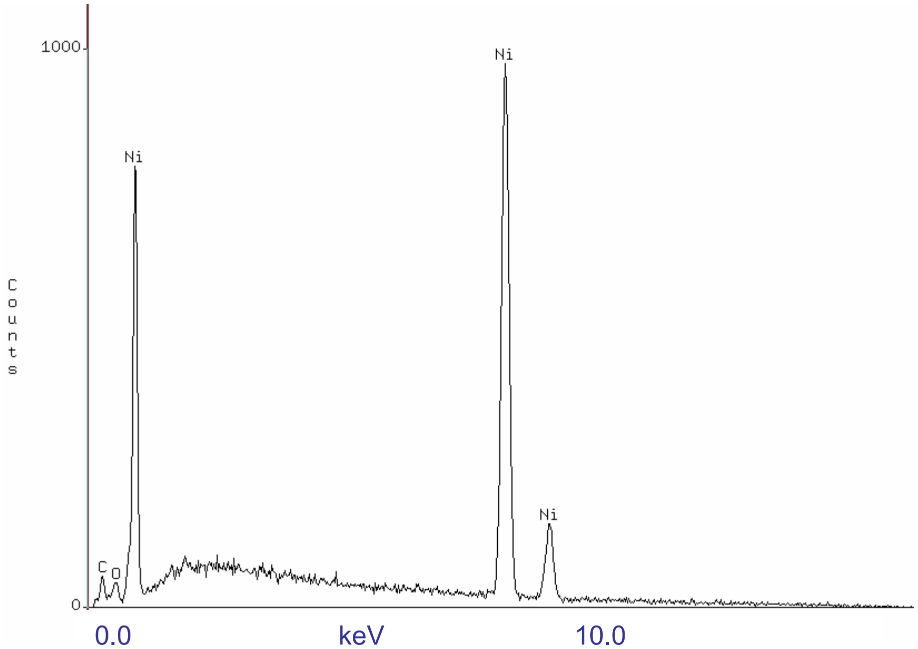

Figure 3.17: EDX of the substrate region of Sample type A after thermal reduction at 700°C for 3 hours in methane

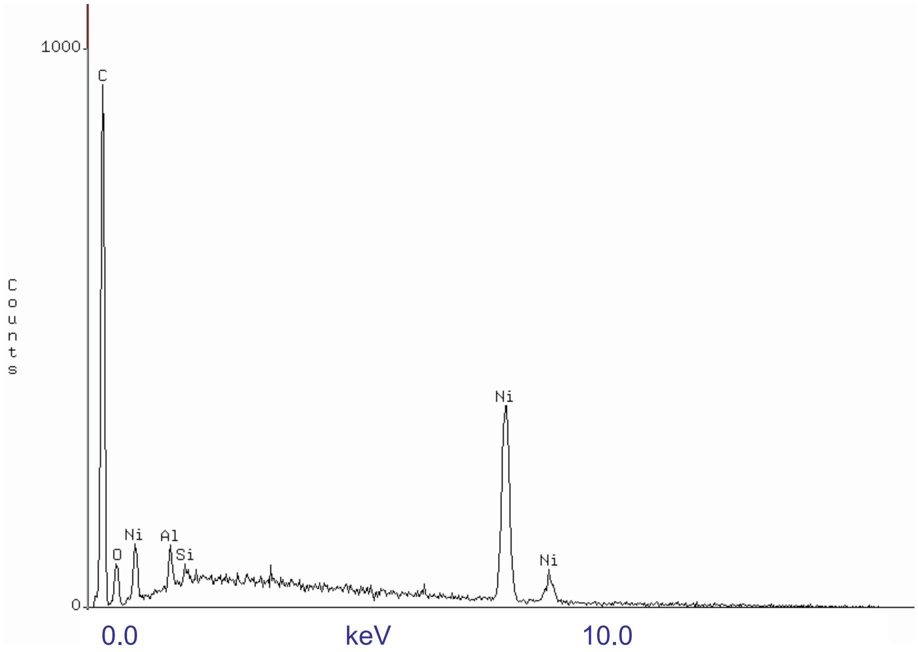

Figure 3.18: EDX of the porous nickel region of Sample type A after thermal reduction at 700°C for 3 hours in methane

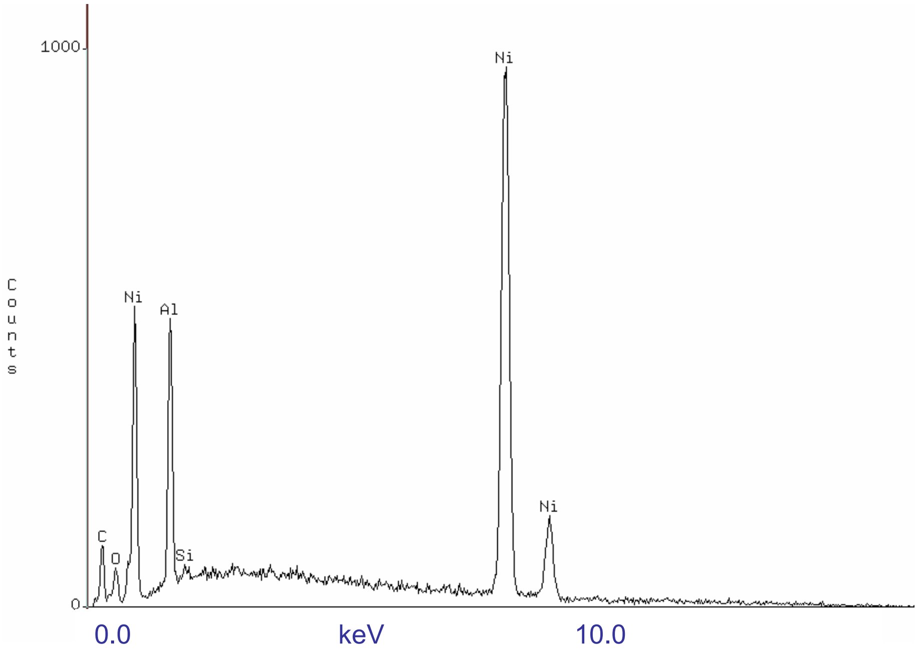

Figure 3.19: EDX of the nickel substrate region of Sample type B after thermal reduction at 700°C for 3 hours in methane

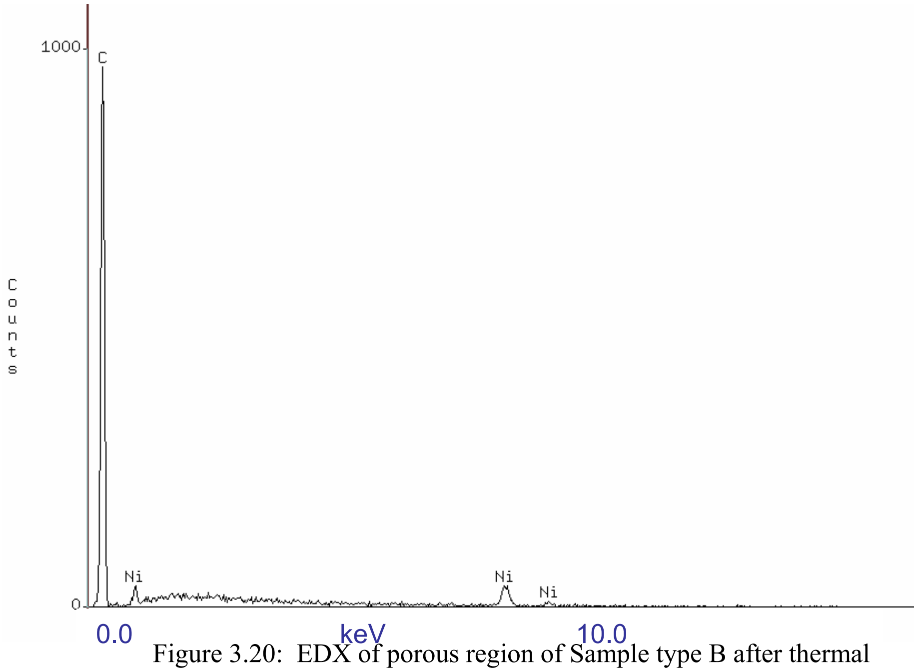

Figure 3.20: EDX of porous region of Sample type B after thermal reduction at 700°C for 3 hours in methane

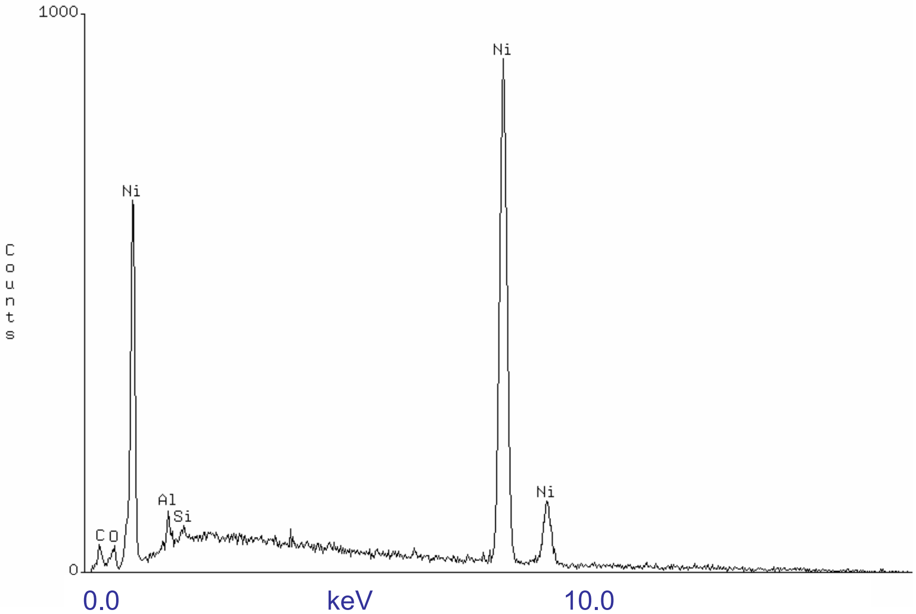

Figure 3.21: EDX of the nickel substrate region of Sample type C after thermal reduction at 700°C for 3 hours in methane

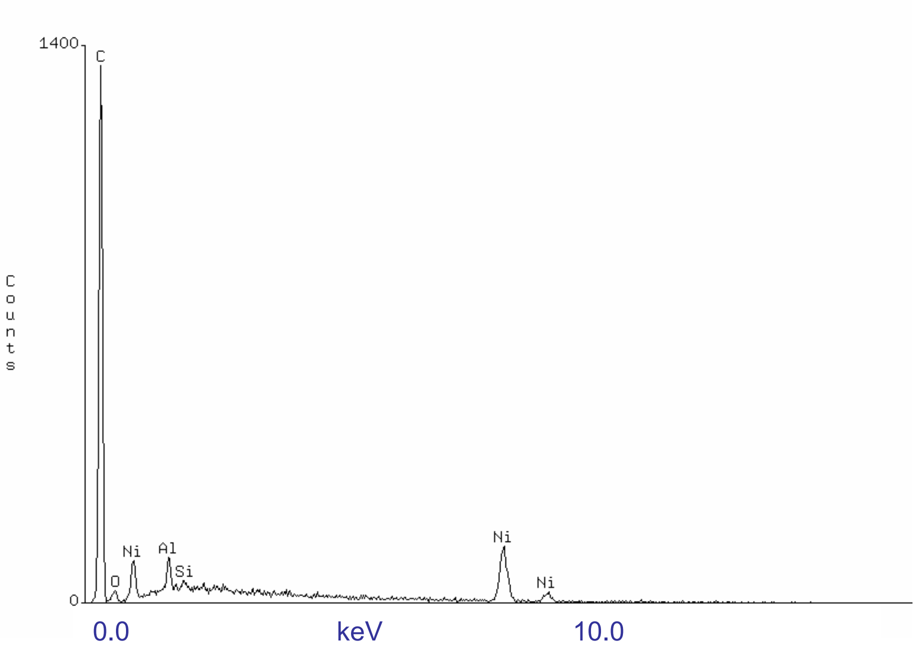

Figure 3.22: EDX of the porous nickel region of Sample type C after thermal reduction at 700°C for 3 hours in methane

Figures 3.17, 3.19 and 3.21 show the EDX results of the nickel substrate of Sample types A, B and C, respectively. These figures should be similar to Figures 3.5, 3.7 and 3.9, since those figures also show the nickel substrate regions of Sample types A, B and C, respectively. With the exception of the silicon peaks in Figures 3.19 and 3.21, this is the case. Like carbon and oxygen, silicon peaks could be present simply from exposing a sample to air, and is therefore not a concern. Comparing Figures 3.17, 3.19 and 3.21 to Figures 3.5, 3.7 and 3.9 shows that in the thermal reduction process of the nickel oxide to form the porous nickel, the substrate region is not impacted. This is to be expected since heating a nickel substrate in the presence of methane gas should not impact the composition of the nickel substrate region.

Figures 3.18, 3.20 and 3.22 show the EDX results of the porous nickel region of Sample types A, B and C. In these figures, the carbon peak was the most dominant peak. This was due to the residual carbon left behind after the reduction process using methane as the reducing agent. Equations 3.3-3.5 show the possible combustion reactions which may take place between the nickel oxide and the methane gas at elevated temperatures.

$$CH_4 + 4\ NiO \xrightarrow{\Delta} CO_2 + 4\ Ni + 2\ H_2O \qquad [3.3]$$

$$CH_4 + 3\ NiO \xrightarrow{\Delta} CO + 3\ Ni + 2\ H_2O \qquad [3.4]$$

$$CH_4 + 2\ NiO \xrightarrow{\Delta} C + 2\ Ni + 2\ H_2O \qquad [3.5]$$

These three equations suggest that in the combustion of methane and nickel oxide would yield water and nickel, which might be porous. Furthermore, three possible carbon compounds could be produced. These compounds might be carbon dioxide, carbon monoxide and carbon, as shown in the above equations. Complete combustion would result in the production of only carbon dioxide. Since combustion was typically incomplete, the other two carbon compounds, carbon monoxide and carbon also formed. Carbon dioxide, carbon monoxide and the water vapor were all purged from the system in the exhaust out of the quartz tube in the experiment, however the carbon was left behind in the matrix of the porous nickel electrode. The size of the carbon particles left in the porous nickel structure would depend on the reduction conditions. In the experiments, lower temperatures resulted in a much finer residual carbon than at higher temperatures.

Figures 3.23-2.25 show the XRD analysis of the samples after reduction for 3hrs in methane at 700^{o}C.

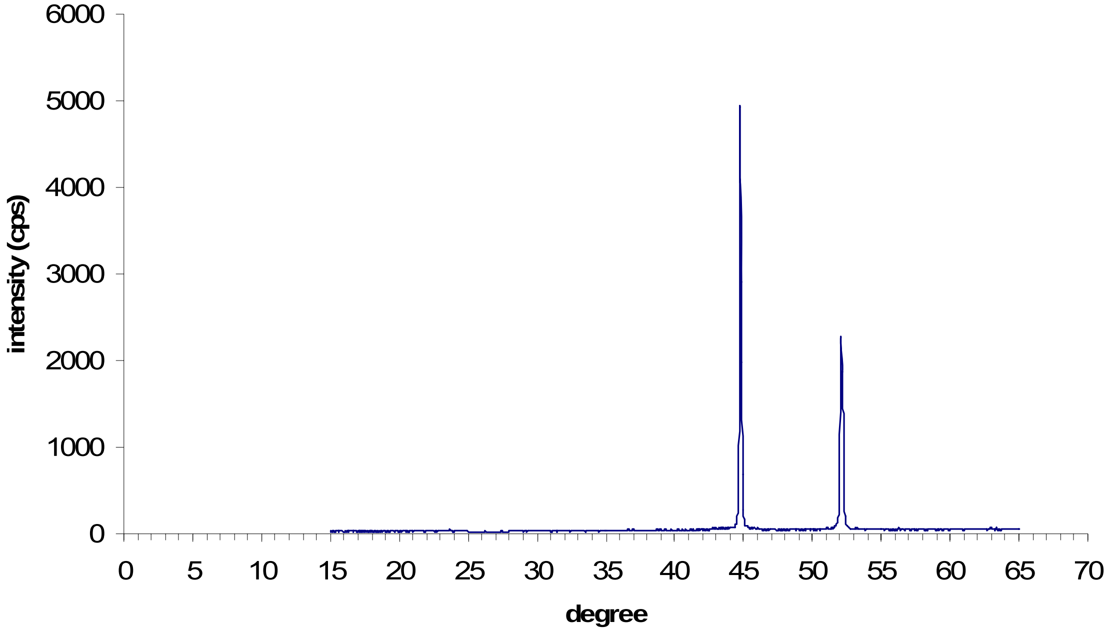

Figure 3.23: XRD results of Sample type A after thermal reduction of nickel oxide at 700°C for 3 hours in methane

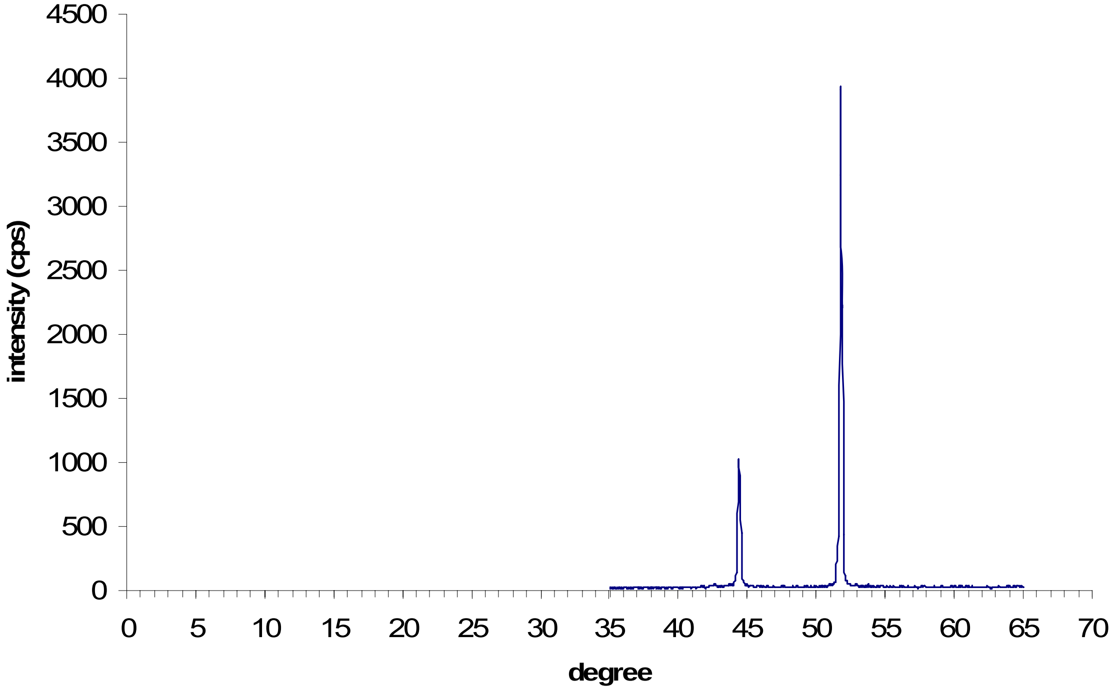

Figure 3.24: XRD results of Sample type B after thermal reduction of nickel oxide at 700°C for 3 hours in methane

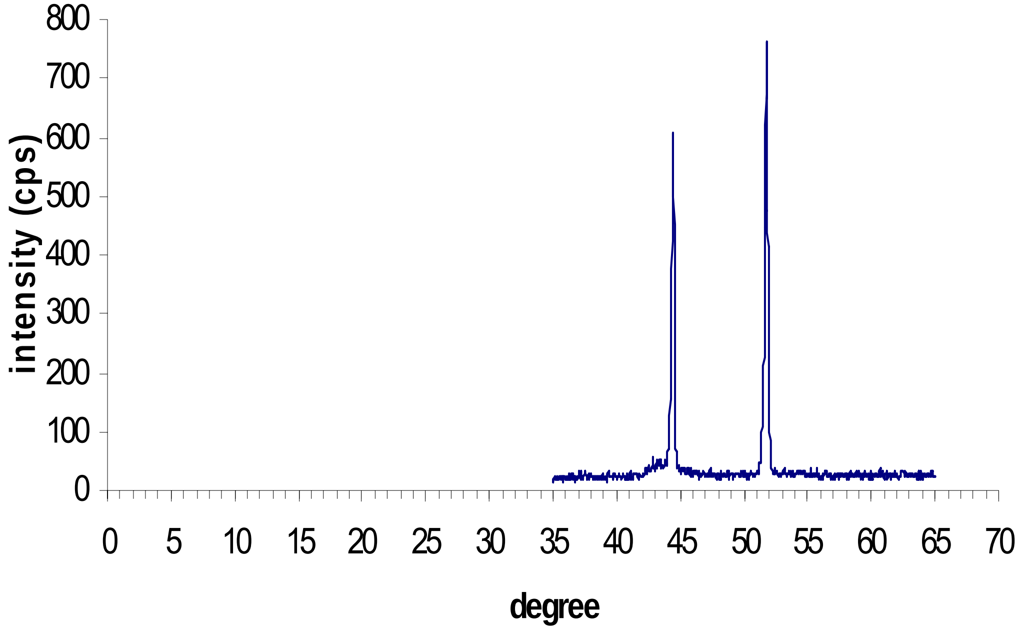

Figure 3.25: XRD results of Sample type C after thermal reduction of nickel oxide at 700°C for 3 hours in methane

XRD was used to analyze the composition of the nickel electrodes after they were thermally reduced at 700°C in the presence of methane gas. After the thermal reduction, the composition of these samples should be only nickel. All of the oxygen in the samples should be removed in the reduction process. Figures 3.23-3.25 show peaks at only 44.5 and 51.9 degrees. These peaks correspond to nickel. Therefore, with these results, it can be concluded that the oxygen was removed from the surface of the surface enhanced electrodes after thermal reduction.

III.2 Capacitance Measurements

Sample types A, B and C were reduced for 24 hours in methane gas at various temperatures ranging from 700°C-1000°C. The capacitances of these samples were measured in series using a counter electrode and a 2M potassium hydroxide electrolyte.

A function generator and an oscilloscope were used to determine the time that it took to charge the electrode at a constant resistance. Equation 1.7 was used to calculate the capacitance of the electrode. The specific capacitance was determined by dividing the capacitance by the area of the electrode. Since not all of the samples were the same size, this served as a method of uniformly comparing all of the electrodes that were tested. Figure 3.26 shows the specific capacitances of the electrodes as a function of the reduction temperature of the electrode.

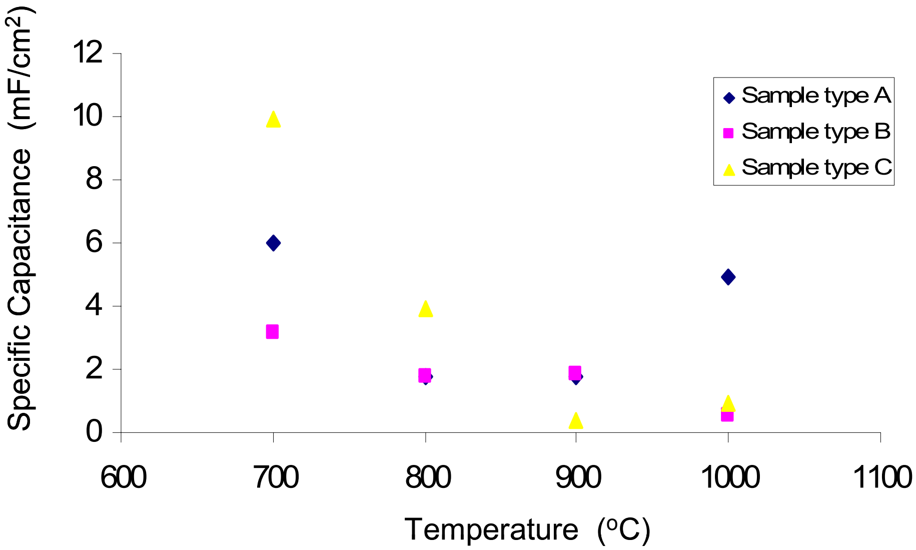

Figure 3.26: Specific capacitance versus temperature of samples reduced for 24 hours with a 2M KOH electrolyte

Figure 3.26 shows a significant increase in specific capacitance compared to a sheet of nickel before surface enhancement. This figure shows that the highest specific capacitance for a nickel electrode in 2M potassium hydroxide is 9.90mF/cm^2. The surface enhanced nickel electrode was 350 times greater than that of a plain nickel plate. This can be determined using equation 1.1. The dielectric coefficient of the electrolyte, the permittivity in a vacuum and the distance between the electrodes were held constant when determining the specific capacitance of the surface enhanced nickel and the nickel plate before surface enhancement. Therefore, equation 1.1 could be modified to equation 3.6:

$$A_2 = A_1 \frac{C_2}{C_1} \qquad [3.6]$$

where C_1 and A_1 are the capacitance of the capacitance and area of the nickel electrode before surface enhancement, respectively. The value of C_2 is the capacitance of the electrode after thermal reduction and A_2 is the area of the surface enhanced nickel electrode. Using this equation, the surface area of the surface enhanced nickel sample was estimated to be 875cm^2.

In general, the results indicated that the higher reduction temperatures result in lower specific capacitances. It was feasible that at a higher temperature of reduction, the oxygen was evacuated from the pores more rapidly, and consequently, the pores that formed were larger. Figures 3.27-3.38 show cross section SEM images of the electrodes of Sample types A, B and C at the different temperatures, respectively. There was inconsistency observed in the experimental results. The inconsistency could be attributed to the residual carbon left on the sample after the thermal reduction. The carbon particles were not well adhered to the surface of the sample, and consequently, the quantity of carbon remaining on the sample would affect the specific capacitance of the testing sample. In general, the lower reduction temperatures resulted in a finer residual carbon powder while the higher reduction temperatures resulted in a thick, flaky carbon powder. This assessment could be substantiated for the experimental results showing that the higher reducing temperature led to a lower specific capacitance. The flaky residual carbon was also not well packed in the pores of the enhanced nickel layer at the higher reduction temperatures.

Figure 3.26 also shows that there is no consistency in which preparation method results in the best specific capacitance. At temperatures of 700°C and 800°C, Sample type C performed best while at 900°C, Sample type B performed the best at Sample type A performed the best at 1000°C. While all of the samples performed comparably, it should be noted that the thickness of the oxide layer before reduction was less in the case of Sample type A than Sample types B and C. Therefore, it is possible that preparing a surface enhanced nickel electrode using a thermal oxidation and reduction procedure could result in a higher specific capacitance than the other preparation methods if the thicknesses of the oxide layer before reduction were equal.

While the quantitative assessment of the enhanced nickel layer could be affected by the presence of the carbon particles, it would be clear that the surface enhancement of the nickel layer improved the specific capacitance compared to that of a plain nickel substrate. Even in the instance of the lowest specific capacitance shown in Figure 3.26, the surface enhancement was still fifteen times greater than that of a plain nickel substrate. Therefore, regardless of the inconsistent results, qualitatively, this experiment showed that thermally reducing nickel in the presence of methane gas is a viable option as a method of creating a high charge storing ultracapacitor. The affect of the surface enhancement can be seen in Figures 3.27-3.38. All of the samples were reduced for 24hrs in methane. The cross sections were taken at 6500x magnification.

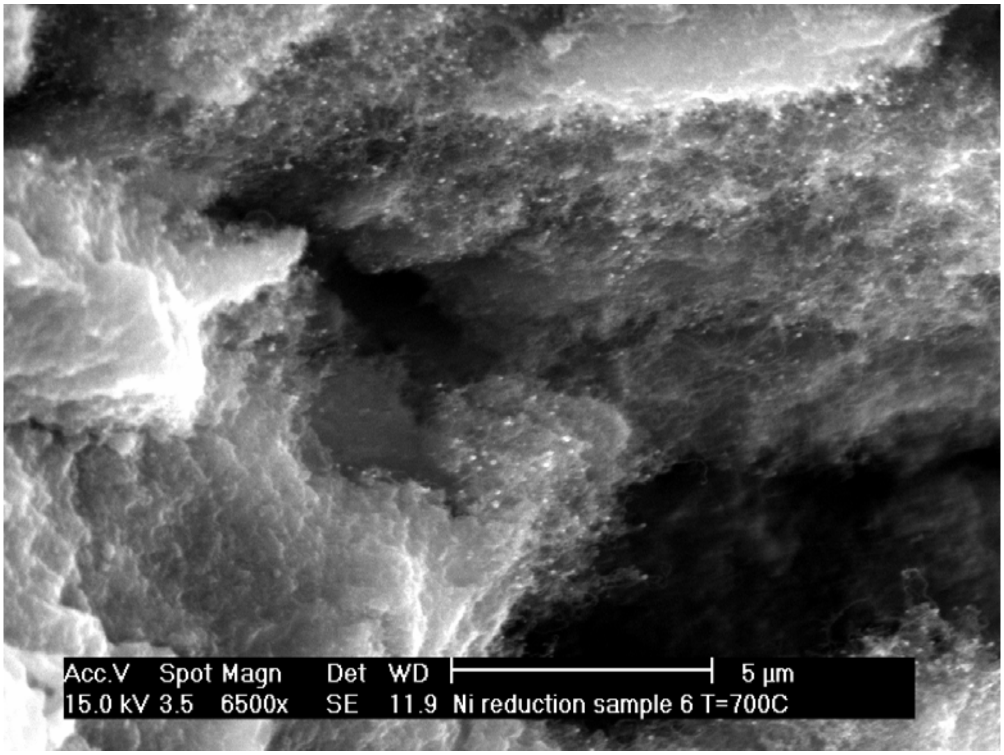

Figure 3.27: SEM cross section of porous Ni region after thermal reduction of Sample type A, T=700°C

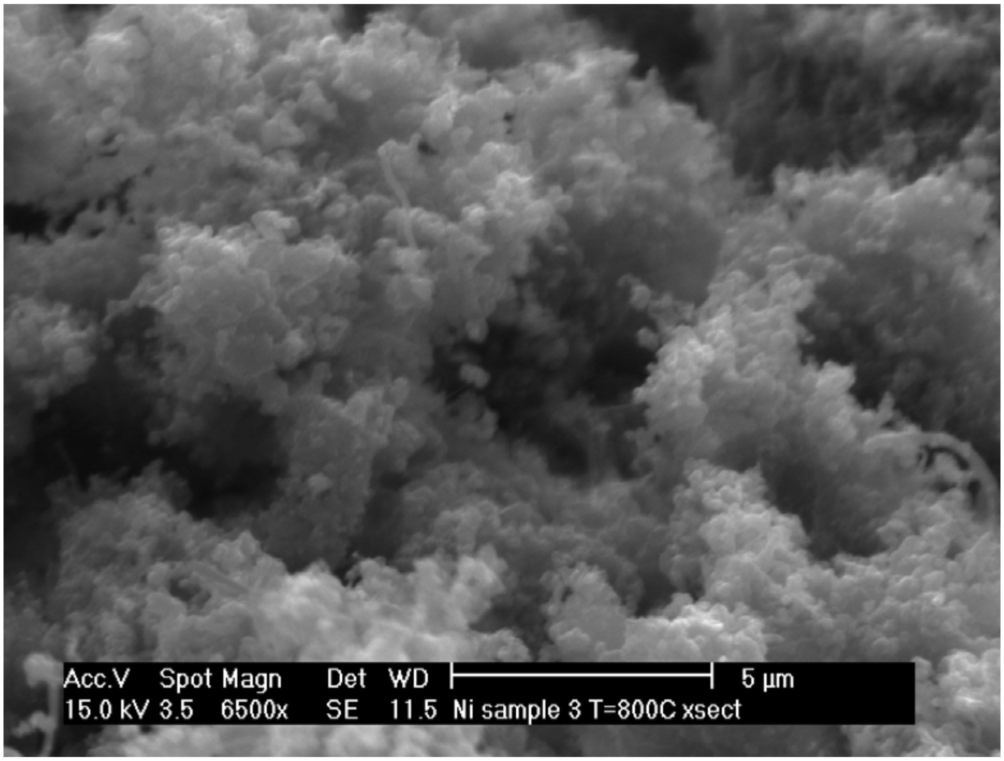

Figure 3.28: SEM cross section of porous Ni region after thermal reduction of Sample type A, T=800°C

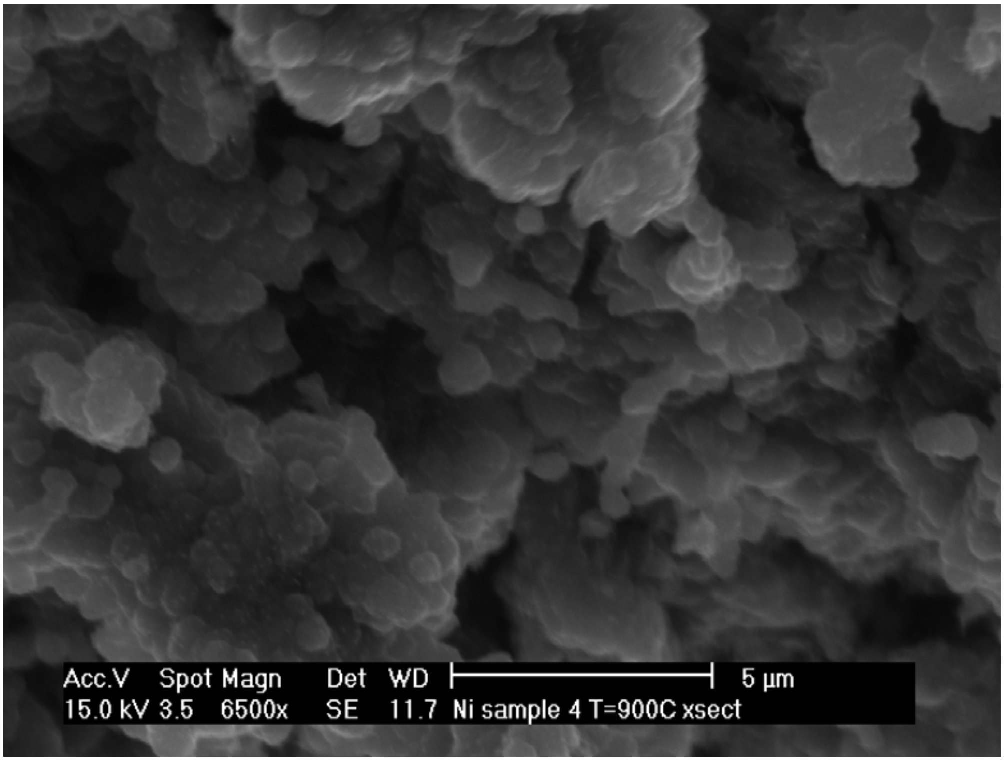

Figure 3.29: SEM cross section of porous Ni region after thermal reduction of Sample type B, T=900^oC

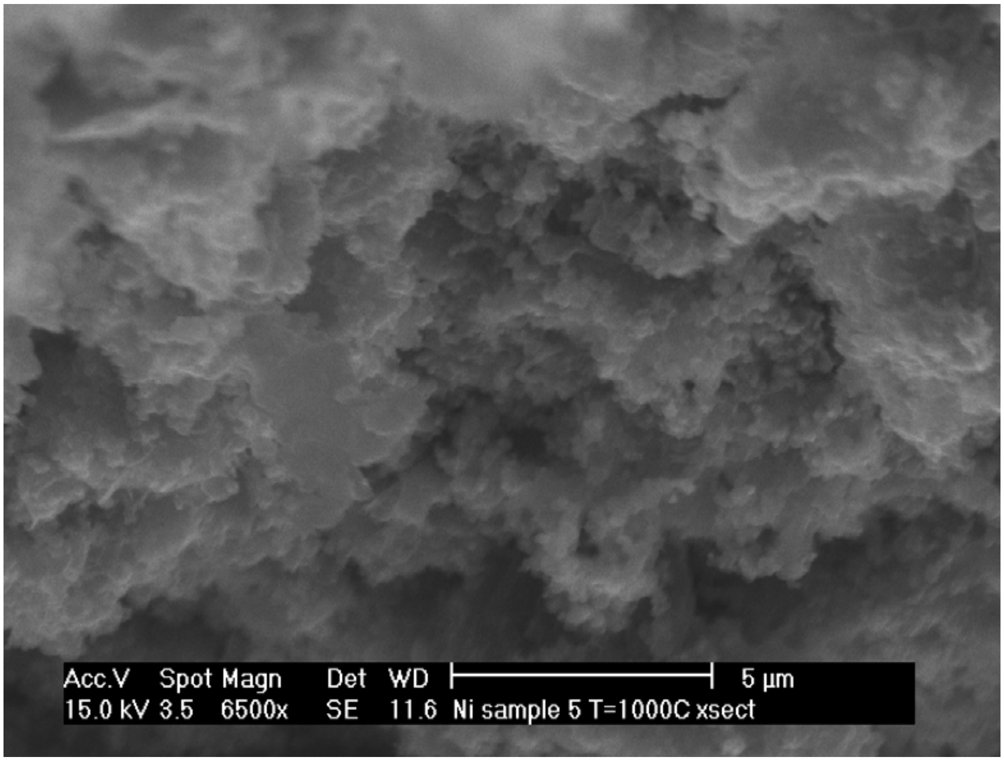

Figure 3.30: SEM cross section of porous Ni region after thermal reduction of Sample type A, T=1000^oC

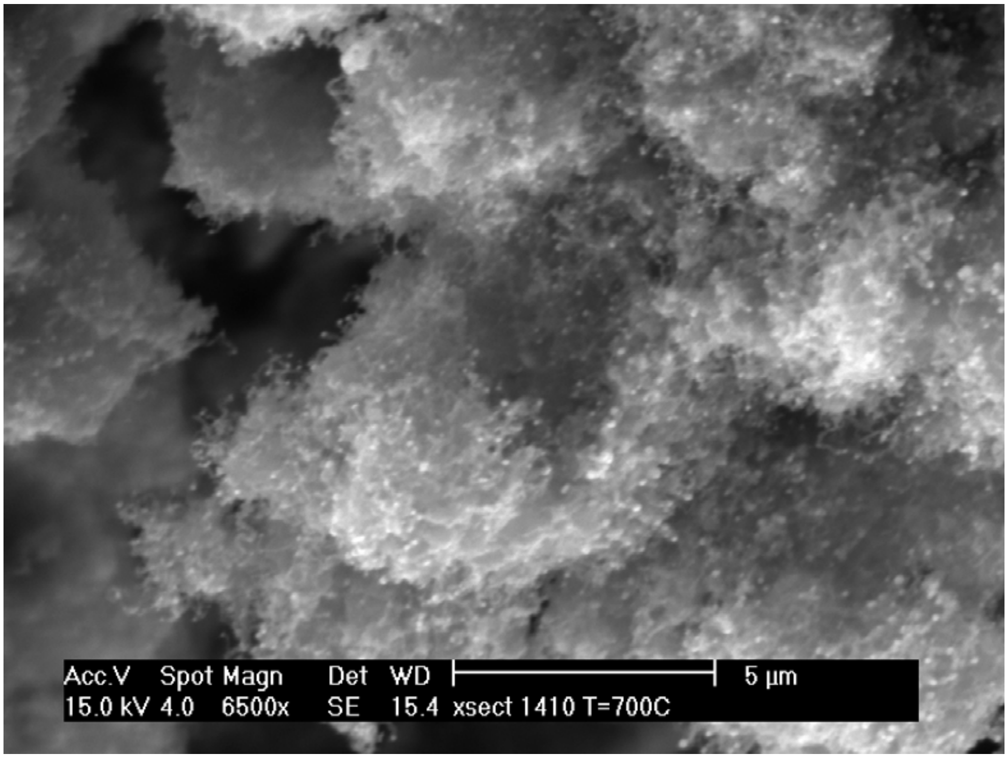

Figure 3.31: SEM cross section of porous Ni region after thermal reduction of Sample type B, T=700°C

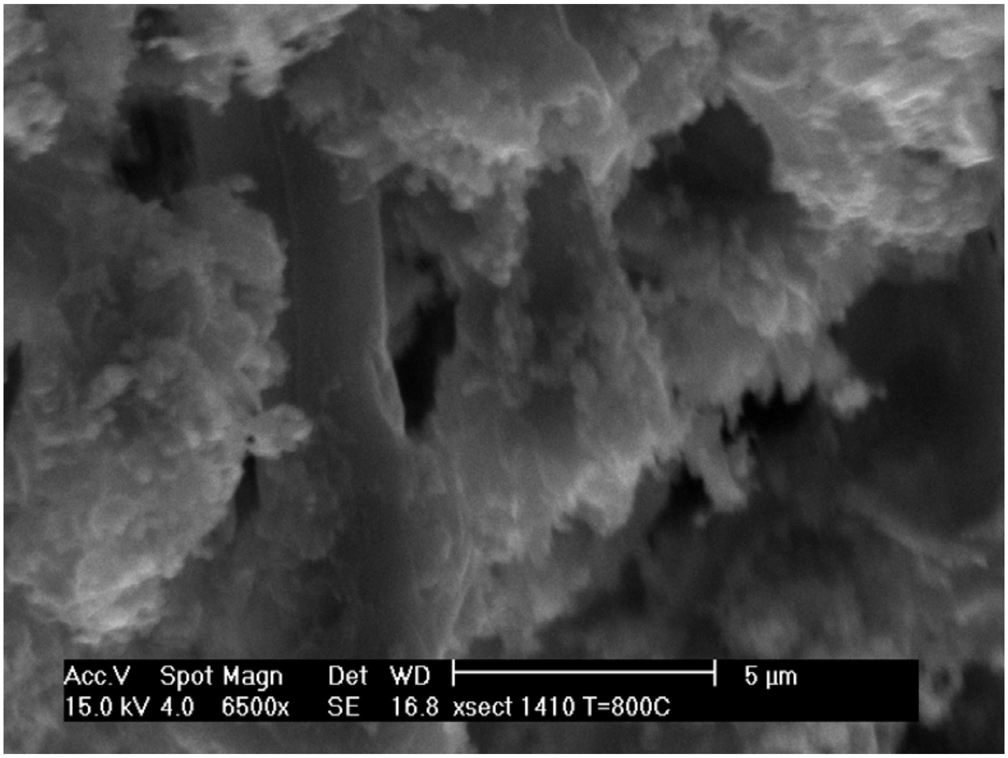

Figure 3.32: SEM cross section of porous Ni region after thermal reduction of Sample type B, T=800°C

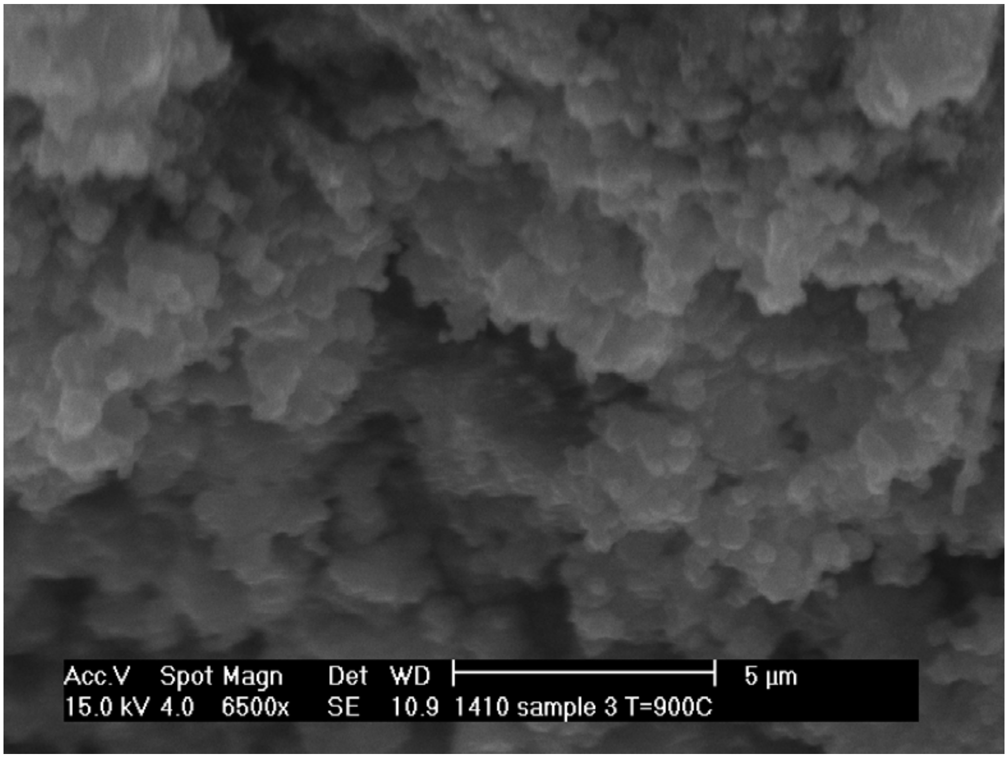

Figure 3.33: SEM cross section of porous Ni region after thermal reduction of Sample type B, T=900^{o}C

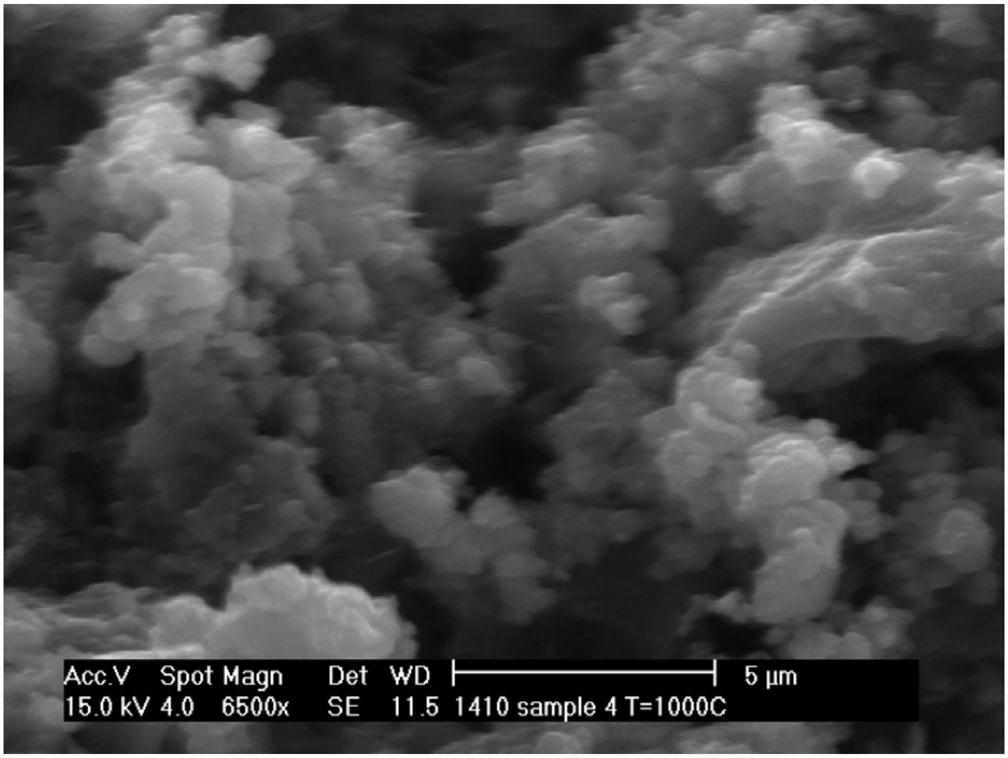

Figure 3.34: SEM cross section of porous Ni region after thermal reduction of Sample type B, T=1000^{o}C

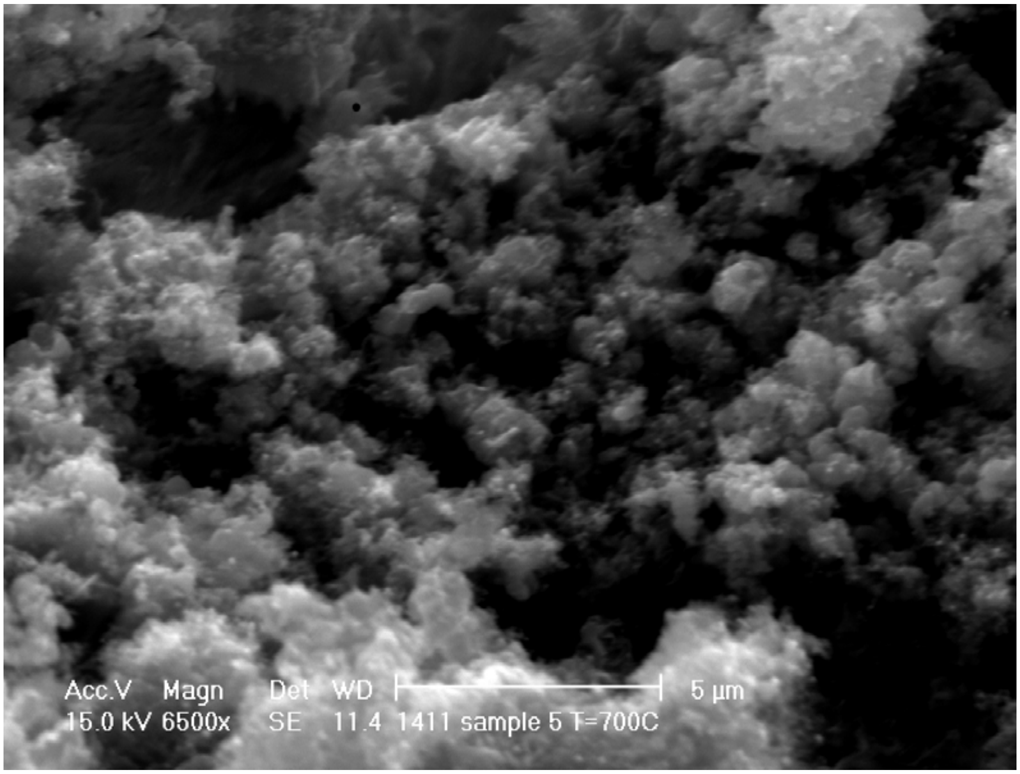

Figure 3.35: SEM cross section of porous Ni region after thermal reduction of Sample type C, T=700^{o}C

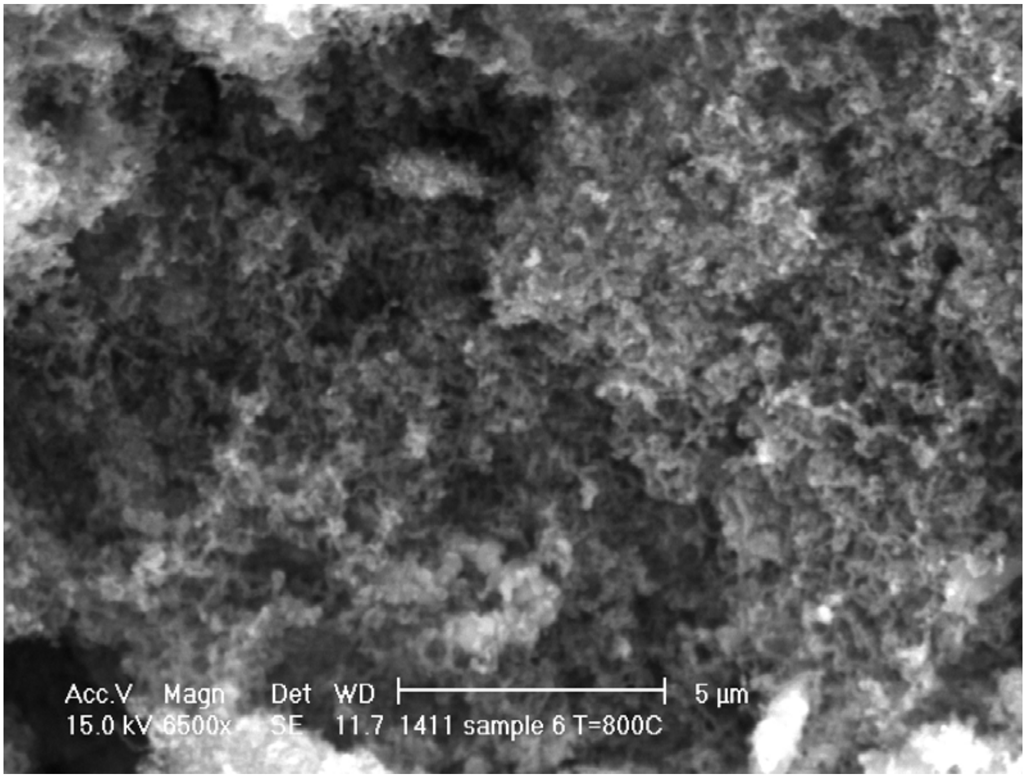

Figure 3.36: SEM cross section of porous Ni region after thermal reduction of Sample type C, T=800^{o}C

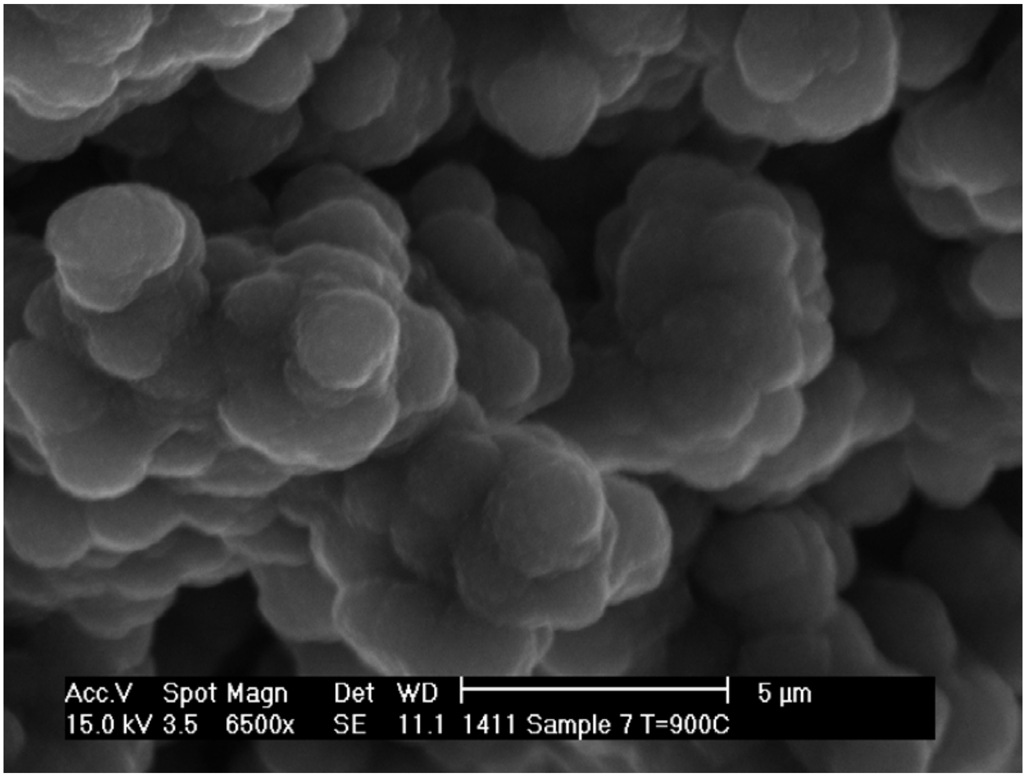

Figure 3.37: SEM cross section of porous Ni region after thermal reduction of Sample type C, T=900^{o}C

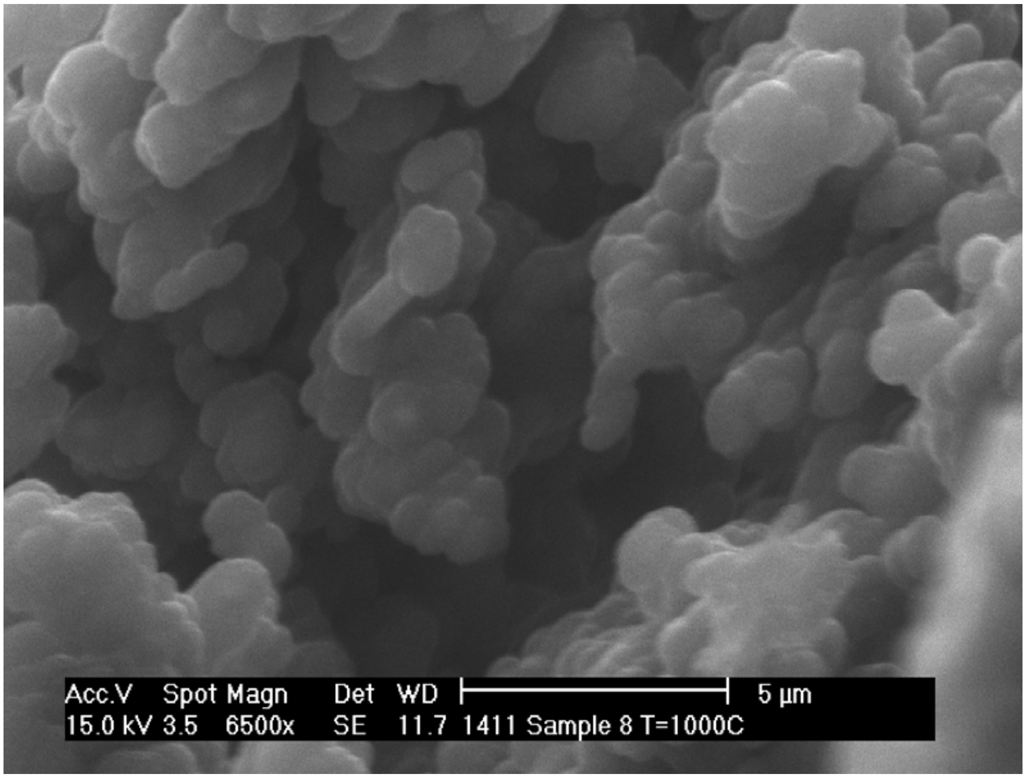

Figure 3.38: SEM cross section of porous Ni region after thermal reduction of Sample type C, T=1000^{o}C

These figures show the porous nickel region of each sample. The surface enhancement was significant compared to the morphology of the samples before reduction. One important thing to note is the structure of the samples. Some pores seem to be much finer than others. For example, Figure 3.31 has very fine features while Figure 3.37 has much larger features. Lower reduction temperatures generally resulted in much smaller features than samples reduced at higher temperatures. The impact of the different sized features can be seen in Figure 3.26. Samples reduced at lower temperatures in general have a higher specific capacitance than samples reduced at higher temperatures. A lower reduction temperature results in a slower reduction process. This means that the oxygen is removed much slower and as a result, the pores formed are finer. A finer pore results in a higher surface area.

Figures 3.27, 3.31 and 3.35 were all reduced at 700^{o}C using the three different sample preparation methods. Comparing these figures shows that the sample preparation method plays little role in the final structure of the electrode. All of these figures show very fine pore sizes. The same can be said if Figures 3.28, 3.32 and 3.36 are compared. All of these figures show SEM images of samples reduced at 800^{o}C. The samples reduced at 900^{o}C and 1000^{o}C all show similar features as well. All of the images show that at a higher temperature, the features are much larger, regardless of the preparation method. This supports the fact that the specific capacitance does not depend on the preparation method as much as the residual carbon left on the sample after reduction.

Another impact of reduction temperature can be seen in Figures 3.39 and 3.40. These samples were viewed at a lower magnification than Figures 3.27-3.38. Figures 3.40 and 55 show the cross section of samples reduced at 700^{o}C and 1000^{o}C respectively.

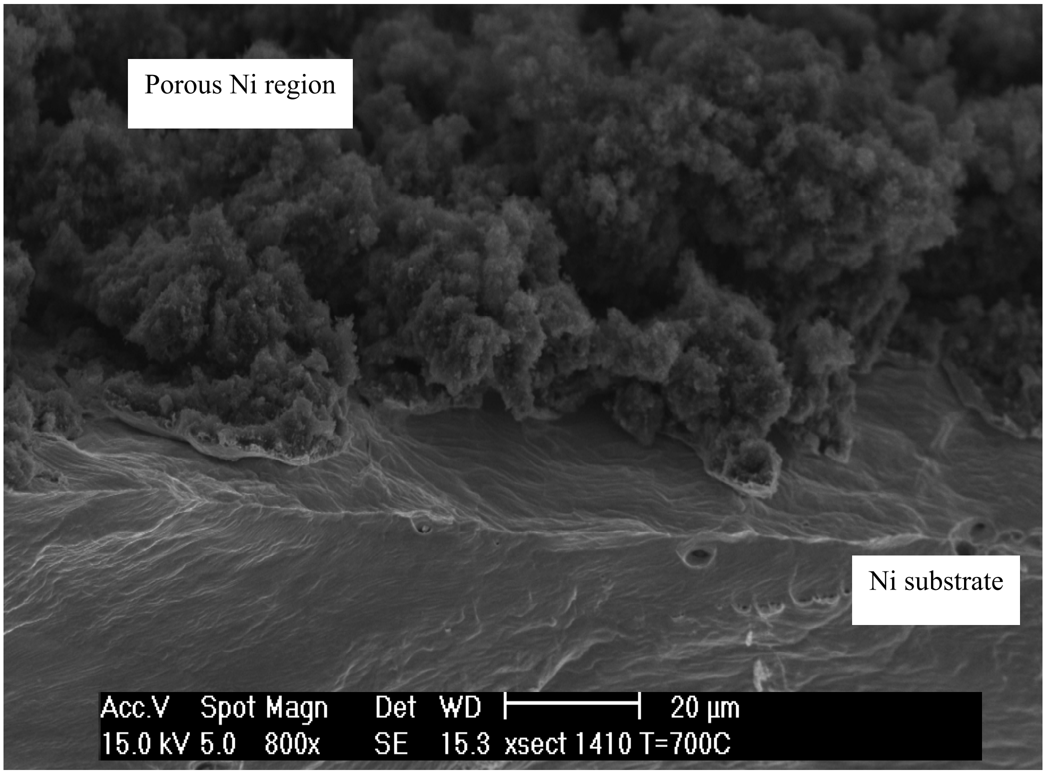

Figure 3.39: SEM cross section of sample at 800x magnification

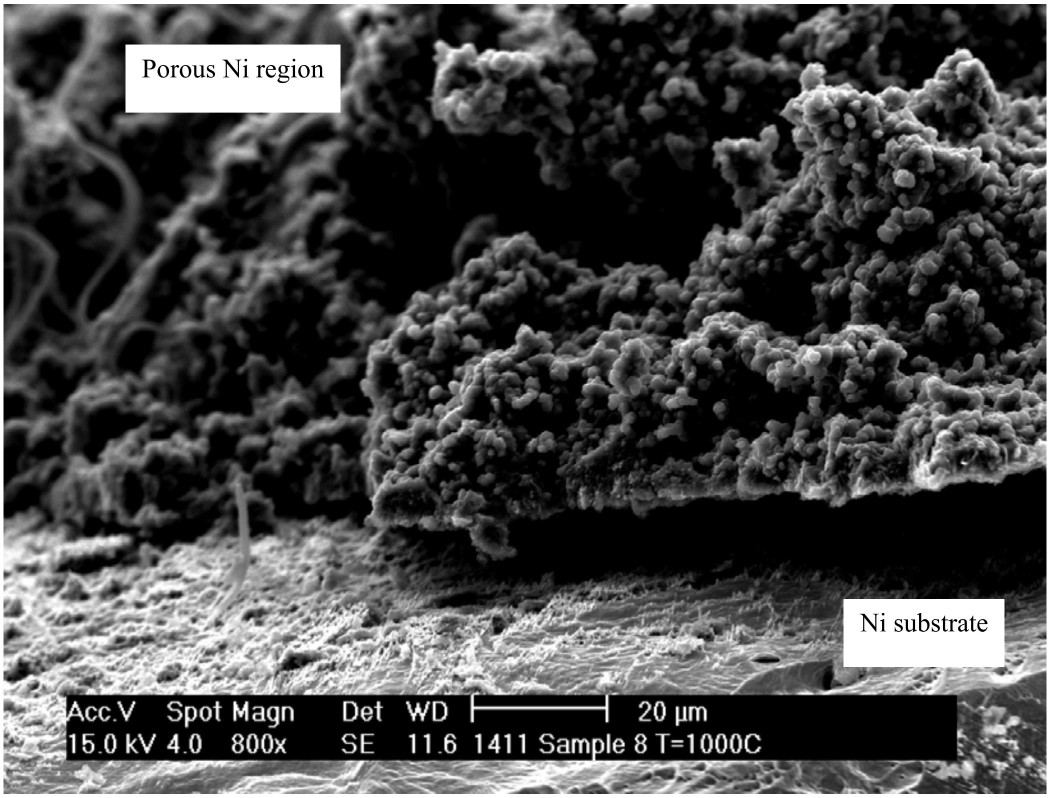

Figure 3.40: SEM Cross section showing a delaminated interface

In Figures 3.39 and 3.40, the lower region is the nickel substrate and the top region is the porous nickel. The important difference in these figures is the nickel substrate/porous nickel interface. This region is distinguishable since there is a significant difference between the structure of the porous nickel region and the nickel substrate. In order for the capacitor to be effective, the porous region and the substrate must be in close contact. Particularly at a higher temperature, the porous region could delaminate from the substrate. This phenomenon can be observed in Figure 3.40 at the nickel substrate/porous nickel interface. This delaminating resulted in a deficiency in the charge storage capability. In order to avoid this delaminating due to high temperature reduction temperatures, lower reduction temperatures would then be used. The experimental result shown in Figure 3.39 was reduced at 700^{o}C. This image shows that there was no delaminating at the nickel substrate and the porous nickel interface.

In order to better understand the morphology and composition of the electrodes that were fabricated, an FEI Nova Nanolab 200 SEM was used to obtain much higher magnification micrographs of the cross section of Sample type B. EDS was also used to qualitatively analyze the composition of the samples. The sample analyzed was reduced at 800^{o}C for 24hrs. The sample was tilted to 45^{o} inside of the tool. This image can be seen in Figure 3.41.

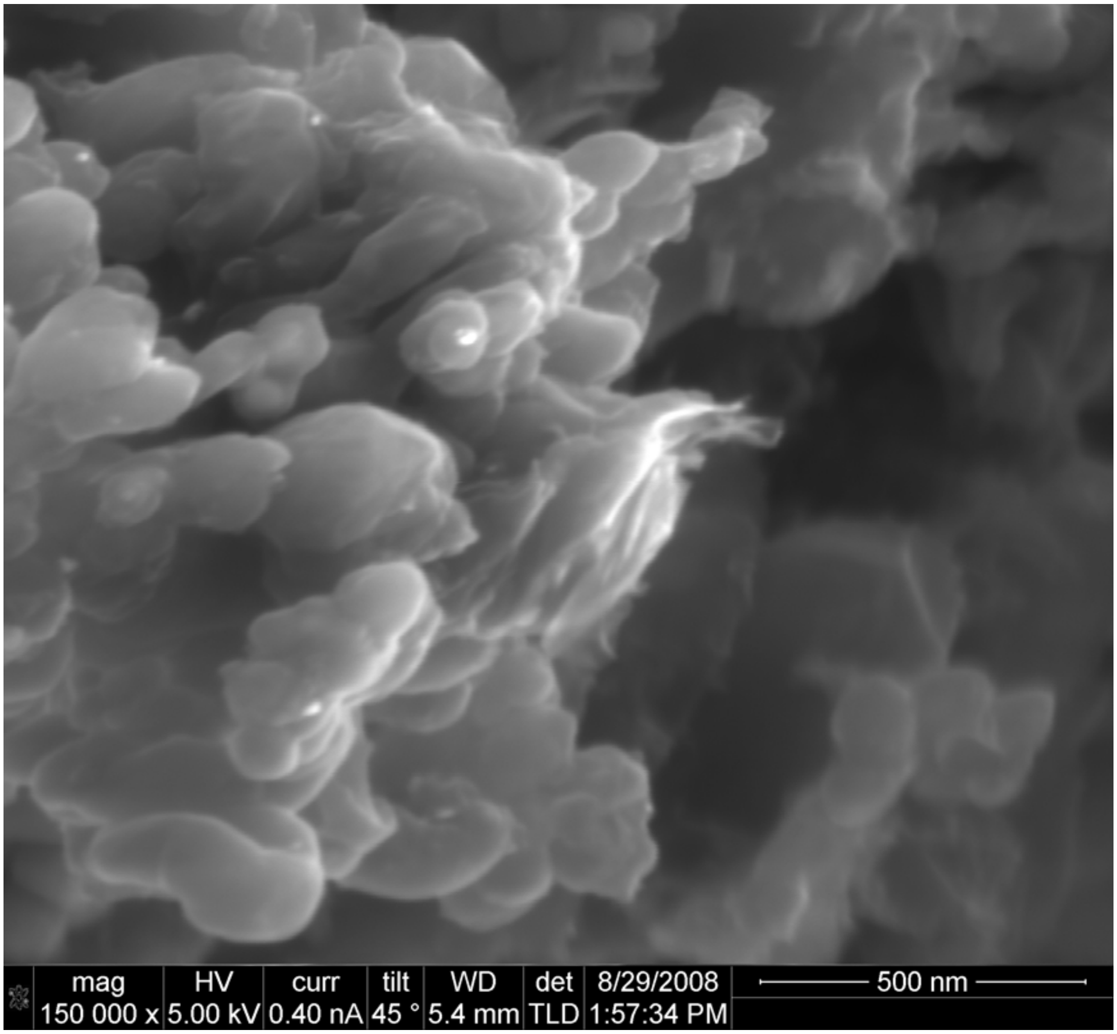

Figure 3.41: SEM Cross section of porous Ni Region of Sample type B after thermal reduction, T=800^{o}C, t=24hrs, 150,000X magnification

Figure 3.41 has two distinct regions. The grey region that was most prevalent was carbon based on the EDS analysis. The less prevalent bright region was nickel. A limitation of the SEM was that only the surface of a sample could be analyzed. Since carbon was coating the nickel, it was much more prevalent in the SEM image. Similar to nickel, carbon was also conductive. Therefore, electrical charge could be stored on the surface of the carbon as well as on the surface of the nickel. In fact, most commercial ultracapacitors were made using carbon. The presence of carbon was also beneficial for it prevented the nickel from oxidizing to form nickel oxide in the presence of air. Even at a low temperature, avoiding the oxidation of nickel would be difficult. Carbon served as a protective layer to the nickel, and aided in obtaining a higher capacitance, since nickel oxide was not a good material for fabricating ultracapacitor electrodes.

Viewing these testing samples at a 45° tilt allowed for an interesting surface discovery. This can be observed in Figure 3.42. In addition to the micrograph, the EDS mapping was performed to determine the composition of the different regions of this image. This can be observed in Figure 3.43.

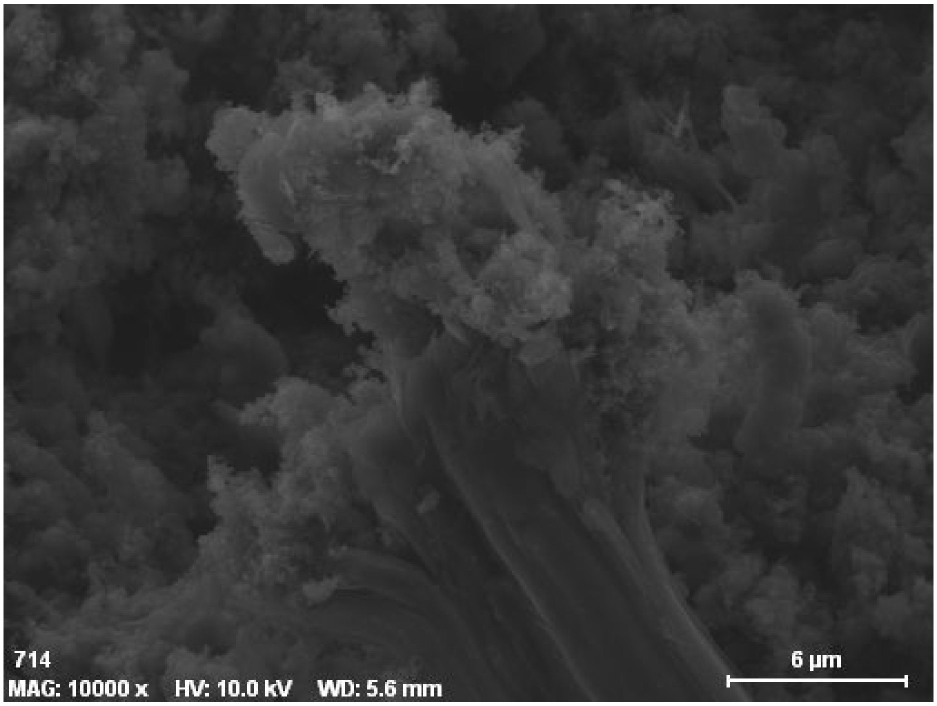

Figure 3.42: 45° tilt view of the porous Ni region of Sample type B after thermal reduction, T=800°C, t=24hrs, 10,000X magnification

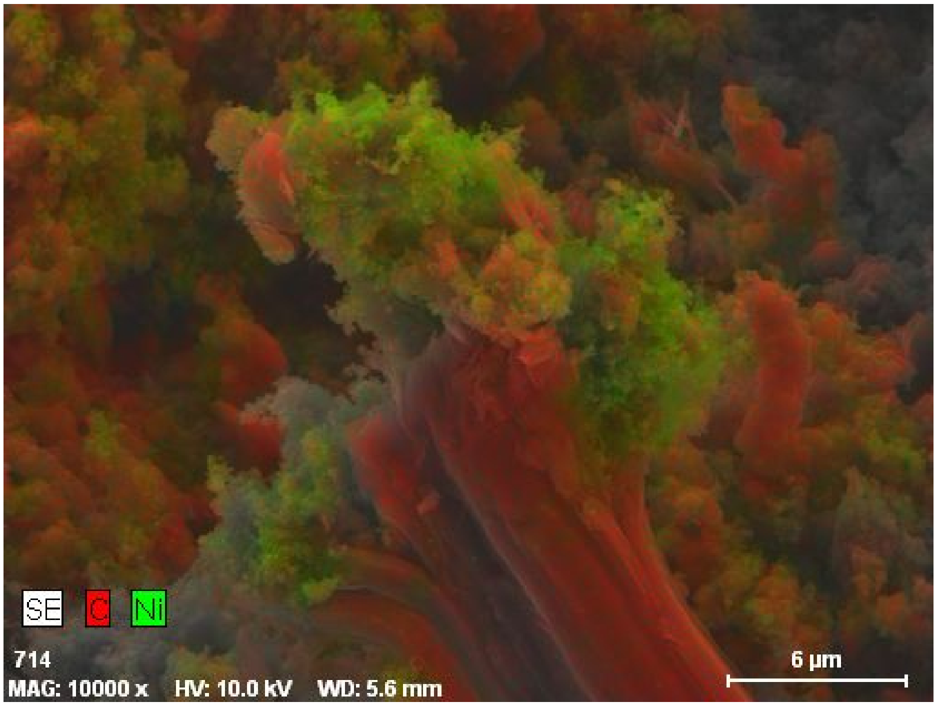

Figure 3.43: EDS mapping of the porous Ni region of Sample type B after reduction, T=800°C, t=24hrs, 10,000X magnification

In Figure 3.43, the red regions represent carbon and the green regions represent nickel. The large rod structure consists of all carbon and the region with the smaller features is nickel. This figure shows that it may be possible that the nickel serves as a catalyst for forming the carbon microtubes. While the formation of carbon nano and microtubes was not addressed in this investigation, the possibility of forming them is interesting since carbon nanotubes are also considered a viable option as an electrode material for ultracapacitor devices. Since this carbon microtube also contains nickel, it becomes more conductive than it would be without the presence of nickel.

Nickel electrodes were thermally reduced for 3 hours at various temperatures ranging from 600°C-900°C in order to determine if there was consistency in the impact of temperature on the surface enhancement of the porous nickel region. Figure 3.44 shows the specific capacitance of these electrodes as a function of reduction temperature of

Sample types A, B and C. A 2M potassium hydroxide electrolyte was used to measure the capacitance.

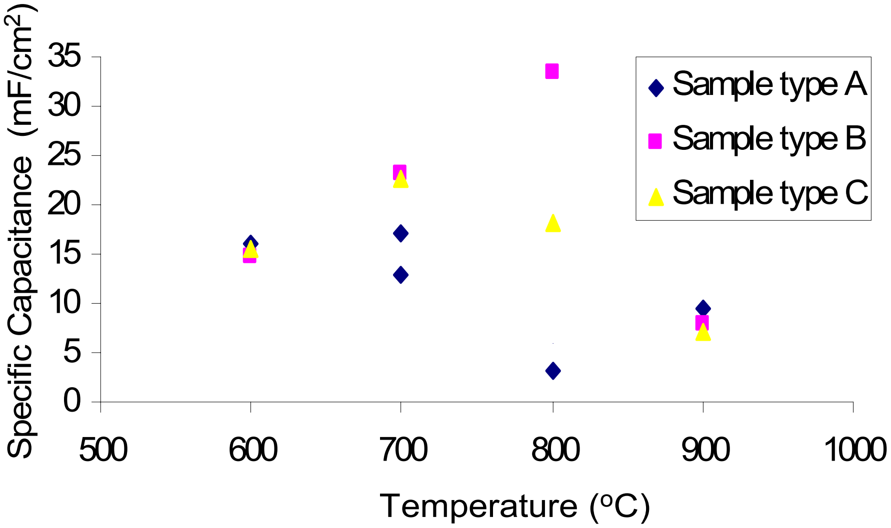

Figure 3.44: Specific capacitance as a function of time of samples thermally reduced for 3hrs with a 2M KOH electrolyte

Equation 1.7 was used to calculate the capacitance of the electrode. The specific capacitance was determined by dividing the capacitance by the area of the electrode. These samples were thermally reduced from 600-900°C instead of 700-1000°C. This is because the samples thermally reduced at 1000°C resulted in delaminated samples that did not perform as well as samples reduced at lower temperatures. The results shown in Figure 3.44 shows that the specific capacitances were greater at lower temperatures than at higher temperatures. The highest increase in surface area of the surface enhanced nickel electrodes was 1000 times greater than the surface area of a nickel plate before surface enhancement. Unlike with other electrodes, at a reduction temperature of 600°C, the samples all performed relatively uniformly. The residual carbon left behind after reducing the samples at 600°C was much less than at higher temperatures. This could be related to the combustion reactions that take place at this temperature. If equations 3.3

and 3.4 represented the reactions that were taking place rather than equation 3.5, then the products of combustion would be carbon dioxide and carbon monoxide rather than carbon. These gases would be purged from the system leaving behind a sample with much less carbon. If the residual carbon is decreased on the sample, the results could be more consistent since the electrode conditions after reduction would be more stable.

Nickel electrodes were prepared by reducing Sample types A, B and C at 700^{o}C in methane gas while varying the temperature. The reduction temperatures were 1, 3, 6, 12 and 24 hours. The specific capacitances were measured using a 2M potassium hydroxide electrolyte and a set-up similar to Figure 2.5. Figure 3.45 shows the specific capacitance as a function of reduction time for these samples.

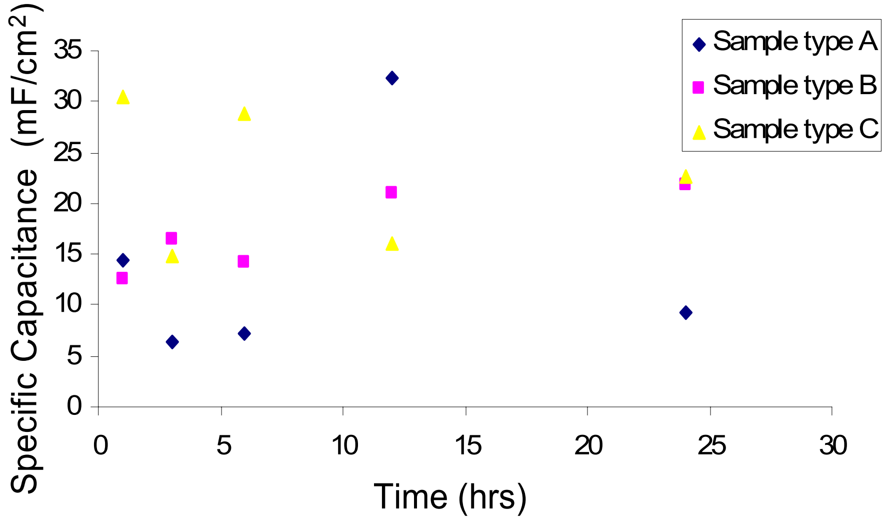

Figure 3.45: Specific capacitance as a function of time of samples thermally reduced at 700^{o}C with a 2M KOH electrolyte

Equation 1.7 was used to calculate the capacitance of the electrode. The specific capacitance was determined by dividing the capacitance by the area of the electrode. As in Figure 3.26, the specific capacitance of all of the electrodes is at least 150 times greater than the specific capacitance of a nickel plate before the surface enhancement. In fact, in some instances the surface enhancement was greater than 1,000 times that of the nickel before the thermal reduction. The specific capacitance results shown in Figure 3.45 are inconsistent, just as the results in Figure 3.26 show.

There is also no consistency in which type of Sample type results in the highest specific capacitance. In general, all of the results are relatively close in specific capacitance, regardless of the amount of time the sample is reduced. This was expected since the role that the amount of reduction time plays should only impact the amount of oxygen removed from the system. If the thermal reduction process goes to completion, then the electrodes should perform uniformly, even if the sample reduction time is 1 hour or 24 hours. The residual carbon does play a role in the uniform performance of the electrodes as in the electrodes represented in both Figures 3.26 and 3.44.

Figures 3.46-3.57 show the SEM images for samples reduced at 700°C in methane at different temperatures for Sample types A, B and C. Samples 3.46-3.49 represent Sample type A reduced at 12, 6, 3 and 1 hour respectively. Figures 3.50-3.53 and Figures 3.54-3.57 represent Sample types B and C, respectively, reduced at the same temperatures as Sample type A.

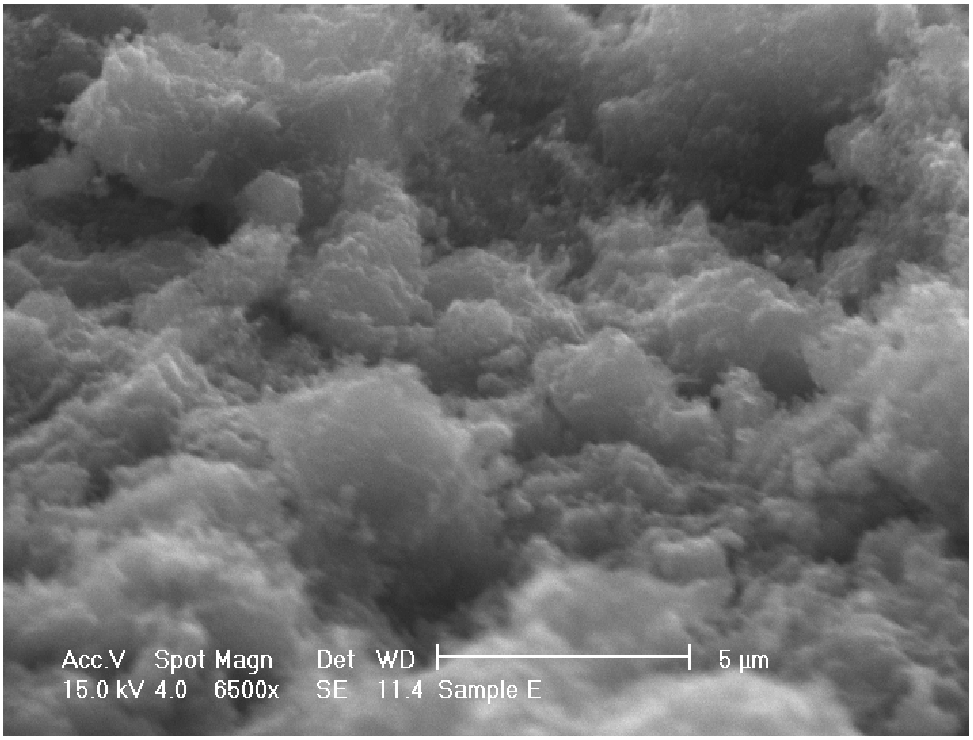

Figure 3.46: SEM cross section of porous Ni region after thermal reduction of Sample type A, t=12hrs

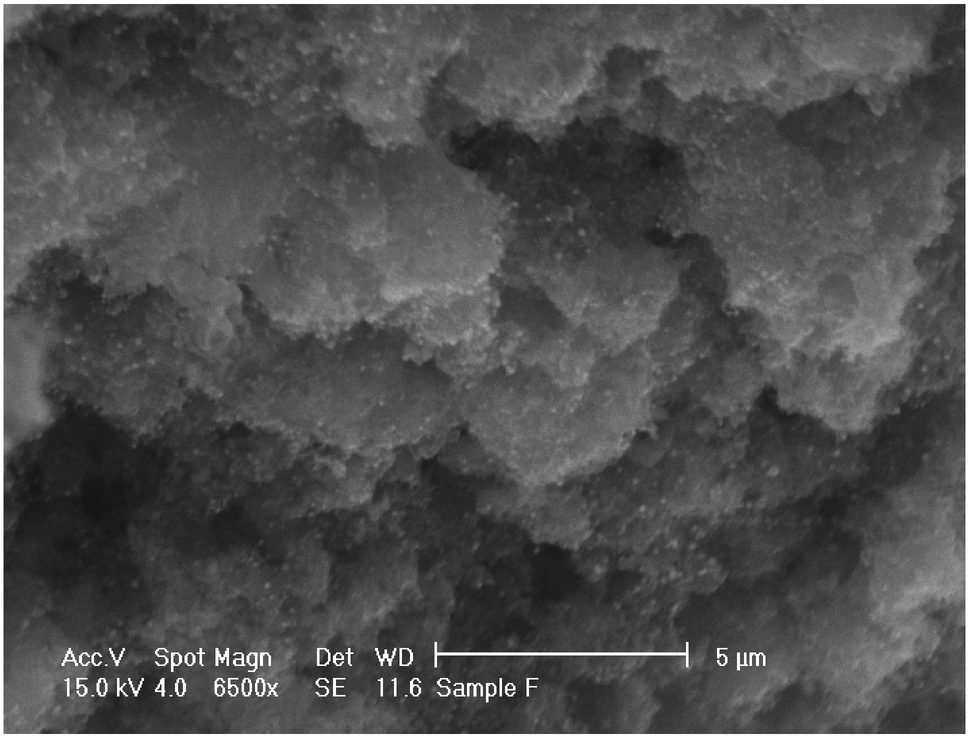

Figure 3.47: SEM cross section of porous Ni region after thermal reduction of Sample type A, t=6hrs

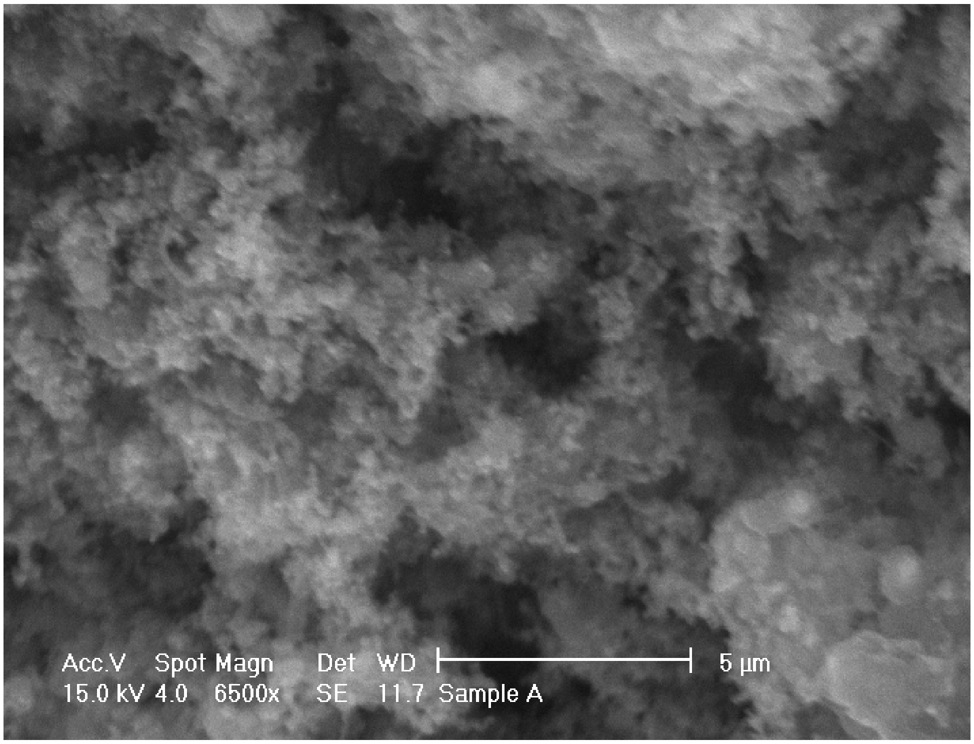

Figure 3.48: SEM cross section of porous Ni region after thermal reduction of Sample type A, t=3hrs

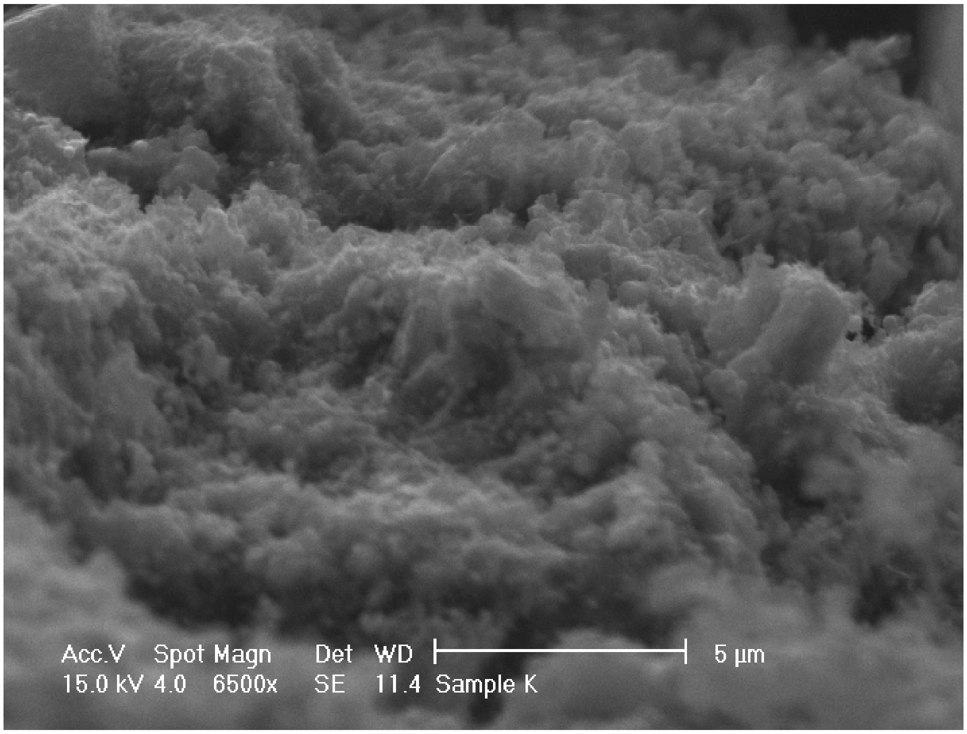

Figure 3.49: SEM cross section of porous Ni region after thermal reduction of Sample type A, t=1hr

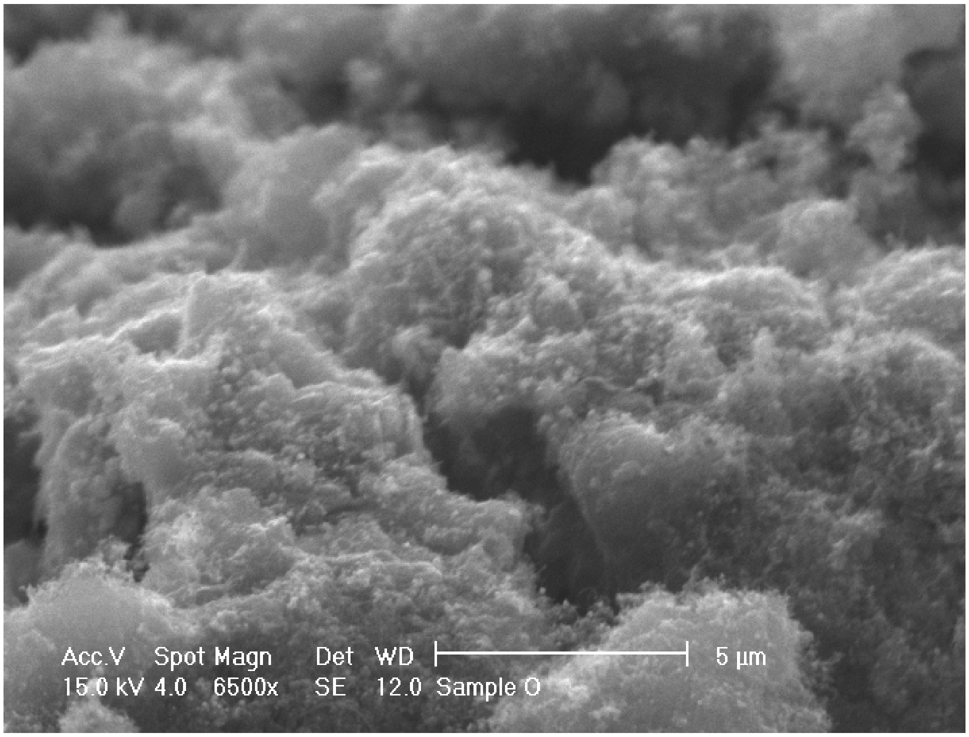

Figure 3.50: SEM cross section of porous Ni region after thermal reduction of Sample type B, t=12hrs

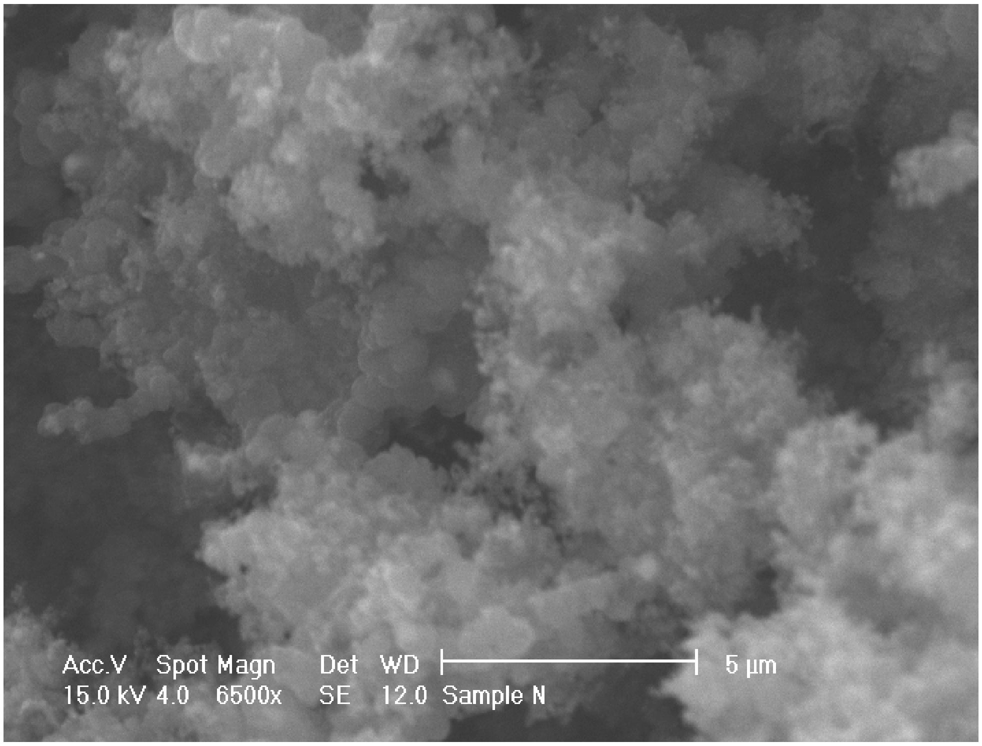

Figure 3.51: SEM cross section of porous Ni region after thermal reduction of Sample type B, t=6hrs

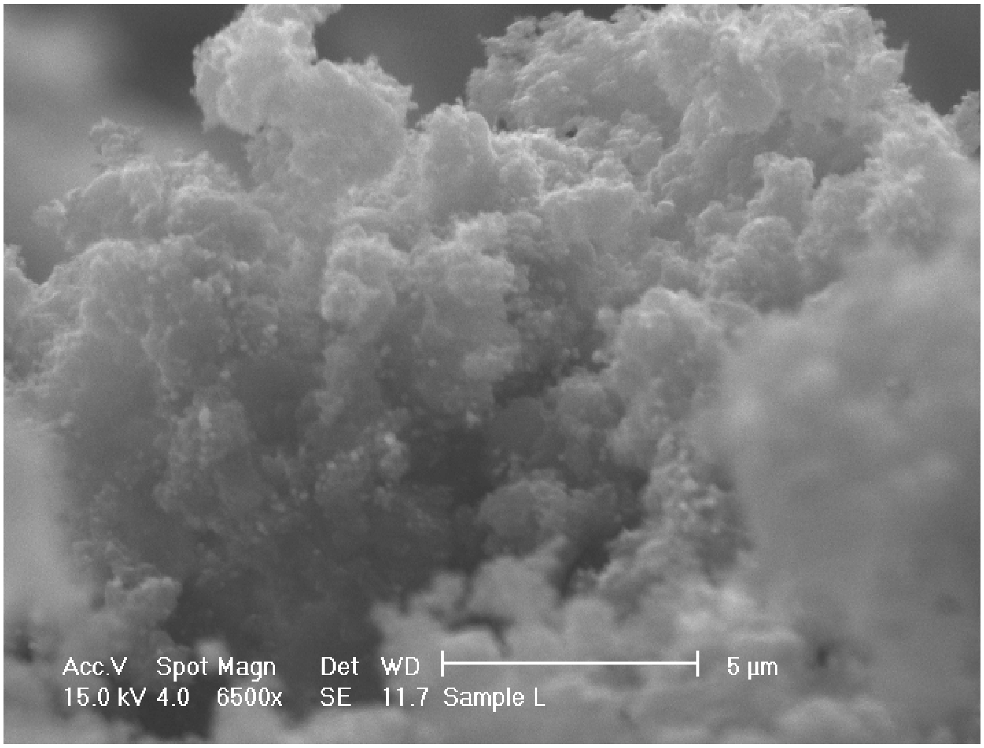

Figure 3.52: SEM cross section of porous Ni region after thermal reduction of Sample type B, t=3hrs

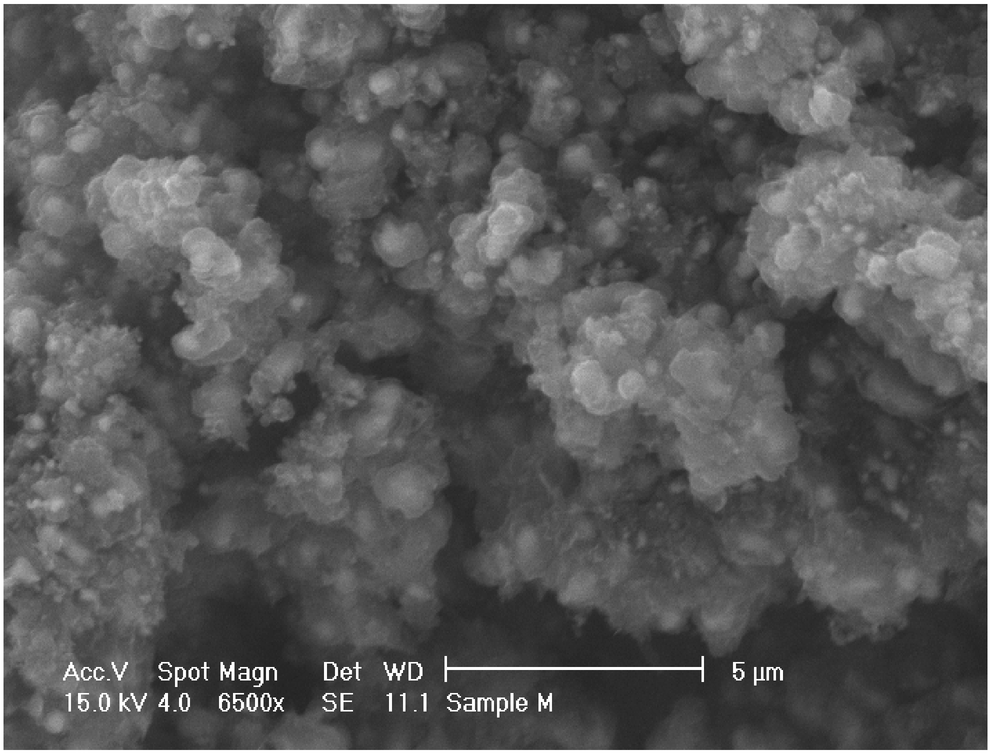

Figure 3.53: SEM cross section of porous Ni region after thermal reduction of Sample type B, t=1hr

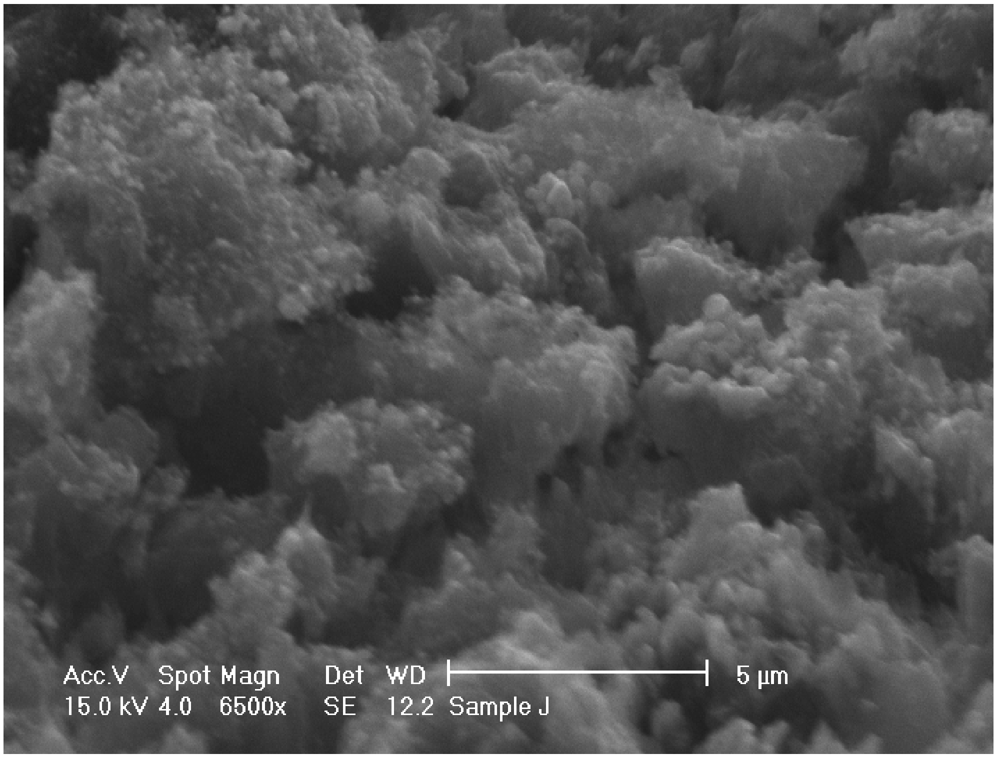

Figure 3.54: SEM cross section of porous Ni region after thermal reduction of Sample type C, t=12hrs

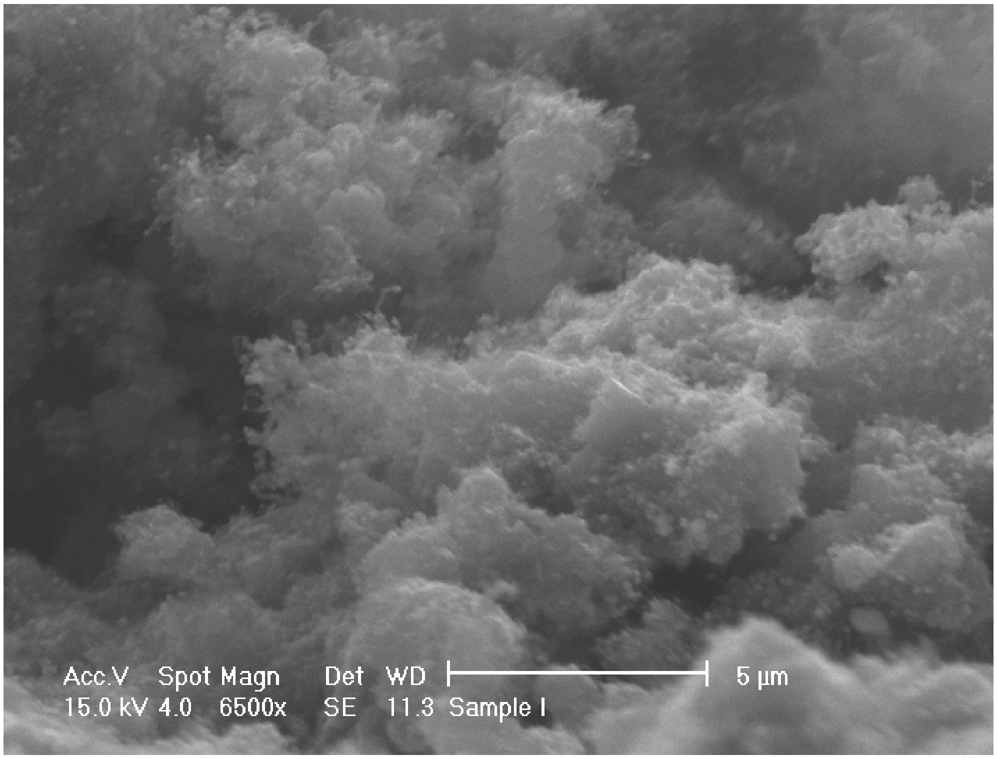

Figure 3.55: SEM cross section of porous Ni region after thermal reduction of Sample type C, t=6hrs

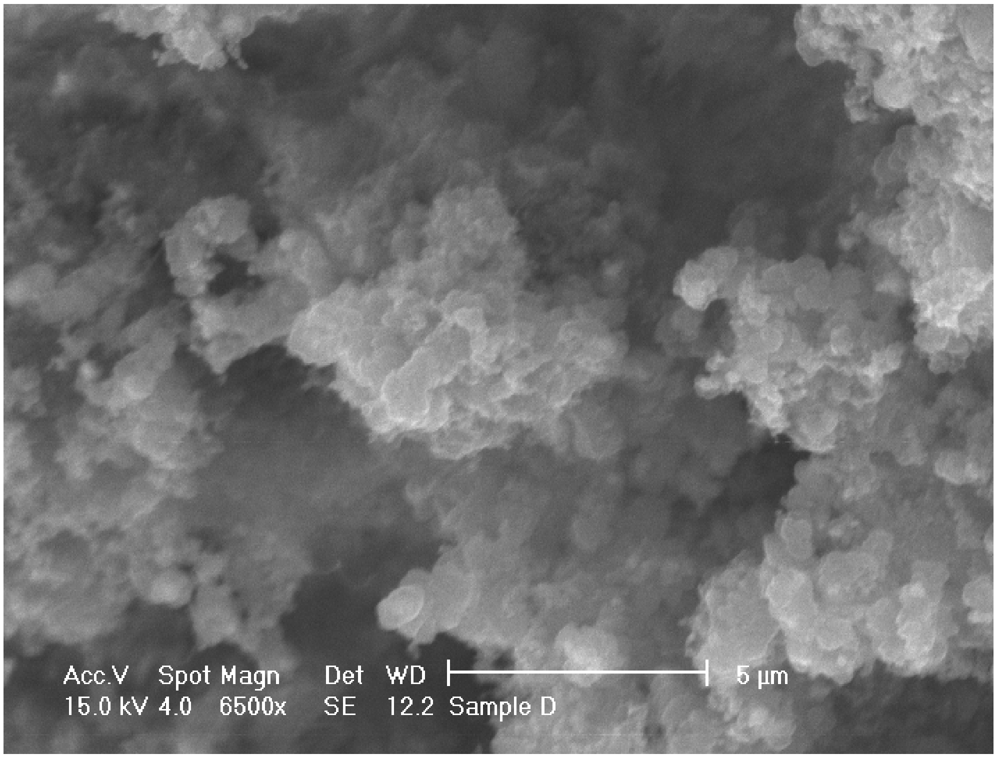

Figure 3.56: SEM cross section of porous Ni region after thermal reduction of Sample type C, t=3hrs

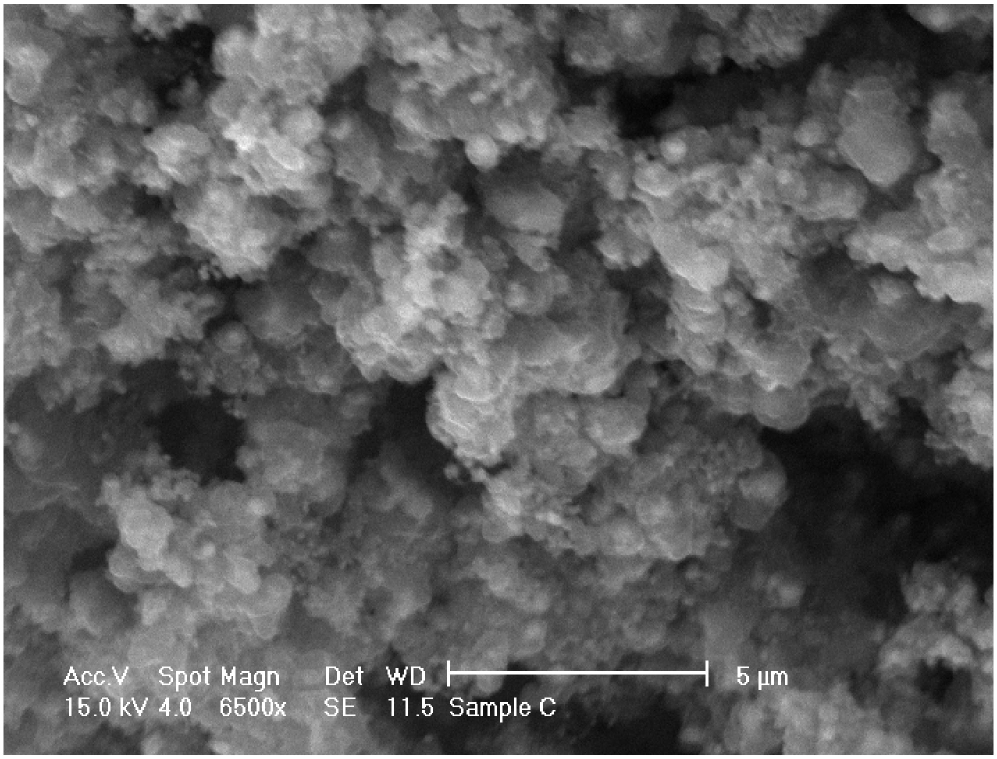

Figure 3.57: SEM cross section of porous Ni region after thermal reduction of Sample type C, t=1hr

Figures 3.46-3.57 show the porous nickel regions of each sample. These figures show a significant increase in the surface area compared to the nickel electrodes before reduction. Figures 3.46-3.57 also show that regardless of the reduction time, the cross section SEM images of each sample seem to be extremely similar. All of the figures also seem to be similar to Figures 3.27, 3.31 and 3.35, which represent Sample types A, B and C reduced at 700°C for 24 hours, respectively. This could be a result of the fact that reduction time does not impact the surface enhancement of the samples, which is also shown in Figure 3.45.

Surface enhanced nickel electrodes were prepared at 800°C in methane while varying the thermal reduction times. The reduction times were 1hr, 3hrs, 6hrs, 12hrs and 24hrs. These experiments were done to serve as a method of comparison to the samples reduced in methane at various times but at 700°C. Figure 3.58 shows the specific capacitance as a function of reduction time of samples reduced at 800°C in methane. The specific capacitances were measured in a 2M potassium hydroxide electrolyte.

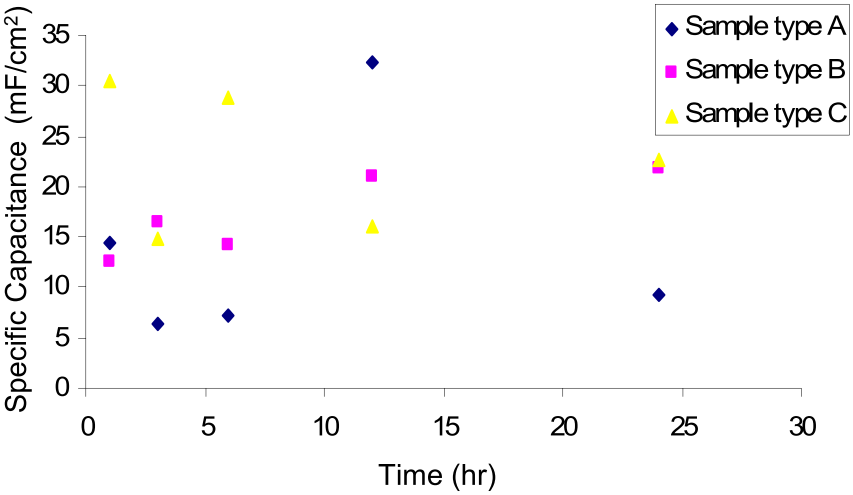

Figure 3.58: Specific capacitance as a function of time for samples thermally reduced in methane at 800°C using a 2M KOH electrolyte

Equation 1.7 was used to calculate the capacitance of the electrode. The specific capacitance was determined by dividing the capacitance by the area of the electrode. Figure 3.58 shows a significant increase in specific capacitance of the surface enhanced electrodes compared to the specific capacitance of the nickel substrate before surface enhancement. The highest specific capacitance is estimated to be 32mF/cm^2. This is about 1,000 times greater than the specific capacitance of a nickel substrate before surface enhancement.

Figure 3.58 is very similar to Figure 3.45 in that all of the specific capacitances are relatively near the same value, although there is no trend in which reduction conditions result in the highest specific capacitance. All of the reduction conditions, however, do result in a much higher specific capacitance than that of a nickel substrate before surface enhancement. In fact, the electrode with the lowest specific capacitance still has a specific capacitance that is over 200 times greater than a nickel substrate before surface enhancement. The inconsistency in the results could be attributed to the residual carbon. Just as in the results shown in Figures 3.26, 3.44 and 3.45, the results in Figure 3.58 shows no real trend in which reduction conditions result in the best performing electrode. This significant improvement in the specific capacitance compared to the specific capacitance of a nickel substrate before surface enhancement shows extremely promising results, however, since these electrodes do allow for a very high capacitance in a compact device.

The effect of the concentration of the electrolyte on the specific capacitance was investigated by testing the capacitance of the electrodes while varying the electrolyte concentration. The different electrolytes tested were 0.1M, 1M, 2M and 3M potassium hydroxide. The experimental arrangement was similar to Figure 2.5. The electrodes tested were reduced for 3 hours in methane while varying the temperature of reduction from 600°C-900°C in 100°C intervals. Figures 3.59-3.62 show the specific capacitance of the surface enhanced nickel electrodes as a function of electrolyte concentration. Figure 3.59, 3.60, 3.61 and 3.62 represent samples reduced at 600°C, 700°C, 800°C and 900°C, respectively.

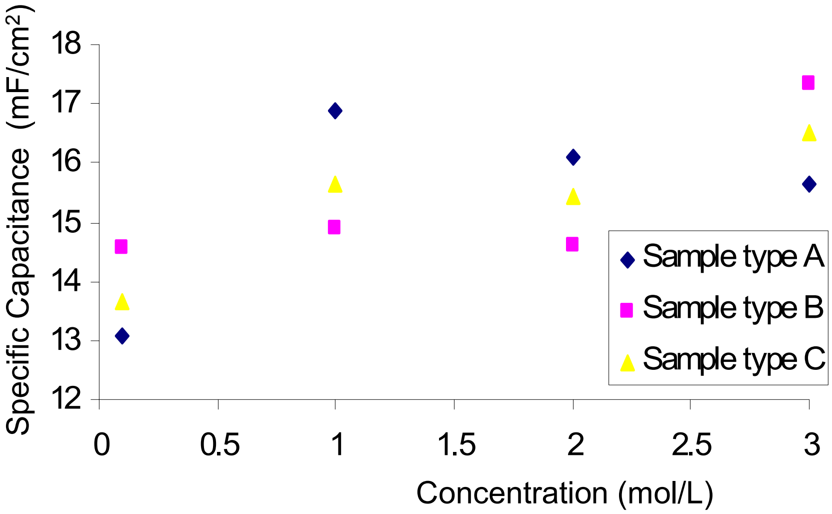

Figure 3.59: Specific capacitance versus electrolyte concentration of nickel electrodes reduce at 600°C

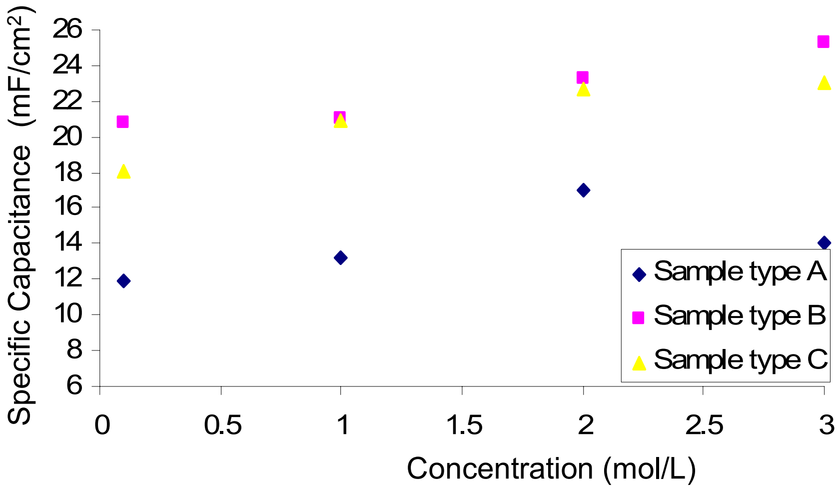

Figure 3.60: Specific capacitance versus electrolyte concentration of nickel electrodes reduce at 700°C

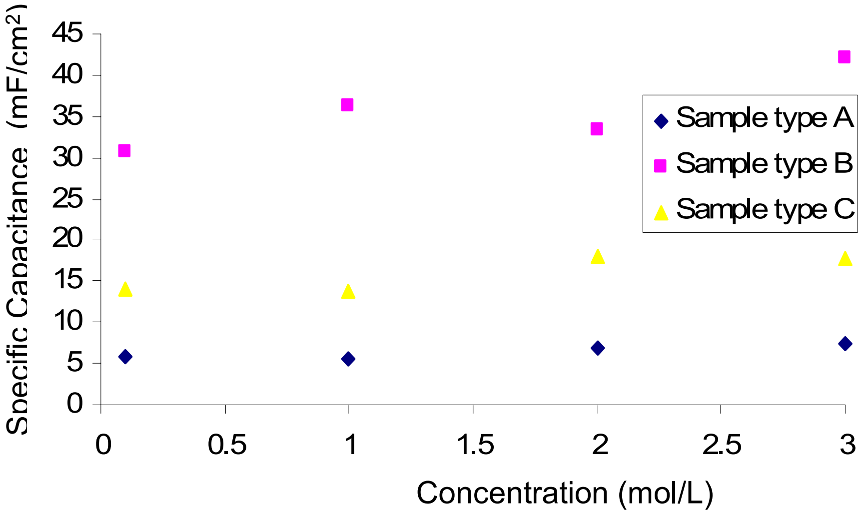

Figure 3.61: Specific capacitance versus electrolyte concentration of nickel electrodes reduce at 800°C

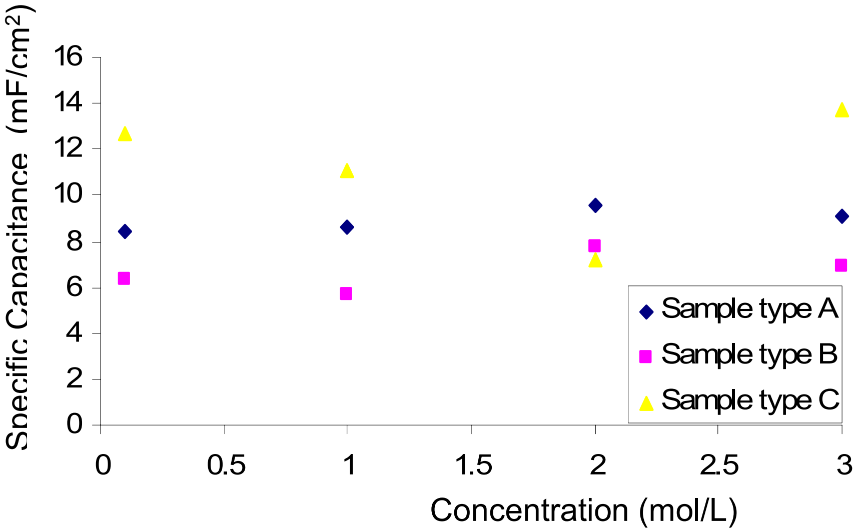

Figure 3.62: Specific capacitance versus electrolyte concentration of nickel electrodes reduce at 900°C

Equation 1.7 was used to calculate the capacitance of the electrode. The specific capacitance was determined by dividing the capacitance by the area of the electrode.

Figures 3.59-3.62 show that the in general, as the electrolyte concentration increased from 0.1M to 3M potassium hydroxide, the specific capacitance increased slightly. As the potassium hydroxide concentration increases, the conductivity of the electrolyte also increases until a maximum conductivity is reached. At this point, the interaction of ions in the electrolyte causes the conductivity to begin to decrease as the concentration increases. Since the specific capacitance is greater when a 3M potassium hydroxide electrolyte was used, it can be assumed that the conductivity of the electrolyte is still increasing at this point.

The surface enhanced nickel ultracapacitors were built using six nickel electrodes assembled in parallel similar to Figure 2.3. The oscilloscope was used to measure the voltage achieved while charging the capacitor and the time it required to charge the ultracapacitor. The change in the instantaneous voltage was also measured. Equation 1.7

was used to calculate the capacitance of the ultracapacitor and equation 2.3 was used to determine the series resistance.

Two types of ultracapacitors were built in this study. The first ultracapacitor consisted of six electrodes of a nickel substrate before surface enhancement. The second ultracapacitor consisted of six electrodes thermally reduced nickel electrodes of Sample type B at 700^{o}C in methane at either 3hrs or 6hrs. Table 3.3 summarizes the values measured and calculated for the two types of the ultracapacitors built.

Table 3.3: Summary of values used to test the ultracapacitors

	Sample type B	Ni substrate
V_3	10.17mV	13.40mV
t	238mS	0.580mS
ΔV	2.0mV	2.8mV
C	74.56mF	0.14mF
R_s	0.75Ω	1.04 Ω

Table 3.3 shows that the capacitance of the ultracapacitor built with Sample type B electrodes have a capacitance of 74.56mF while the ultracapacitor built with the nickel electrodes before surface enhancement has a capacitance of only 0.14mF. The capacitance of the ultracapacitor built with surface enhanced electrodes is more than 500 times greater than that of an ultracapacitor built with the nickel substrate. This value shows significant improvement of the capacitance due to surface enhancement accomplished by thermal reduction. This result was consistent with the specific capacitance results measured for one nickel electrode measured using the counter electrode. This was highly encouraging since no effort was made to optimize the volumetric capacitance. If additional surface enhanced electrodes were placed in parallel, this capacitance could increase significantly. As demonstrated, the scale-up from one

electrode to six electrodes yielded consistent results, indicating that the scale-up to a larger system may yield similar results.

The series resistance for both types of the ultracapacitors was approximately 1Ω. This value was expected since the series resistance would be impacted by the thickness of the layer of built up charge on the electrodes. However, the electrolyte was a simple aqueous electrolyte and this layer of charge would not be substantial, which allowed for easy movement of the ions throughout the system. This low series resistance would be beneficial if the charge and discharge time could be optimized.

Both of the series resistances were approximately equal for the two types of the ultracapacitors. This could be the result of the same electrolyte being used in both ultracapacitors and the layer of the charge build up on the surface of the electrodes was similar. While the surface area of the ultracapacitor built using the surface enhanced nickel electrode was higher than that of the nickel substrate, the thickness of this ion layer would be similar since the size of the ions in both systems was the same. If the pores in the surface enhanced nickel ultracapacitor were greater than the size of the ions, the device would not be diffusion limited and the series resistance should be low. The experimental results supported this assessment. If a larger more complex electrolyte was used, such as the commercially available complex organic electrolytes, this might not be the case. Consequently, the series resistance of the surface enhanced ultracapacitor would be larger than that of the nickel substrate ultracapacitor.

IV. CONCLUSIONS

This research showed the feasibility of using a thermal reduction procedure in an appropriate environment could produce a surface enhanced nickel ultracapacitor using a potassium hydroxide electrolyte. First the specific capacitance of a nickel electrode before surface enhancement was tested. The specific capacitance of this electrode was estimated to be $28\mu F/cm^2$. Nickel electrodes that were surface enhanced demonstrated specific capacitances that were more than 1,000 times greater than that of the nickel electrode before surface its enhancement.

The nickel electrodes were prepared using thermal reduction in the presence of methane gas. The reduction temperature and time were varied in order to determine the best conditions for reducing the nickel oxide sample to form the highly porous nickel electrode. The temperatures used ranged from $600\text{-}1000^{o}C$ and the reduction time ranged from 1hr-24hrs. The specific capacitances were then measured in order to determine the best reduction conditions. It was found that a lower reduction temperature resulted in higher specific capacitance since the removal of the oxygen from the nickel electrode was slower at a lower temperature. The slower reduction process resulted in finer pores than the samples reduced at higher temperature. The reduction time did not appear to play a role in the performance of the specific capacitance. Once all of the oxygen was removed, the reactions ceased. Therefore, as long as the reduction time is sufficient for removing the oxygen, then the specific capacitances should be similar for electrodes reduced at the same temperature.

In addition to using the specific capacitance measurements, electrodes were analyzed using an SEM in order to compare the degree of surface enhancement between the electrodes before and after the thermal reduction as well as the variations in the cross section of the electrodes based on the variations in the thermal reduction conditions. These SEM images supported that the surface area had increased significantly once the sample was reduced. The SEM results were in agreement with the specific capacitance results at high reduction temperatures. High reduction temperatures could result in lower specific capacitances because of the rapid removal of the oxygen from the system.

In addition to SEM, EDX analysis was performed to qualitatively analyze the compositions of the system. The EDX analysis found that all of the various reduction conditions were adequate in removing the oxygen from the electrode. Finally, XRD analysis was performed to determine the overall composition of the surface of the samples before and after the thermal reduction. These results supported the EDX results, and the results showed that after the thermal reduction, the composition of the surface of the sample consisted of only nickel. This indicated that all of the oxygen had been removed from the surface of the sample.

The effect of the electrolyte was also measured by varying the electrolyte concentration used to determine the specific capacitances of the surface enhanced nickel electrodes. Four different concentrations of the potassium hydroxide were used to measure the specific capacitances. The concentrations used ranged from 0.1M to 3M potassium hydroxide. As the concentration of the electrolyte increased, the specific capacitance also increased. This increase in specific capacitance corresponds to the fact that the conductivity of the electrolyte also increases as the concentration increases, at least up to a concentration of 3M potassium hydroxide.

Finally, ultracapacitors were built in order to determine the feasibility of scaling up the results found when only testing one electrode. These ultracapacitors consisted of six nickel electrodes arranged in parallel. The electrolyte used was 2M potassium hydroxide. Two types of the ultracapacitors were built. One ultracapacitor was built using surface enhanced nickel electrodes while the other was made of the nickel electrodes before surface enhancement. The series resistance and the capacitance were calculated for each of these ultracapacitors. The series resistance for the two ultracapacitors was approximately 1Ω for each ultracapacitor. This could be due to the potassium hydroxide electrolyte used to construct the ultracapacitors. A low series resistance was encouraging for a device that could be scaled up even further since a low series resistance would lead to a high charge and discharge time compared to the commercially available ultracapacitors.

The capacitance of the ultracapacitor fabricated using the surface enhanced nickel electrodes was 74.56mF while the capacitance of the ultracapacitor built using the nickel substrate before the surface enhancement was 0.14mF. The surface enhanced nickel ultracapacitor was more than 500 times greater in capacitance than the nickel substrate ultracapacitor. This significant improvement in capacitance is extremely encouraging since the ultracapacitor built was only 30mL in volume. If this ultracapacitor was scaled up, the capacitance could be competitive with the commercially available capacitors today.

If this ultracapacitor could be competitive with the commercial devices, it would provide a new, novel method of storing a large quantity of electrical charges in a compact device using a relatively low cost material. Due to the continually high demand of alternative methods of charge storage, ultracapacitors such as this one could serve as a means of meeting the increasing energy demands.

V. FUTURE WORK

This research considered the ideal reduction temperature and times for fabricating an ultracapacitor. Another important consideration would be the impact of the reducing agent. Both hydrogen gas and carbon were considered as possible the reducing agents, however neither yielded results comparable to that of the methane gas. In the case of carbon, however, it was difficult to remove all of the oxygen from the nickel oxide region of the electrode. Hydrogen gas was capable of removing all of the oxygen of the electrode, however the surface area of the electrode was not improved significantly and as a result, the specific capacitance of this device was in the same order of magnitude as the nickel plate before the surface enhancement. If it was possible to find suitable reduction conditions, hydrogen may still be a viable option as a reducing gas.

Additional tests would be necessary to determine the longevity of the electrode. The lifetime of the device would be an important aspect of an ultracapacitors. Ultracapacitors were designed to have a lifetime up to 1,000 times greater than that of a battery. Ideally, an ultracapacitor would not break down regardless of the application and therefore it could be maintenance free. In order to determine the lifetime of the high surface area nickel ultracapacitors, the device would have to be continuously charged and discharged and the performance of the device would then be measured. Ideally, the device would show no depreciation in the charge storing capabilities.

Experiments should also be performed to determine the power and energy density of the ultracapacitors. Since the series resistance appeared to be low, the power density of these devices should be higher than those of commercially available ultracapacitors.

Finally, larger ultracapacitors should be constructed to determine if further scale-up would be feasible. The scale-up from one electrode to six electrodes resulted in a capacitance expected. Ideally, more numbers of electrodes or a larger size of electrode was used, a higher capacitance would be obtained.

APPENDIX

List of symbols

In order of appearance:

C	capacitance, F
κ	dielectric coefficient of the electrolyte
ε_o	permittivity in a vacuum, $8.85x10^{-12}$ F/m
A	surface area of an electrode, m^2
d	distance between two electrodes, m
l	length of an electrode, m
E	energy accumulated on an ultracapacitor, J
V_o	applied voltage used to charge an ultracapacitor, V
C_{tot}	total capacitance of the ultracapacitors added either in parallel or series, F
C_1	capacitance of ultracapacitor 1, either in parallel or series, F
C_2	capacitance of ultracapacitor 2, either in parallel or series, F
R_{tot}	total resistance of resistors added either in parallel or series, Ω
R_1	resistance of resistor 1, either in parallel or series, Ω
R_2	resistance of resistor 2, either in parallel or series, Ω
V	actual voltage of an ultracapacitor, V
t	time required to an ultracapacitor, s
R	constant resistance of the resistor used to determine the capacitance of an ultracapacitor, Ω
V_1	maximum applied voltage of the square wave, V

V_2	minimum applied voltage of the square wave, V
y	thickness of the nickel oxide film due to thermal oxidation, μm
t'	time of oxidation of the nickel to form nickel oxide, s
A'	oxidation constant that is dependent on the temperature of oxidation and and the nature of the film, μm^2/s
B	integration constant, μm^2
MW_{NiO}	molecular weight of nickel oxide, 74.7
MW_O	molecular weight of atomic oxygen, 16.0
Δm	change in mass of the nickel plate after thermal oxidation, g
A_{avg}	average area of the nickel plate, cm^2
ρ_{NiO}	density of nickel oxide, 6.67g/cm^3
V_s	voltage of the square wave applied to the circuit set-up used to measure the capacitance of the ultracapacitor, V
R_3	resistance of resistor 3 set up in series, Ω
R_s	series resistance of an ultracapacitor, Ω
ΔV	instantaneous change in the voltage of the square wave due to the series resistance, Ω
V_3	resultant voltage of the circuit set up if R_1 and R_2 are in parallel, V
R_c	resistance applied to the ultracapacitor, Ω

BIBLOGRAPHY

C.R. Bundle, Charles A. Evans, Shaun Wilson. **Encyclopedia of Materials Characterization: Surfaces, Interfaces, Thin Films**. Butterworth-Heineman, Michagan, 1992.

Andrew Burke, *Ultracapacitors: why, how, and where is the technology*, Journal of Power Sources, **91** (2000) 37.

William D. Callister, Jr. **Materials Science and Engineering: An Introduction**. 7th Edition, John Wiley & Sons, Inc., New York, 2007.

B.E. Conway. **Electrochemical Supercapacitors: Scientific Fundamental and Technological Applications**. Klumer Academic/Plenum Publishers, New York, 1999.

Richard C. Dorf. **Introduction to Electric Circuits**. 2nd Edition, John Wiley & Sons, Inc., New York, 1993.

Ch. Emmenegger, Ph. Mauron, P. Sudan, P. Wenger, V. Hermann, R. Gallay, A. Züttel, *Investigation of electrochemical double-layer (ECDL) capacitors electrodes based on carbon nanotubes and activated carbon materials*, Journal of Power Sources, **124** (2003) 321.

Elzbieta Frackowiak, Françios Béguin, *Carbon materials for the electrochemical storage of energy in capacitors*, Carbon **39** (2001) 937.

Kazuo Fueki, J. Bruce Wagner, Jr., *Studies of the Oxidation of Nickel in the Temperature Range of* 900^o *to* 1400^oC, Journal of the Electrochemical Society, **112** (1965) 384.

Christie John Geankoplis. **Transport Processes and Separation Process Principles**. 4th Edition, Prentice Hall, New Jersey, 2003.

Vladimir N. Ipatieff. **Catalytic Reactions at High Pressures and Temperatures**. The MacMillan Company, New York, 1936.

Il-Hwan Kim and Kwang-Bum Kim, *Ruthenium Oxide Thin Film Electrodes for Supercapacitors*, Electrochemical and Solid State Letters, **4** (2001) A62.

Per Kofstad. **High Temperature Corrosion.** Elsevier Applied Science, New York, 1988.

T. Morimoto, K. Hiratsuka, Y. Sanada, K. Kurihara, *Electric double-layer capacitor using organic electrolyte*, Journal of Power Sources, **60** (1996) 239.

A.G. Pandolfo, A.F. Hollenkamp, *Carbon properties and their role in supercapacitors*, Journal of Power Sources, **157** (2006) 11.

Roger Hill Parker. **An Introduction to Chemical Metallurgy**. 1st Edition, Pergamon Press Ltd., Oxford, 1967.

Giuseppe Parravano, *The Reduction of Nickel Oxide by Hydrogen*, Journal of the American Chemical Society, **74** (1952) 1194.

Geoffrey Prentice. **Electrochemical Engineering Principles**. Prentice Hall, New Jersey, 1991.

P. Simon, A. Burke. *Nanostructured Carbons: Double-Layer Capacitance and More*. The Electrochemical Society **Interface**. Spring 2008. pp38-43.

Hong Yong Sohn, Milton E. Wadsworth. **Rate Processes af Extractive Metallurgy**. Plenum Press, New York, 1979.

Makoto Ue, Kazuhiko Ida, Shoichiro Mori, *Electrochemical Properties of Organic Liquid Electrolytes Based on Quaternary Onium Salts for Electrical Double-Layer Capacitors*, Journal of the Electrochemical Society, **141** (1994) 2989.

J.P. Zheng, P.J. Cygan, T.R. Jow, *Hydrous Ruthenium Oxide as an Electrode Material for Electrochemical Capacitors*, Journal of the Electrochemical Society, **142** (1995) 2699.